# UNIVERSITÀ DEGLI STUDI DI TRIESTE

## XXXIII CICLO DEL DOTTORATO DI RICERCA IN BIOMEDICINA MOLECOLARE

---

# Dissecting the role of G9a/GLP histone methyltransferases in Platinum-resistant ovarian cancer

Settore scientifico-disciplinare: BIO/11 BIOLOGIA MOLECOLARE


DOTTORANDA
**Dott.ssa Alice Costa**

COORDINATORE
**Prof.ssa Germana Meroni**

SUPERVISORE DI TESI
**Dott. Gustavo Baldassarre**


**ANNO ACCADEMICO 2019/2020**

This PhD project was carried out at Centro di Riferimento Oncologico (CRO, National Cancer Institute) of Aviano, in the Division of Molecular Oncology directed by Dr. Gustavo Baldassarre, and supported by Biasotto M.D. Foundation OGAP O.N.L.U.S.

*“Illness is the night side of life, a more onerous citizenship. Everyone who is born holds dual citizenship, in the kingdom of the well and in the kingdom of the sick.*
*Although we all prefer to use the good passport, sooner or later each of us is obliged,*
*at least for a spell, to identify ourselves as citizens of that other place.”*
*SUSAN SONTAG, Illness as Metaphor, 1990*

*“La malattia è il lato notturno della vita, una cittadinanza più onerosa. Tutti quelli che nascono hanno una doppia cittadinanza, nel regno dello star bene e in quello dello star male.*
*Preferiremmo tutti servirci solo del passaporto buono, ma prima o poi ognuno viene costretto, almeno per un certo periodo, a riconoscersi cittadino dell’altro paese”*
*SUSAN SONTAG, Malattia come metafora, 1990*

# TABLE OF CONTENTS

# ABSTRACT

Epithelial Ovarian Cancer (EOC) is the most aggressive gynecological malignancy, mainly due to the advanced stage at diagnosis and the development of drug-resistant recurrences. Epigenetic modifications, such as histone methylation/acetylation, are emerging as key regulators of tumor growth and response to therapies. To verify if they are also involved in the onset of drug resistance in EOC, we performed a high-throughput Epigenetic Modifiers (EMs)-based screening using four different models of EOC isogenic Platinum-Resistant (PT-Res) cells. The screening identified G9a/GLP histone methyltransferases (HKMTs) inhibitors (*G9a/GLPi*) as the most active compounds in killing all tested models. Based on these results and the current literature proposing a role for G9a in EOC progression, the aim of this thesis was to dissect the role of these HKMTs in the development of EOC PT-resistance.

Using biochemical and cell biology approaches we characterized the activity of the *G9a/GLPi* UNC0631 in inducing cell death alone or in combination with cisplatin (PT), demonstrating that UNC0631 was able to improve PT efficacy and increase PT-induced DNA damage both in parental but especially in PT-Res cells.

Using OVSAHO parental and PT-Res cells as a study model we observed an altered expression of cell-cell junction markers (i.e. β-catenin, occludin and p120-catenin) modified by PT and then reverted by UNC0631, indicating a role of G9a/GLP in cell-cell junction organization. Accordingly, PT-Res clones displayed greater ability to form spheres in extracellular matrix respect to their parental counterpart and UNC0631 treatment decreased their sphere forming activity.

In search of the possible molecular mechanism(s) explaining UNC0631 activity we verified that G9a expression and localization is regulated by PT and is altered in PT-Res EOC cells. Accordingly, PT treatment increased H3K9me2 and these effects were completely reverted by UNC0631 treatment. Then Gene Expression Profile (GEP) in OVSAHO parental and PT-Res cells treated with PT and/or UNC0631, combined with Gene Set Enrichment Analyses (GSEA), reveled that Focal Adhesion and Canonical Wnt pathways were the most significantly enriched in PT-Res respect parental cells in untreated condition. Moreover, genes belonging to Tight Junction, Canonical Wnt and Focal Adhesion pathways were all enriched in PT-Res cells treated with PT and reverted by UNC0631. qRT-PCR analysis confirmed that two genes of the Wnt pathway, namely FBXW11 and BTRC, were modified by PT in a G9a/GLP-dependent manner in all tested PT-Res isogenic models. Chromatin immunoprecipitation analyses demonstrated that G9a bound the distal region of BTRC promoter, more efficiently in PT-Res respect to the parental cells and, accordingly, that BTRC promoter had a higher degree of H3K9me2 in PT-Res cells. Finally, to prove the role of G9a/GLP in mediating the effects of UNC0631 we generated OVSAHO PT-Res G9a/GLP$^{KO}$. When compared with than PT-

Res wild type cells PT-Res G9a/GLP$^{KO}$ cells were more sensitive to PT, had increased PT-induce DNA damage, and the partial recovery of properly organized cell-cell junctions.

Collectively, our data suggest that G9a/GLP inhibition could represent a good strategy to overcome PT-resistance in EOC. Mechanistically the data support a role for G9a/GLP HKMTs in the regulation of Wnt/β-Catenin pathway that could explain the acquisition of a mesenchymal stem-like phenotype observed in PT-Res cells that, in the end, could affect the response to anticancer drugs.

# 1. INTRODUCTION

## 1.1 Epithelial Ovarian Cancer

Ovarian cancer (OC) is the eighth most common cancer in women worldwide and the fifth leading cause of cancer death in women in the western world, with 259,400 new cases and 184,800 deaths worldwide annually (Cabasag et al., 2020; Ferlay et al., 2019; Jayson et al., 2014). This high mortality is mainly due to asymptomatic early-stages that lead to late-stage detection and diagnosis, the peculiar way of metastatic dissemination, and the intrinsic or acquired drug resistance (Gao et al., 2017; Van Zyl et al., 2018).

Based on cell types of origin, ovarian cancer can be subdivided in three main clinical categories, according to the anatomic structures from which they arise: epithelial ovarian carcinoma (EOC), originating from the epithelial cells that cover the ovaries and the fallopian tubes; sex cord-stromal tumor, arising from the gonadal stromal surrounding the ovary; and germ cell tumor from germ cells. Among ovarian carcinomas, EOC is the most lethal group, representing 90% of malignant ovarian tumors (Stewart et al., 2019; X. Y. Zhang & Zhang, 2016). The International Federation of Gynecology and Obstetrics (FIGO) has updated the staging system and proposes a four-steps staging for EOCs, based on the degree of its dissemination at diagnosis. At stage I cancer is limited to ovaries only. By stage II the disease involves one or both ovaries, extended to pelvis and affects tubes and uterus. Stage III results from spread to the abdominal cavity and lymph nodes. Lastly, stage IV is characterized by distant metastasis formation (Javadi et al., 2016).

EOC is a heterogeneous disease and can be subdivided in four main histological subtypes, which differ in etiology, morphology, molecular biology and prognosis: serous (SC), endometrioid (EC), clear cell (CCC) and mucinous (MC) epithelial ovarian cancers. Serous tumors include two categories: high-grade (HGSC) and low-grade serous (LGSC) and represent the majority of advanced-stage ovarian cancers. The second most common subtype is the clear cell carcinoma, followed by endometrioid that could also be divided in high and low grade tumors; finally mucinous ovarian cancer is a less common tumor histotype (Ramalingam, 2016). HGSCs represent the 70% of all the epithelial ovarian cancers, whereas LGSCs, ECs, MCs and CCCs subtypes account for <5%, 10%, 3% and 10%, respectively (Javadi et al., 2016; Stewart et al., 2019).

Based on their aggressiveness and invasiveness, EOCs are also subdivided in two main categories: low-grade type I and high-grade type II (**Figure 1.1**). Type I includes low-grade serous, clear cell, endometrioid, and mucinous tumors, and account for 10% of ovarian cancer related death. These neoplasms believed to arise from endometriosis or borderline serous tumors, are well-differentiated, generally confined to the ovary and exhibit relatively stable genomic profile. They are often mutated in PIK3CA, PTEN, ARID1A, ERBB2, KRAS and BRAF genes (Rojas et al., 2016; Testa et al., 2018),

are relatively indolent and usually diagnosed at an early stage (Kossaï et al., 2018). Type II lesions, that include high-grade serous and endometrioid cancers, undifferentiated carcinomas, malignant mixed mesodermal tumors (carcinosarcomas) and some clear cell carcinomas, principally originate in the Fallopian tube, are diagnosed at an advanced stage, have an aggressive behavior and disseminate rapidly. These tumors exhibit marked genomic instability, widespread DNA copy number abnormalities and recurrent mutation in TP53, RB1, BRCA1, BRCA2 and NF1. In addition, these tumors frequently show altered Homologous Recombination (HR) repair pathway, defective in nearly half of HGSCs (Jayson et al., 2014; Jones & Drapkin, 2013; Kurman & Shih, 2016; Rojas et al., 2016; Testa et al., 2018).

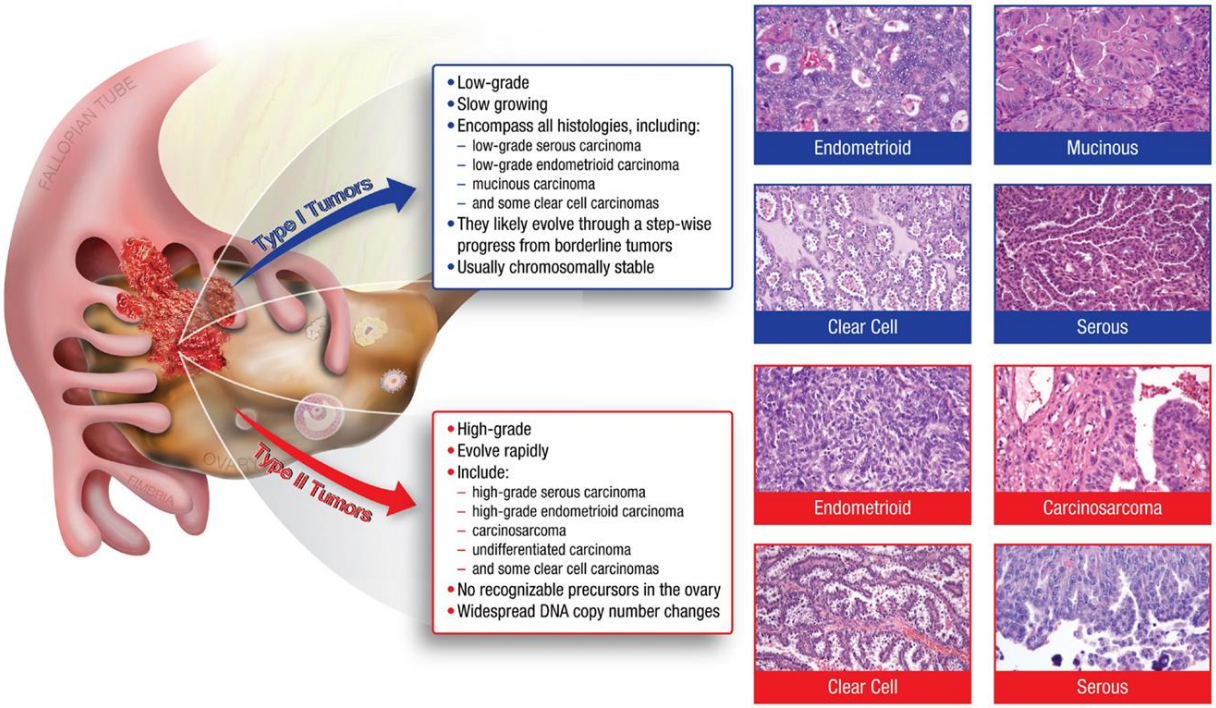


**Figure 1.1. Classification and histopathology of Epithelial Ovarian Cancers.** EOCs are molecularly and morphologically subdivided in two groups: Type I tumors (in blue) comprise low-grade serous, mucinous, endometrioid, and clear cell carcinomas; Type II tumors (in red) include high-grade serous, endometrioid, clear cell carcinomas and carcinosarcoma. The architectural complexity of tissue structures increases from Type I to Type II tumors (Jones & Drapkin, 2013).

### 1.1.1 Current treatment for Epithelial Ovarian Cancer

Despite the classification, all EOC patients are equally treated in first instance with platinum-based and taxane-based combination chemotherapy, including carboplatin and taxol, following cytoreductive surgery, as total hysterectomy, bilateral salpingo-oophorectomy, tumor debulking and omentectomy, that has the purpose to provide a histopathological diagnosis and to establish FIGO stage (Jayson et al., 2014; Reid et al., 2017). The anticancer activity of platinum (i.e. cisplatin and

carboplatin) is exploited by the induction of cross-linking within and between DNA strands, causing single-strand (SS) and double-strand (DS) breaks. Cisplatin particularly reacts with the nucleophilic N7-sites of purine bases, and a double reaction may covalently link purines. Intrastrand adducts are produced when purines are located on the same strand, alternatively, if purines are on opposite strands an interstrand crosslink (ICL) is generated (**Figure 1.2**) (R. Agarwal & Kaye, 2003; Rocha et al., 2018).

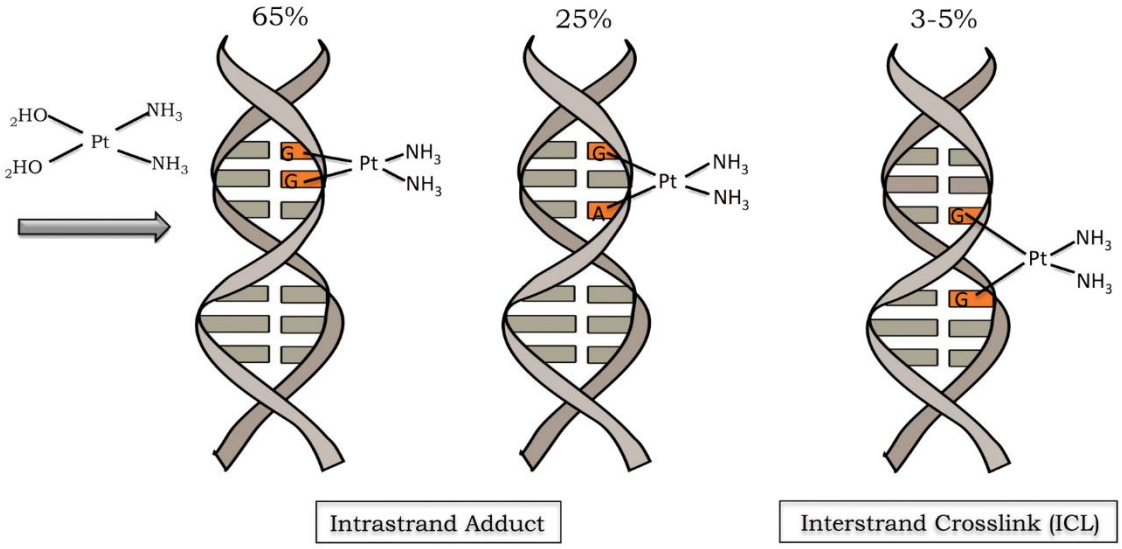


**Figure 1.2. DNA damage induction by cisplatin.** Cisplatin forms covalent bonds with DNA. The major of lesions induced by cisplatin are represented by intrastrand adducts and iterstrand crosslinks (ICL). The percentages represent the frequency of each type of DNA lesions (Rocha et al., 2018).

Platinum-DNA adducts are recognized and removed by specific DNA repair processes, as Nucleotide Excision Repair (NER), MisMatch Repair (MMR) and Homologous Recombination Repair (HRR) systems (R. Agarwal & Kaye, 2003; Van Zyl et al., 2018). In particular, the HRR pathway is involved in the repair of interstrand crosslink, whereas NER and MMR systems participate in the repair of DNA damage caused both by ICL and platinum-intrastrand adducts (Damia & Broggini, 2019).

DNA damage causes cell cycle arrest to allow the repair of the lesions if the damage is limited. When the damage is extended and could not be repaired cells die by apoptosis. Cells with deficient for BRCA1 and BRCA2 genes are not able to use the HRR pathway and, therefore, are highly sensitive to apoptosis triggered by platinum-induced DNA damage. Accordingly, patients with HGSCs due to hereditary BRCA1 or BRCA2 mutation respond well to PT-therapy and present substantially longer survival (Chetrit et al., 2008; Cooke & Brenton, 2011).

The first platinum compound introduced in the clinical practice for the treatment of ovarian cancer is cisplatin. However, because of its dose-limiting toxicity including minor symptoms like nausea and serious injuries on kidney and peripheral neuropathy, it has been replaced by carboplatin, that is

another platinum-analogues with comparable efficacy but less toxicity respect to cisplatin. As already mentioned, platinum compounds are administrated in combination with Paclitaxel, whose mechanism of action consists of binding the intracellular β-tubulin, leading to microtubule stabilization, $G_2$/M cell cycle arrest and apoptosis (R. Agarwal & Kaye, 2003). Paclitaxel and carboplatin are currently recommended by GCIG (The Gynecologic Cancer Inter-Group) as first line chemotherapy in ovarian cancer, administrated intravenously every 3 weeks for six cycles in most of the patients with advanced-stage OC (R. Agarwal & Kaye, 2003; S. Kim et al., 2018). In addition to Paclitaxel, other agents are used in combination with platinum chemotherapy, especially in the relapse setting, including liposomal doxorubicin, gemcitabine, and bevacizumab (Chandra et al., 2019). In the last years platinum-sensitive are also treated with a maintenance therapy with inhibitors of PARP proteins (PARPi) given to patients for up to two-three years after the completion of chemotherapy (Mirza et al., 2020). The use of this highly effective maintenance therapy is based on the concept of synthetic lethality firstly demonstrated in cancer patients for BRCA1/2 mutated tumors (Fong et al., 2009) and then extended to all ovarian cancer exhibiting an HR deficiency (Mirza et al., 2020).

### 1.1.2 Platinum-resistance

Despite the majority of ovarian cancer patients well responds to initial chemotherapy, most of them relapse and develop platinum-resistance (Poveda et al., 2014). Based on the time elapsed between the end of platinum-based treatment and relapse, referred to as platinum-free interval, patients with recurrent OC are subdivided in three groups: refractory, resistant and sensitive. Patients with recurrent disease during or within four weeks following platinum-based chemotherapy are categorized as refractory, within 6 months after the last round of chemotherapy as resistant, and at least 6 months after completion of PT-therapy as sensitive (**Figure 1.3**) (Binju et al., 2019; Oronsky et al., 2017; Van Zyl et al., 2018).

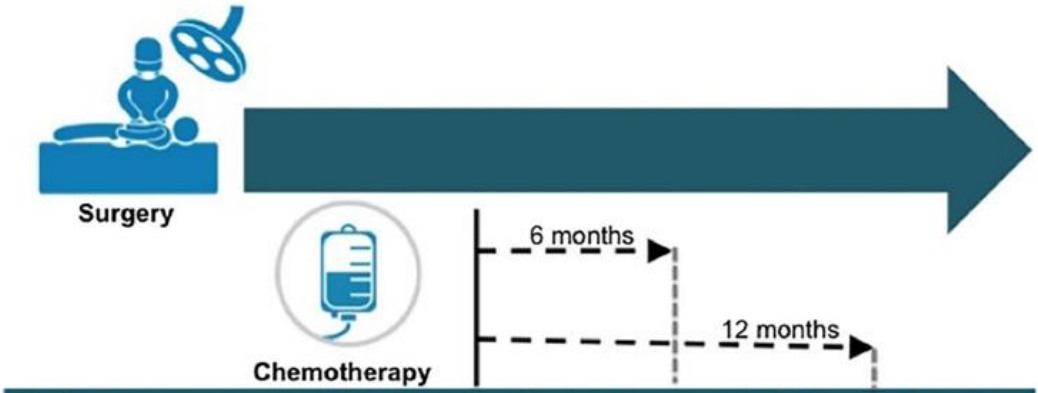


| Platinum sensitivity classification | Refractory | Resistant | Partially sensitive | Sensitive |
|---|---|---|---|---|
| Probability of second platinum response | 0% | <10% | 30% | >50% |

**Figure 1.3. Platinum sensitivity classification.** Based on response to platinum chemotherapy patients are classified as refractory, resistant, partially sensitive or sensitive, according to the time elapsed between the end of first-line treatment and the relapse. Probability of re-treatment response is shown (Oronsky et al., 2017).

It is well established that HGSEOC patients with HRR deficiency, for instance those carrying BRCA mutations accumulate double-strand breaks after platinum chemotherapy, leading to increased apoptosis and higher sensitivity to platinum treatment. Based on the absence of any pre-existing resistant cells within the tumor mass, any residual disease or regrowth, platinum-sensitive patients are typically re-treated with platinum-based chemotherapy, although the persistence of previous therapy side-effects such as neuropathy and pancytopenia, dictate the choice of subsequent treatments (Cooke & Brenton, 2011). As mentioned above platinum-sensitive either in first line or after recurrences, can be treated with PARP inhibitors as maintenance therapy after platinum. Indeed, this class of agents is extremely active in HRR-deficient cells and their activity has been validated in clinical trials in BRCA1/2 mutation carriers with ovarian carcinomas (Damia & Broggini, 2019). The mechanism of action of PARP inhibitors, including Olaparib, Rucaparib and Niraparib, is exploited by base excision repair inhibition and PARP-DNA complexes trapping at the replication fork, leading to synthetic lethality of HRR-defective cells (Konstantinopoulos & Matulonis, 2018). However, restoration of HR repair system by reversion mutations or intragenic deletions in BRCA1 and BRCA2 mutated genes, can lead not only to platinum-resistance but also to PARP-inhibitors acquired resistance development (Van Zyl et al., 2018).

Intrinsic drug resistance assumes that in HGEOC a small population of platinum-resistant cancer cells exists before treatment and emerges once treatment has killed their platinum-sensitive counterpart. These results in re-growth of the tumor and low probability that will respond to further treatment with platinum drugs (Cooke & Brenton, 2011; Holmes, 2015). Approximately the 14% of HGSC patients

(refractory patients) present intrinsic (primary) drug resistance, not responding to initial platinum therapy. Platinum-resistant patients, instead, despite their initial sensitivity to chemotherapy, develop an acquired resistance selected by drug treatment (**Figure 1.4**) (Cooke & Brenton, 2011; Van Zyl et al., 2018). In this case, small populations of cells adapt to prevent death and continue to grow after platinum, repopulating tumor bulk and lead to rapid relapse and resistance to further treatment. For these patients is excluded the possibility to be re-treated with the standard platinum-based chemotherapeutic regimen, thus alternative treatment is needed. Currently, platinum-resistant patients can be subsequently treated with alternative drugs, as liposomal doxorubicin, topotecan, gemcitabine, etoposide and vinorelbine, with an average response rate only about 10-15% and a median progression-free survival of 3-4 months (Lisio et al., 2019; Van Zyl et al., 2018).

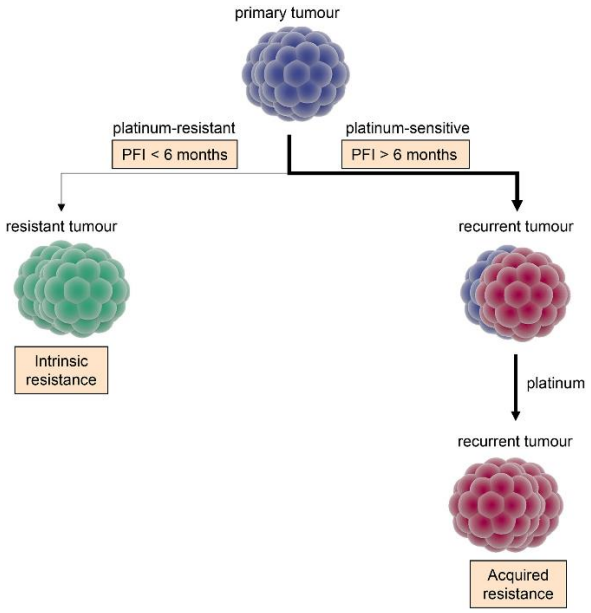


**Figure 1.4. Schematic model of intrinsic and acquired resistance in HGSC.** As indicated by the violet mass, platinum-resistant cells are present in the tumor before treatment and emerged once platinum-base chemotherapy has killed their platinum-sensitive counterpart (Binju et al., 2019).

Different mechanisms are responsible of platinum-resistance, in particular dysfunctional DNA repair and/or tolerance to DNA lesions (Van Zyl et al., 2018). Indeed, the response of a cancer cell to DNA alkalylatin-like agents, as cisplatin and carboplatin, is dictated by its ability to detect and repair DNA damage. For this reason, primary resistance, that occur in 15-25% of HGSC patients, is principally associated with HRR-proficient tumors (Konstantinopoulos & Matulonis, 2018; Van Zyl et al., 2018). About the 50% of HGSCs harbor genetic or epigenetic alterations in Homologous Recombination Repair. Germline and somatic mutations in BRCA1/2 are present in 22,6% and 6-7% of high-grade serous EOCs, respectively. In addition to mutations, BRCA1 can be inactivated via promoter hypermethylation, that is mutually exclusive respect to BRCA1/2 mutations and is recorded approximately

in 10-20% of EOCs (Konstantinopoulos & Matulonis, 2018). As already mentioned, HRR deficiency is determinant for platinum response and is exploited for treatment with PARP (poly-ADP-ribose polymerase) inhibitors. Clinically, HR-deficient (HRD) EOCs patients, exhibit significantly higher response rates and prolonged progression-free survival after platinum treatment, and commonly well respond to platinum treatment in case of recurrent disease. However, the restoration of HRR pathway for instance by a decrease of BRCA1 promoter methylation or by the acquisition of secondary mutation in BRCA1/2 of germline mutation carriers (reversion mutations) that restore BRCA1/2 function, can lead to drug resistance (Freimund et al., 2018).

Among the other biological processes contributing to platinum-resistance, Epithelial Mesenchymal Transition (EMT) emerges. During this process tumor cells switch from an epithelial to a mesenchymal phenotype, determined by the upregulation of transcriptional repressors, such as Snail, Slug, Zeb1/2 and Twist, that leads to loss of epithelial markers (i.e. E-cadherin) and concomitant acquisition of the mesenchymal ones (i.e. Vimentin and N-cadherin) (Schwarzenbach & Gahan, 2019). Typical phenotypic hallmarks of EMT are the loss of cell-cell junctions, loss of apical-basal polarity and acquisition of migratory and/or invasive properties (Haslehurst et al., 2012).

Likewise, the acquisition of epigenetic alterations, as DNA methylation and histones post-translational modifications, has demonstrated to be implicated in drug resistance, because of their role in transcriptional repression of tumor suppressor genes, involved in different biological processes, as apoptosis, cell cycle regulation and DNA repair. Platinum-resistance can be also owed to the presence of Cancer Stem Cells (CSCs), a small subset of cancer cells that indefinitely self-renew, and initiate and maintain tumor growth. Remaining in quiescence for prolonged periods, they are not interested by chemotherapy effects, and for this reason can cause relapsed disease (R. Agarwal & Kaye, 2003; Schwarzenbach & Gahan, 2019; Van Zyl et al., 2018). Other mechanisms contributing to PT-resistance are represented by a decrease drug influx or increase drug efflux, or mutations in membrane transporter proteins. For example, overexpression of the two copper efflux transporters ATP7A and ATP7B, involved in the efflux of platinum drugs, lead to PT-resistance, as well as enhanced expression of ATP-binding cassette (ABC) proteins. Among them, ABCG2 (ATP-binding cassette subfamily G member 2), ABCB1 (or MDR1, multidrug resistance protein 1) and ABCC1 (or MRP1, multidrug resistance associated protein 1) overexpression in tumor tissues is considered a major cause of limited efficacy of anticancer drugs (Spitzwieser et al., 2016; Toh et al., 2017). Similarly, a decreased expression of the copper influx transporter CTR1, has been shown to be involved in PT-resistance, leading to reduced intracellular drug accumulation (Kilari et al., 2016; Samimi et al., 2004; Sonego et al., 2017). Of course all mechanisms able to prevent apoptotic cell death are considered

bona fide mechanisms of PT-resistance. In **Figure 1.5** are shown some of the mechanisms involved in drug resistance discussed above.

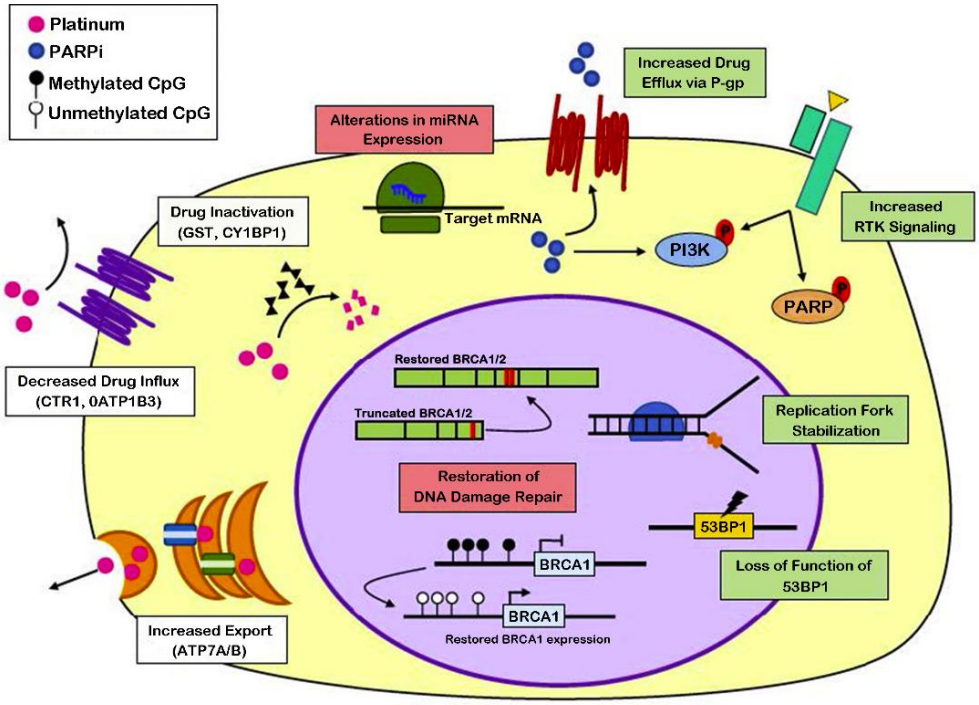


**Figure 1.5. Mechanisms involved in platinum- and PARP inhibitors-resistance of EOC.** Alterations in drug efflux and influx, suppression of apoptosis via 53BP1 loss of function, increased DNA damage repair are some of the potential mechanisms involved in drug resistance of Epithelial Ovarian Cancer (Freimund et al., 2018).

## 1.2 Wnt signaling pathway in Ovarian Cancer

The Wnt signaling is divided into the β-catenin dependent (Canonical) and the β-catenin independent (non-Canonical) pathways. Here we will focus on the Canonical Wnt pathway since it relates to cancer progression and seems to play a relevant role in ovarian cancer (Arend et al., 2013).

The Wnt/β-catenin pathway activation is determined by the binding of WNT molecules to the Frizzled (FZD) family receptors and low-density lipoprotein receptor-related proteins (LRP5/6) on cells surface. Upon receptor-ligand binding, two kinases (CK1 and GSK3β) phosphorylate LRP5/6 and Dishevelled (Dvl) molecules are recruited to the plasma membrane where they interact with FZD proteins. The subsequent interaction of Axin with phosphorylated LRP5/6 and Dvl inactivates the destruction complex of β-catenin, that, therefore, is now able to enter the nucleus. Here β-catenin forms a complex with the transcription factors TCF/LEF, leading to the expression of Wnt target genes (i.e. CCND1, c-Myc) eventually controlling cell proliferation, differentiation and migration. In absence of WNT ligands, β-catenin is recognized and bound by the destruction complex, composed by CK1, Axin, APC and GSK3β. More specifically, GSK3β and CK1 phosphorylate β-catenin, then

ubiquitylated by β-TRCP1 and β-TRCP2 E3 ligases and rapidly degraded by 26S proteasome. Low β-catenin cytoplasmic levels lead the recruitment of the co-repressor Groucho to TCF/LEF transcription factors, preventing the transcriptional activation of target genes (**Figure 1.6**) (Arend et al., 2013; Daugherty & Gottardi, 2007; Katoh, 2017).

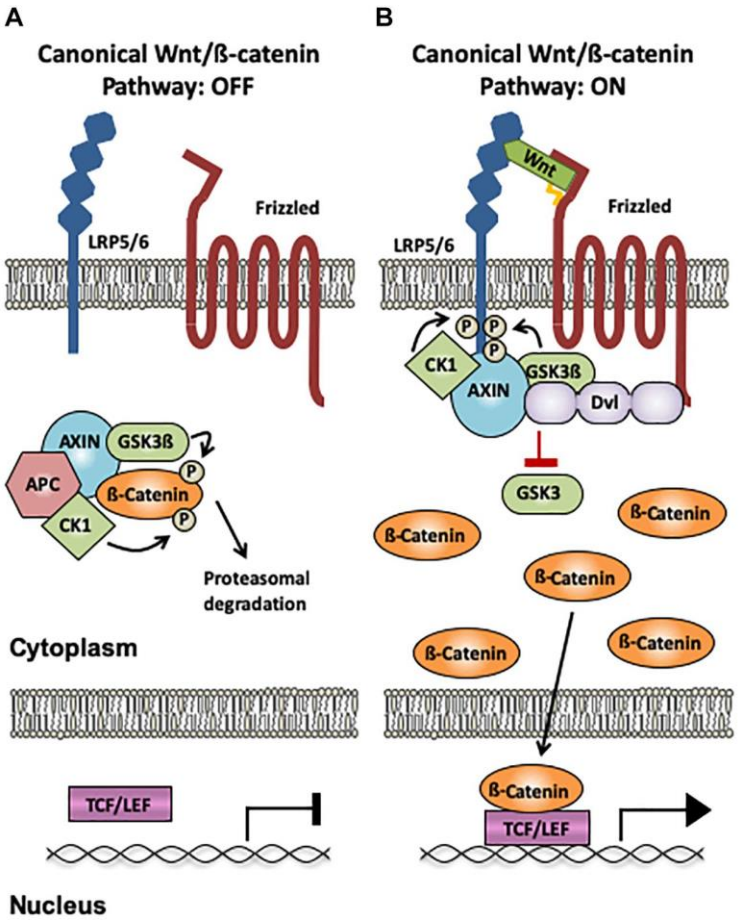


**Figure 1.6. Canonical Wnt signaling pathway. A)** Wnt/β-catenin pathway OFF: in the absence of WNT molecules bound to Frizzled receptors and LRP5/6 co-receptors, β-catenin is recognized and bound by the destruction complex (CK1, GSK3β, Axin and APC), leading to the phosphorylation and subsequent proteasomal degradation of β-catenin. **B)** Wnt/β-catenin pathway ON: after the Wnt ligand binding with FZD and LRP5/6, Dvl recruits Axin, CK1 and GSK3β on the membrane, disrupting the destruction complex. β-catenin is accumulated in the cytoplasm and subsequently enters the nucleus, where it forms a complex with the transcription factors TCF/LEF and activates the Wnt target genes transcription (Palomer et al., 2019).

Dysregulations in Wnt signaling have been described in many cancers, principally due to mutations in β-catenin or other members of the pathway, hypermethylation and silencing of secreted frizzled-related proteins, and overexpression of WNT ligands or receptors, that overall result in increased cancer cell proliferation and migration, and often the development of PT-resistance (Schwarzenbach & Gahan, 2019). It has been demonstrated that Wnt/β-catenin pathway is involved in the carcinogenesis of all ovarian cancer subtypes, and its target genes are subdivided in two groups: stemness/proliferation and EMT/dissemination genes, which are active early in tumor progression and expressed

in late stage tumors, respectively. As already stated, EMT has been reported to be associated with chemoresistance, and the major pathways involved in this process include the Wnt/β-catenin pathway (Arend et al., 2013).

## 1.3 Epigenetics of Ovarian Cancer

Cancer can be considered a genetic disease, in which DNA alterations have profound and ubiquitous roles. Yet, genome-wide alterations in DNA methylation, chromatin structures and regulatory element activities are also frequent event in malignant cells (Flavahan et al., 2017). Epigenetic mechanisms allow genetically identical cells to reach different stable phenotypes by modifying various parts of the genome through differential chromatin marking and packaging. These modifications can directly affect the DNA, as cytosine-phosphate-guanine (CpG) dinucleotide sequences methylation, hydroxylation, formylation and carboxylation, but can also involve nucleosome positioning and alterations (H. Shen & Laird, 2013). The main component of nucleosome is the histone, around which is wrapped a 147bp segment of DNA. Each histone has a side (NH2-terminal) tail rich in basic lysine and arginine residues, that is often interested by extensive post-transcriptional chemical modifications (PTMs), including methylation, acetylation, phosphorylation and ubiquitylation (**Figure 1.7**), affecting gene transcription, replication and DNA repair processes by influencing chromatin compaction or signaling to other proteins (E. L. Greer, 2002; Marsh et al., 2014). It is well accepted that PTMs of histones mediate a variety of critical biological processes, generally via chromatin modification that lead to target genes expression or silencing (Audia & Campbell, 2016). Epigenetic modifications, that have been proven to play an important role in carcinogenesis, tumor growth, and progression (Flavahan et al., 2017), correlate with different gene expression patterns and changes in cell plasticity during tumorigenesis, and could lead to short- or long-term alterations in the activity of anticancer treatments, for instance the development of acquired resistance to chemotherapy (Brown et al., 2014; Ivanov et al., 2014).

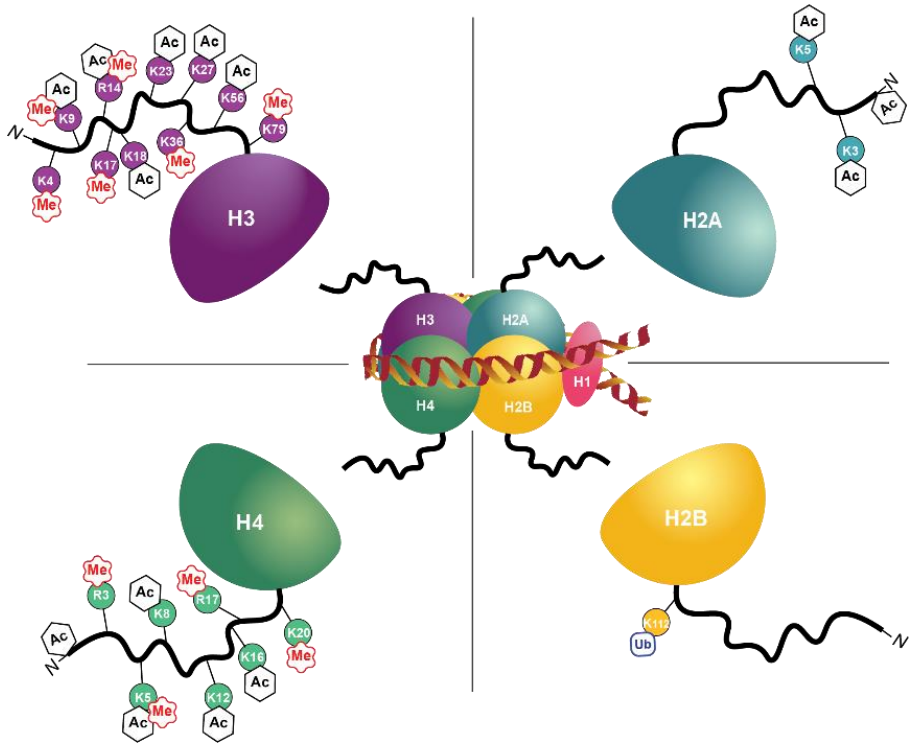


**Figure 1.7. Schematic drawing of a nucleosome with the four canonical histones (H3, H4, H2A, and H2B).** The covalent PTMs of the histone tails are shown. (Me = methylation, Ac = acetylation, Ub = ubiquitylation, K = lysine, R = arginine).

### 1.3.1 DNA methylation

Among the epigenetic modifications, DNA methylation is the most studied and best understood, representing a frequent event in cells continuously exposed to cisplatin (Kouzarides, 2007; D. W. Shen et al., 2012; Smith et al., 2017). Early evidences suggest that this type of epigenetic modification can be useful for the detection of acquired resistant changes linked to clinical outcome (Brown et al., 2014). DNA methylation, known to be involved into the regulation of gene expression, usually occurs at the carbon-5 position of cytosine residues of CpG dinucleotide sequences, causing the inhibition of gene transcription (Ivanov et al., 2014; Smith et al., 2017). Several evidences support that CpG islands cover the transcription start sites of about half of human genes either actively expressed or poised for transcription (H. Shen & Laird, 2013). The enzymes responsible of this type of modification belong to the DNA methyltransferases (DNMTs) protein family (DNMT1, DNMT3a and DNMT3b), able to transfer a methyl group (CH3) from S-adenosylmethionine to cysteines in CG sequences, and upregulated in cancer cells compared to normal cells (Schwarzenbach & Gahan, 2019). Indeed, 5–10% of CpG islands resulted abnormally methylated in cancer genomes, leading to the silencing or preventing re-activation of multiple tumor suppressor genes, as well as other genes involved in regulation of cell growth, angiogenesis, and DNA repair (Dawson & Kouzarides, 2012;

Flavahan et al., 2017). Moreover, in a range of tumor cell line models, CpG promoter islands hypermethylation has been shown to be the cause of acquired resistance to cytotoxic chemotherapy drugs (Brown et al., 2014; Nogales et al., 2016), by inactivating genes required for drug response (D. W. Shen et al., 2012). A series of genes have been found hypermethylated in ovarian cancer, and the degree of abnormal methylation correlates with disease progression and decreased survival. As already stated, the 15-35% of patients with sporadic ovarian cancer exhibit BRCA1 promoter hypermethylation, that results in decreased BRCA1 protein expression and thus failure in DNA damage repair with accumulation of mutations (Koukoura et al., 2014). Hypermethylation contributes to silencing multiple other tumor suppressor genes in ovarian cancer, including p53, leading to decreased DNA damage response and activation of the apoptotic pathway, and E-cadherin, contributing to the epithelial-mesenchymal transition, invasion and metastasis (Sharma et al., 2019; Smith et al., 2017). Epigenetic changes have been described also in genes encoding drug transporters, as ABC efflux proteins, resulting in altered expression that contributes to drug resistance (D. W. Shen et al., 2012). However, several studies demonstrate that tumor treatment with DNA methyltransferases (DNMTs) inhibitors can cause a global DNA hypomethylating activity, allowing the ra-activation of those genes linked to chemotherapy response (Fang et al., 2014).

### 1.3.2 Histone modifications

Among the epigenetic modifications involved in ovarian carcinogenesis, histones post-translational alterations play a central role. As already stated, these changes in the NH2-terminal tails of histones can result in chromatin remodeling and thus modification of genes expression. The type and the degree, as well as the type of residue interested by epigenetic modification, regulate gene transcription activation or repression (Schwarzenbach & Gahan, 2019; Sharma et al., 2019; Smith et al., 2017; Yang et al., 2018). PTMs of histones are carried out by a group of histone modification enzymes, which generally act in complexes, and include histone acetyltransferases (HATs)/deacetylases (HDACs), histone methyltransferases (HMTs)/demethylases (KDMs), and writers and erasers of phosphorylation, as well as many other modifications (Chi et al., 2010).

#### 1.3.2.1 Acetylation and deacetylation of histones

Histone acetylation is an epigenetic process by which lysine's positive charge is neutralized, leading to weakening histones-DNA electrostatic interactions. For this reason, histone acetylation is commonly associated with euchromatin, an open and transcriptional permissive conformation of chromatin (Dawson & Kouzarides, 2012). Histone acetylation is regulated by the competing activities of two

enzymatic families: the histone lysine acetyltransferases (HATs) and the histone deacetylases (HDACs), which, respectively, add and remove the acetyl groups on lysine residues of histone tails, resulting in a less or more accessible chromatin to transcriptional factors, and thus regulating gene expression (Smith et al., 2017; Yang et al., 2018). Therefore, the imbalanced expression of HATs and HDACs is associated to aberrant genes expression and thus carcinogenesis. Unlike HATs, which are downregulated in ovarian cancer, HDACs result overexpressed, also in a series of other cancers, and have a central role in promoting cell proliferation and migration, as well as in tumor progression and platinum-resistance development (Sharma et al., 2019; Smith et al., 2017).

### 1.3.2.2 Methylation and demethylation of histones

Histone methylation is a reversible epigenetic modification, thanks to the combined action of methyl-transferases (HMTs) and demethylases (HDMTs) that, respectively, catalyze methyl group addition and removal from different histone residues (E. L. Greer, 2002). This type of modification occurs on all histone basic residues: on arginines, mono- or di-methylated on their guanidinyl group; on lysines, mono-, di- or tri-methylated on their ε-amine group; and on histidines, rarely, as mono-methylation (E. L. Greer, 2002). Depending on the particular residue methylated, the degree of methylation and the site of the methylated histone within a specific gene locus, histone methylation involves either transcriptional activation or gene silencing (Yang et al., 2018).

Among the best studied histone lysine methylation sites are H3K4, H3K9, H3K27, H3K36, H3K79 and H4K20. Different lysine methylation markers have specific role in terms of chromatin accessibility, therefore, of genes expression regulation. For example, H3K4, H3K36 and H3K79 methylations are preferentially associated with euchromatin and gene activation, instead, methylation on H3K9, H3K27 and H4K20 leads to heterochromatin structure and gene silencing. However, the final effect on chromatin structure and gene expression is often due to the combination of multiple histone modifications, called “histone crosstalk” (Morera et al., 2016). As already mentioned, the state of histone methylation is maintained by a balance between HMTs and HDMTs. Therefore, imbalance between these two enzyme families leads to aberrant gene expression and thus carcinogenesis (Yang et al., 2018). Ovarian cancer is characterized by HMTs overexpression, that lead to an aberrant silencing of tumor suppressor genes, as well as an aberrant HMDTs upregulation (Flavahan et al., 2017; Yang et al., 2018).

As already described for DNA methylation, also histone methylation is involved in acquired resistance to cytotoxic chemotherapy drugs. As previously stated, the aberrant promoter methylation of ATP-binding cassette (ABC) family of drug efflux transporters coding genes has been associated with drug resistance in cancer stem cells (Toh et al., 2017). However, their expression is affected not only

by CpG island methylation, but also by histone modifications. In particular, ABCG2, known to confer resistance to cancer cells to a variety of anticancer drugs (To et al., 2008), results overexpressed when permissive histone modifications, as H3 acetylation, increased H3K4 tri-methylation, H3S10 phosphorylation and decreased H3K9 tri-methylation, occur. In this context, chromatin remodeling proteins and RNA polymerase II are able to access the DNA and activate ABCG2 transcription, contributing to an increased drug efflux capacity of cancer cells and a reduced chemotherapy sensitivity (Toh et al., 2017).

Numerous studies support that, among histone modification enzymes, the H3K27-methyltransferase EZH2 is upregulated in many carcinomas, playing a role in drug resistance through gene silencing and chromatin remodeling (Yang et al., 2018). Has been demonstrated that the decrease in H3K27 methylation following loss of EZH2 alters the expression of specific cisplatin resistance-related genes in platinum-resistant ovarian cancer cells, as RASSF1A, MLH1 and CYT19, resulting in increased drug accessibility and re-sensitization to cisplatin. Moreover, downregulated H3K27 methylation by EZH2 depletion leads to the inhibition of ovarian cancer tumor xenografts growth (Hu et al., 2010).

## 1.4 G9a/GLP Histone lysine methyltransferases

It is worth noting that histone lysine methylation is, at the same time, a marker of active and inactive transcription status, depending on the lysine residue that is methylated and the degree of methylation (me1, me2 or me3) (Mozzetta et al., 2014). Lysine methylation is commonly controlled by a family of proteins that contains the so called SET-domain (Su(var)3-9, Enhancer-of-zeste and Trithorax) and that includes, among the others, the G9a and G9a-like protein (GLP) histone lysine methyltransferases (HKMTs) (Stein et al., 2014; H. Zhang et al., 2014). G9a (also known as EHMT2 or KMT1C) and GLP (also known as EHMT1 or KMT1D) are the major H3K9 methyltransferases able to catalyze the majority mono- and di-methylation of Lysine 9 in Histone H3 (H3K9me1/H3K9me2) in most of mammalian cell type, and have been found to play a central role in many biological processes associated with gene regulation (Krishnan et al., 2011; Poulard et al., 2017). Even though G9a and GLP can form homodimers, they predominantly exist in human cells as heteromeric complex, that is stabilized by the interaction with Wiz (a multi-zinc finger-containing molecule) and is required for G9a-GLP methyltransferase activity on H3K9 *in vivo* (Casciello et al., 2015; Shinkai & Tachibana, 2011).

### 1.4.1 G9a/GLP structure and activity

Two isoforms of the human G9a protein are known: the full length G9a (isoform a), a product of both G9a (24 exons) and NG36 (4 exons) transcripts, and the shorter one (isoform b), which lacks exon 10 (**Figure 1.8**). GLP, the closely G9a related paralog, displays 45% identity with G9a and differs

principally for the N-terminus (Shankar et al., 2013). As previously described, G9a belongs to the family of S-adenosylmethionine (AdoMet)-dependent enzymes, containing the catalytic SET domain at the C-terminus, which contributes to its methyltransferase activity, flanked by a pre- and a post-SET regions. Moreover, the protein has an ankyrin repeats region (ANK), involved in protein-protein interaction, and nuclear localization signals (NLS) at N-terminus (Estève et al., 2005). The SET domain is necessary for the substrate binding groves by the interaction with the post-SET region, and for the interaction with GLP in the heteromeric complex assembly (**Figure 1.8**).

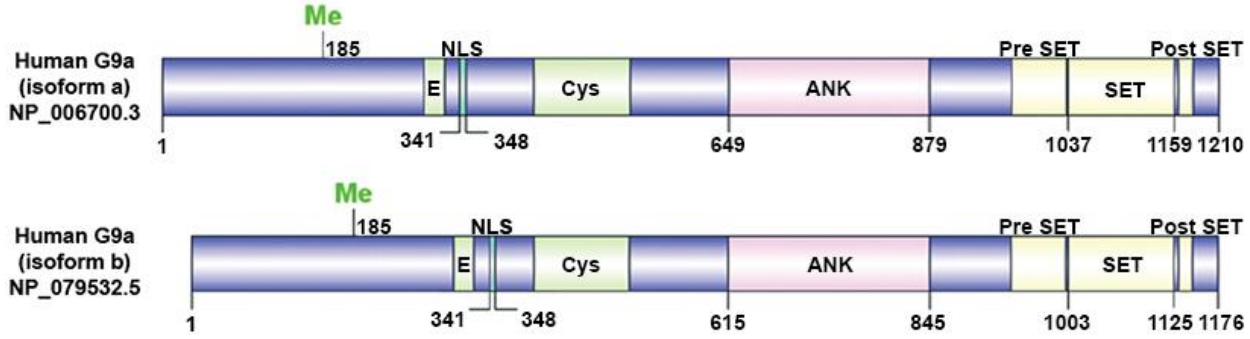


**Figure 1.8. Schematic representation of human G9a protein structure.** Human full-length G9a (isoform a) and short length G9a (isoform b) are shown with their respective NCBI accession ID (left). The Cysteine (Cys) rich region, ankyrin repeats (ANK), the catalytic SET domain with flanking Pre-SET and Post-SET regions, the site for methylation (Me), nuclear localization signal (NLS) and the glutamic acid (E) rich region are denoted. Numbers indicate amino acid residues (Shankar et al., 2013).

H3K9 mono- and di-methylation by G9a activity, result from the transfer of methyl groups (CH3) from S-adenosyl-l-methionine (SAM) to ε-amino group of the Lysine 9 in Histone H3 and leads to gene silencing. G9a Y1154 and Y1067 tyrosine residues are of particular importance for catalytic activity and H3K9 methylation. In particular, Y1067 replacement to phenylalanine allows G9a to tri-methylate its target (H3K9me3) (Shankar et al., 2013). In addition, G9a/GLP methylate also non-histone substrates, like GLP, Wiz, CDYL1, Reptin, CSB, HDAC1, DNMT1 and KLF12. Furthermore, G9A methylates Lys373 within the regulatory domain of transcription factor p53, resulting in the inhibition of its tumor-suppressor activity. However, the biological significance of non-histone lysine methylation currently is not completely understood. Furthermore, G9a itself presents a motif at its N-terminus which is automethylated. Auto-methylation of the enzyme does not affect its catalytic activity, and has been reported to be necessary for the interaction with HP1, by which other repressors, such as HDAC1 and DNMT1, are recruited on chromatin (Collins & Cheng, 2010; Shankar et al., 2013; Vedadi et al., 2011). Interestingly, G9a positively correlates with DNA methylation, resulting implicated in DNA CpG methylation of silencing genes by directly interacting with

DNA methyltransferases DNMT1 and DNMT3 (Krishnan et al., 2011; Xiaodong Cheng and Robert M. Blumenthal, 2010).

### 1.4.2 Role of G9a/GLP complex in Ovarian Cancer

Examination of the Oncomine database and the recent literature show that G9a is overexpressed in a number of cancers, including ovarian carcinoma, in which the high expression of G9a correlates with poor prognosis, suggesting that it is a putative oncogene in this context and that the analysis of its expression may represents a novel prognostic/predictive marker (Casciello et al., 2015; Hua et al., 2014a). Some *in vitro* studies on highly invasive ovarian cancer cells (ES-2, OVCAR-3, OV-90, SKOV-3 and TOV-21G), demonstrated a higher protein levels of G9a compared to poorly aggressive tumor cells. Moreover, a higher expression of G9a was observed in metastatic lesions of ovarian cancer xenografts respect to the primary tumors (Casciello et al., 2015). Accordingly, ovarian cancer cells knockout for G9a showed decreased pro-metastatic ability in mice, confirming a linkage between the methyltransferase and the metastatic process (Hua et al., 2014a). Increased G9a activity and concomitant increase in global H3K9 di-methylation levels have been observed in mammalian cells under hypoxic conditions, which represent an important factor in the development of metastasis of solid tumors. Furthermore, the acquisition of cell motility under hypoxic conditions has been connected to a decreased expression of cell adhesion molecules (Casciello et al., 2015; Ke et al., 2014). In this context, G9a inhibits the expression of cell adhesion factors such as E-cadherin, promoting the Epithelial-mesenchymal transition. This provides evidence for a critical role of G9a as a factor that enhances survival, proliferation, and metastasis of malignant cells, by regulating the expression of genes involved in the metastatic dissemination and the EMT (Casciello et al., 2015).
Interestingly, it has been recently proposed that G9a/GLP heterodimeric complex could also participate in the response to DNA damage, directly linking their expression with the response to chemotherapy. Indeed, it has been observed that decreased expression of G9a/GLP impairs cancer cells ability to repair the damage, eventually enhancing the sensitivity of cancer cells to both radiation and chemotherapeutic drugs such as cisplatin or doxorubicin (P. Agarwal & Jackson, 2016; Ginjala et al., 2017). Overall, these findings highlight the oncogenic potential of G9a and GLP, rendering these enzymes potential targets for novel chemotherapeutic drugs (Krishnan et al., 2011).

### 1.4.3 G9a/GLP inhibitors

Given the involvement of G9a/GLP complex in the initiation and progression of solid tumors, in the recent past has been hypothesized that targeting G9a could promote the re-expression of tumor

suppressor genes, reduce metastasis and inhibit cancer cell proliferation (Casciello et al., 2015). Two classes of G9a/GLP inhibitors have been developed through structure-based design: SAM competitive and substrate competitive inhibitors. Among the first class of compounds, chaetocin was the first developed, with a broad range of activity against HKMTs belonging to SUV-39 family (Shinkai & Tachibana, 2011). However, substrate competitive inhibitors resulted have a better selectivity than SAM inhibitors against G9a (Cao et al., 2019). The first competitive inhibitor of the N-terminal peptides of Histone H3 produced was BIX01294, showing high specificity against G9a/GLP (Krishnan et al., 2011). Nonetheless, BIX01294 causes high toxicity in cells, limiting its usefulness as a G9a/GLP chemical probe (Vedadi et al., 2011). Thus, more potent and less toxic inhibitors have been developed by further modifications of BIX01294, such as UNC0224 and UNC0321. Both these compounds displayed higher binding affinity for G9a compared to the previous molecule, but their low lipophilicity limit their effects (Cao et al., 2019). Thus, to improve the ratio of toxicity to functional potency of G9a inhibitors, UNC0638, UNC0631, UNC0642 and UNC0646 were developed. In particular, UNC0631 exhibits a good toxicity/function ratio and has an excellent cell permeability, as well as UNC0638. UNC0642 not only exhibits high potency and selectivity, but has also excellent *in vivo* pharmacokinetic properties, which makes it an excellent candidate in animal model experiments (Cao et al., 2019; Casciello et al., 2015; Vedadi et al., 2011).

G9a activity turned out fundamental for the malignant phenotype maintenance in several cancer types, thus modulating the expression of genes methylated by G9a could represent a good treatment strategy for ovarian cancer, by using G9a inhibitors alone or in combination with other standard-of care therapies currently used in the clinic. In fact, the inhibition of histones methylation leads to a decrease of chromatin condensation, allowing the platinum-compounds a greater access to DNA, and thus, re-sensitizing PT-resistant cells to chemotherapy (Casciello et al., 2015; Smith et al., 2017; Van Zyl et al., 2018).

# 2. AIM OF THE STUDY

In the last few years, increasing attention has been given to epigenetic alterations in cancer research. These alterations have been observed early during cell transformation and are thought to play a role in cancer onset, progression and response to therapies. Recently has been proposed that epigenetic changes are implicated in acquired resistance to chemotherapy and that they play a central role in ovarian carcinomas progression. Accumulating clinical evidences suggest that the combination treatment of targeted therapy and standard chemotherapy could significantly improve the disease free survival and the quality of cancer patients, including EOC patients, with implications for the design of new clinical intervention strategies aiming at preventing the emergence of drug resistance. In this context, aberrant epigenetic changes emerge as possible new therapeutic target in countering drug resistance, since they can be readily reversed by targeting epigenetic maintenance enzymes with new class small-molecules, generally referred as Epigenetic Modifying Drugs (EMDs).

In this PhD project, using our isogenic PT-Resistant EOC cells as a model, we aim to study the role of EMDs as novel therapeutic targets to treat PT-Resistant EOC and in particular we will focus on the anticancer role of G9a/GLP histone methyltransferases (HMTs) inhibitors. G9a/GLP HMTs are principally involved in H3K9 methylation and are able to catalyze the majority mono- and di-methylation of H3K9 in the cell. G9a/GLP inhibitors have been selected using an unbiased EMD screening on a large number of cells where they resulted the most active EMDs in killing isogenic PT-Resistant EOC cells. Therefore, we aim to dissect the role of G9a/GLP inhibitors in mediating EOC response to PT and to characterize the molecular mechanisms underling their activity in EOC. Finally, we will use a genetic approach to confirm that the effects observed with the inhibitors were effectively due to G9a/GLP inhibition.

Overall, we hope to demonstrate that targeting these HMTs with specific inhibitors is a pursuable anticancer strategy to improve low survival of patients with PT-resistant diseases.

# 3. MATERIALS AND METHODS

## 3.1 Cell lines

MDAH-2774 (CRL-10303), TOV-112D (CRL-11731), OVCAR-8 (NCI 60-0507712), TOV-21G (CRL-11730), ES-2 (CRL-1978) cells were from ATTC, OVSAHO (JCRB-1046) cells were from JCRB Cell Bank, and ID8 CRISPR/Cas9-modified mouse epithelial ovarian cells were a gift of Dr I. McNeish (Hammersmith Hospital, London). All human cell lines were maintained in RPMI-1640 medium (Sigma-Aldrich Co.) supplemented with 10% heat-inactivated FBS, 100 µg/ml penicillin and streptomycin (complete medium) at 37 °C in 5% $CO_2$ atmosphere. ID8 cells were maintained in DMEM medium supplemented with 4% fetal calf serum, 100 µg/ml penicillin and streptomycin, 5 µg/ml insulin and transferrin, and 5 ng/ml sodium selenite, at 37 °C in 5% $CO_2$ atmosphere. The subsequent drug treatment was administrated when the cells reached again a 70-80% of confluence. 293FT cells (Invitrogen Inc.), used for lentivirus production, were grown in DMEM supplemented with 10% heat-inactivated FBS (Sigma-Aldrich Co.).

## 3.2 Reagents

Cisplatin (CDDP) (TEVA Italia), Paclitaxel (TAXOL®) (ACTAVIS Dublin, Ireland), and Doxorubicin (Ebewe Italia) were used for *in vitro* experiments. Carboplatin (CBDCA) (TEVA Italia) was used for *in vivo* experiments. Epigenetics Screening Library (11076) was purchased from Cayman Chemical. G9a/GLP specific inhibitors were purchased from Cayman Chemical (UNC0631 -11084, UNC0638 -10734, UNC0642 -14604) and resuspended in DMSO. The WNT pathway inhibitors WNT-C59 and XAV-939 were purchased from Selleckchem. Recombinant Human Wnt-3a (5036-WN-010) was purchased from R&D Systems.

## 3.3 Epigenetic screening

The timeline of the epigenetic screening has been structured as follow. On day 1, $9x10^3$ OVSAHO cells/well, $8x10^3$ TOV-112D PT-Sensitive (parental) cells/well, $7x10^3$ TOV-112D PT-Resistant (PT-Res) cells/well, $4x10^3$ MDAH-2774 parental cells/well, $7x10^3$ MDAH-2774 PT-Res cells/well, $4x10^3$ ES-2 parental cells/well and $6x10^3$ ES-2 PT-Res cells/well were seeded in 96-well plates using a robotic liquid handling Hamilton's MICROLAB STARlet. On day 2 cells were treated with the Epigenetic Screening Library (Cayman Chemical) for 72 hours at the final concentration of 5 µM. Cell viability was evaluated at the end of the treatment using CellTiter 96® AQuesous cell proliferation assay kit (Promega). The screening was performed three times on each cell line and statistical analysis was conducted. Compounds that presented synthetic lethality were ranked using a moderated *t-test* statistic. The 75% of cell viability was selected as limit for a compound to be considered active.

## 3.4 Lentiviral production and transduction

EHMT1/EHMT2-knockout OVSAHO cells were generated by lentiviral transduction. Briefly, 293FT cells were co-transfected, using a calcium phosphate precipitation, with the gRNA-SpCas9(BB)-2A-GFP plasmid together with ViraPower Packaging Mix (PAX2 and pLP/VSV-G) (Invitrogen, Thermo Fisher Scientific, Eugene, OR, USA). The lentiviral particles were collected from the culture medium of these cells after 48h and 72h to transduce OVSAHO cells.

## 3.5 FACS analysis

For the production of OVSAHO PT-Res EHMT1/EHMT2 knockout, cells were plated in 100 mm dish and transduced with the transfected-239FT medium. OVSAHO cells were then collected 72 hours post transduction and fixed in ice-cold 70% ethanol, washed twice in PBS 1x and resuspended in propiudium iodide (50 μg /ml supplemented with 100 μg/ml RNase A in PBS 1x). Stained cells were subjected to FACS analyses with FACScan instrument (BD Biosciences), and GFP-positive cells were sorted and pooled together.

## 3.6 Cell viability assay

Parental and PT-Res OVSAHO, TOV-112D, MDAH-2774 and ES-2 cells were seeded in 96-well culture plates (as described in 3.3) and after 24 hours treated with increases doses of CDDP, UNC0631, UNC0638 or UNC0642 for 72 hours. Cell viability was evaluated at the end of the treatment using the CellTiter96 AQueous cell proliferation assay kit (Promega). Same schedule of treatment was used for WNT-C59 and XAV-939 in OVSAHO cells and for ID8 cells treatment with increases doses of CDDP and UNC0631, by plating $2{,}5x10^3$ $PTEN^{KO}$ cells/well, $4X10^3$ $TP53^{KO}$ cells/well, $4X10^3$ $TP53^{KO}$+$BRCA2^{KO}$ cells/well, and $5X10^3$ $BRCA1^{KO}$ cells /well.

In viability assays using CDDP and UNC0631 combined treatment, EOC cells were seeded in 96-well culture plates, the they after were treated for 48 hours with cisplatin and then released for 24 hours with UNC0631 (± 0,1 μg/μl of recombinant Wnt3a) in cisplatin-free medium, otherwise were treated with UNC0631 for 24 hours and then released for 48 hours with CDDP. Cell viability was determined at the end of treatments using the CellTiter96 AQueous cell proliferation assay kit (Promega).

In viability assays using CDDP and doxorubicin/taxol combined treatment cells were seeded in 96-well culture plates, after 24 hours were treated with CDDP for 48 hours and then released in cisplatin-free medium, otherwise were treated with doxorubicin or taxol for 24 hours. Cell viability was determined at the end of treatments using the CellTiter96 AQueous cell proliferation assay kit (Promega).

In viability assay using CDDP and XAV-939 combined treatments OVSAHO cells were plated in 96-well culture plates, after 24 hours two types of treatment were performed: 1. Cells were treated with increasing doses of XAV-939 (0,1 – 5 – 10 μM) for 24 hours and then released in drug-free medium or treated with CDDP (2 μM) for 48 hours. 2. Cells were treated with CDDP (2 μM) for 48 hours and then released in cisplatin-free medium or treated with increasing doses of XAV-939 (0,1 – 5 – 10 μM) for 24 hours. In all cases cell viability was determined at the end of the treatment using the CellTiter96 AQueous cell proliferation assay kit (Promega).

## 3.7 Luciferase assay

OVSHAO parental cells were seeded in 24-well plate and co-transfected with 1 μg of TOPFlash reporter construct, containing multiple copies of the optimal TCF motif (GATCAAAGG), and 50 ng of pRL-TK vector (Renilla), as internal control for transfection efficiency. The transfection was carried out with FuGENE® HD Transfection Reagent (Promega) in 24-well plates with $35x10^3$ cells/well, plated 24 hours earlier, according to manufacturer's recommendations. After 16 hours cultured medium was changed and at 48 hours after transfection cells were treated with cisplatin and/or UNC0631. At the end of treatments lysates were assayed for luciferase activity using the Dual-Luciferase reporter assay system (Promega). The ratio of expression from TOPFlash to expression from Renilla provided a measurement of Canonical Wnt-specific transcriptional activity.

## 3.8 Three-dimensional ovarian epithelial cell cultures

Three-dimensional culture was performed as described in (Debnath et al., 2003; Segatto et al., 2014). Briefly, OVSHAO parental and PT-Res cells ($10x10^3$ cells) were embedded as single cells in matrigel (Cultrex®, BME), mixed with the appropriate medium and layered on the top of a bottom layer of polymerized matrix (GFR-BME, 8.5mg/ml) (Trevigen). Embedded cells were incubated at 37°C for 3 days, and cisplatin and/or UNC0631 treatments were performed, by adding the drug and/or the inhibitor directly into the cell culture media. PT-Res cells were treated for 72 hours, whereas parental treatment was stopped at 48 hours. At the end point, number of spheres formed was count and images were collected to calculate sphere areas, using ImageJ software. Next, cleaved caspase 3 was analyzed following immunofluorescence staining.

## 3.9 Immunofluorescence

For immunofluorescence (IF) on cultured cells, cells were plated on coverslips and fixed in PBS 4% paraformaldehyde (PFA) at room temperature, blocked in PBS-1% bovine serum albumin (BSA), and permeabilized in PBS 0.2% Triton X-100. Stains were permeabilized with primary antibodies:

cleaved caspase 3 (1:300, Cell signaling), γH2Ax (S139) (1:200, Merk Millipore), occludin (1:200, Invitrogen), p-120-catenin (1:200, BD Biosciences), β-catenin (1:200, Cell signaling), β-catenin (1:200 BD Biosciences), E-cadherin (1:50, BD Biosciences), Zo-1 (1:50, Cell Signaling), γ-catenin (1:100, Bd Biosciences). Then samples were washed in PBS and incubated with secondary antibodies (Alexa-Fluor 488- or 568-conjugated anti-mouse or anti-rabbit antibodies, Invitrogen) for 1 hour at room temperature. TO-PRO-3 iodide (Invitrogen) was used to visualize nuclei and Alexa-Fluor 647-Phalloidin (Invitrogen) for F-actin staining. Coverslips were analyzed using the TCS-SP8 Confocal Systems (Leica Microsystems Heidelberg GmbH, Wetzlar, Germany) interfaced with the Leica Confocal Software (LCS) (version 3.5.5.19976, Wetzlar, Germany) or the Leica Application Suite (LAS) software (version 6.1.1, Wetzlar, Germany). At least 8 fields were scored for each cell population and experimental condition. Fluorescence intensity and protein localization were studied using the Volocity® software (PerkinElmer).

IF analyses on OVSHAO cells grown in three-dimensional culture was performed as described (Debnath et al., 2003; Segatto et al., 2019). Briefly, incubation with cleaved caspase 3 (1:50, Cell Signalin) primary antibody was performed over/night at 4°C, followed by 1 hour at room temperature with secondary antibody (AlexaFluor® 488-, 546-, 568- or 633-conjugated, Invitrogen). Nuclei were counterstained using TO-PRO-3 (Invitrogen) for 30 min at room temperature. Finally, samples were analyzed as above.

## 3.10 Evasion assay

Evasion assay was performed as previously described (Sonego et al., 2019). Briefly, $7{,}5x10^3$ OVSAHO parental, G9a/GLP$^{WT}$ and G9a/GLP$^{KO}$ cells were included in matrigel (Cultrex®, BME) drops (12 µl of matrix volume per drop) at a final concentration of 8 mg/ml. Matrigel was diluted in RPMI 1640 and 0.1% BSA. Drops were dispensed in cell culture dishes and incubated for 1 hour at 37 °C upside down to jellify. Next, dishes were turned up and drops were incubated in complete medium. Images were collected using a stereo microscope Leica M205FA and the evasion ability was evaluated 10 days after inclusion by measuring the distance covered by cells exiting from drops, using ImageJ software.

## 3.11 Permeability assay

OVSAHO parental ($18x10^4$ cells/transwell), G9a/GLP$^{WT}$ ($15x10^4$ cells/transwell) and G9a/GLP$^{KO}$ ($18x10^4$ cells/transwell) have been seeded, in triplicates, on top of transwell filtersin 24-well dishes and grown for 24 hours until they had reached confluence, with 500 µl of complete medium in the upper chamber, and 500 µl in the well's bottom. Then, cells were treated with cisplatin (15 µM) for

16 hours. At the end of treatment, FITC-Dextran 70 kD (1:100) was added on the top of the monolayer and the concentration of the compound at the well's bottom was measured by means of TECAN Infinity 200 PRO instrument detecting the fluorescence at 535 nm. Measurement of FITC-Dextran was performed twice, immediately after the addition of the compound (T0) and 20 minutes later (T1).

## 3.12 Scratch test and cell migration assay

OVSAHO parental, G9a/GLP$^{WT}$ and G9a/GLP$^{KO}$ cells ($18x10^4$ cell/well) were plated in 6-well plates, in duplicate, and allow to grow until they reached confluency. Then, a scratch wound across each well was made using a sterile pipet tip and culture medium was changed (T0). The experiment was stopped after 72 hours of migration (T1). Time course analysis was carried out by means of the LEICA AF6000 Imaging System (LEICA, Wetzlar, Germany).

## 3.13 Preparation of cell lysates and immunoblotting

Cell lysates were prepared using cold RIPA lysis buffer (150mM NaCl, 50mM Tris HCl [ph8], 1% Igepal, 0,5% sodium deoxycholate, 0,1% SDS*)* plus a protease inhibitor cocktail (Complete, Roche),1 mM sodium orthovanadate, and 1 mM dithiothreitol as previously reported (Sonego et al., 2013). Chromatin fraction was prepared by resuspending the un-soluble pellet derived from the lysis in SDS 1%, then sonicated at 30% of amplitude for 10 seconds. Differential extraction of nuclear and cytoplasmic proteins was performed in ES-2 parental and PT-Res cells as previously described (Baldassarre et al., 2005; Schiappacassi et al., 2008). Protein concentrations were determined using the Bio-Rad protein assay (Bio-Rad).

For immunoblotting, equal concentrations of protein samples (35 μg) were separated by 4–20% SDS-PAGE (Criterion precast gel; Bio- Rad) and transferred to nitrocellulose membranes (Hybond C; Amersham). Chromatin samples were loaded considering 1/3 of the volume used for the respective total lysate or cytoplasmic fraction. Immunoblotting were performed using the following primary antibodies: mouse monoclonal anti-Vinculin (1:1000, Cell Signaling), rabbit monoclonal anti-β-Actin (1:1000, Cell Signaling), rabbit monoclonal anti-Fibrillarin (1:250, Santa Cruz), mouse monoclonal anti-GAPDH (1:1000, Cell Signaling), rabbit monoclonal anti-G9a/EHMT2 (1:500, Cell Signaling), mouse monoclonal anti-EHMT1/GLP (1:500, abcam), rabbit monoclonal anti-H3K9me2 (1:1000, Cell Signaling), rabbit monoclonal anti-Histone H3 (1:1000, Cell Signaling), rabbit monoclonal anti-β-Catenin (1:500, Cell Signaling), rabbit monoclonal anti β-TRCP1 (1:1000, Cell Signaling), mouse monoclonal anti- γH2AXpS139 (1:500, Merkmillipore). Antibodies were visualized with appropriate horseradish peroxidase-conjugated secondary antibodies (GE Healthcare) for ECL detection (Biorad)

or Alexa-conjugated secondary antibodies (Invitrogen) for Odyssey infrared detection (LI-COR Biosciences). Quantification of the immunoblots was done using the QuantiONE software (Bio-Rad Laboratories) or the Odyssey infrared imaging system (LI-COR Biosciences).

## 3.14 Cisplatin-DNA (PT-DNA) adducts detection by Dot-blot

DNA was isolated using the Maxwell® DNA-purification kit (Promega) from OVSAHO cells treated as indicated. DNA (500 ng) was denatured at 100 °C for 10 min and spotted onto nitrocellulose membranes (Hybond C; Amersham) using a dot-blot apparatus (Easy-Titer® ELIFA, Pierce). The membranes were then baked for 2 hours at 80 °C and subjected to standard Immunoblot assay using a rat monoclonal anti-cisplatin-DNA Adducts (1:500, EMD Millipore) antibody.

## 3.15 RNA extraction and qRT-PCR analysis

Total RNA for RNA microarray and qRT-PCR analyses was isolated from patient-derived primary tumors or cell cultures using Trizol solution (Roche Applied Science Mannheim, Germany) according to manufacturer protocol. Total RNA was quantified using NanoDrop (Thermo Fisher Scientific Inc., USA). RNA was retro-transcribed with GoScript reverse transcriptase to obtain cDNAs, according to provider's instruction (Promega). Absolute quantification was evaluated by qRT-PCR, using EvaGreen dye-containing reaction buffer (SsoFastTM EvaGreen®, BioRad) and running the reactions in the MyiQ2 Two Color Real-time PCR Detection System (Biorad). Data normalization was performed using ACTIN and GAPDH as housekeeping genes and relative expression was calculated using the mRNA concentration. All the primers for gene expression analyses were purchased from Sigma-Aldrich. Table below reports all the primer sequences.

| Primer | Sequence 5'-3' |
|---|---|
| **ACTIN forward** | GAAGGTGAAGGTCGGAGTC |
| **ACTIN reverse** | GAAGATGGTGATGGGATTTC |
| **BTRC forward** | GCCATACAGGTTCAGTCCTCTG |
| **BTRC reverse** | CGTGTTTAGCATTTCACCTGTAT |
| **FBXW11 forward** | TCGCCTGGTTGTTAGTGGAT |
| **FBXW11 reverse** | CGGACCAATTCTTCATGTCC |
| **FZD1 forward** | TTCAGCAGCACATTCTGAGG |
| **FZD1 reverse** | CCTGCACACTTTTCCCTTT |
| **FZD7 forward** | GCTGCTTTGTTGGAAAGAGG |
| **FZD7 reverse** | GCAGTACGGGAGGAAAAACA |
| **FZD9 forward** | CTGCATCCCCTAGAGACAGC |
| **FZD9 reverse** | ACTAGGACCCTGTGGGGACT |
| **EHMT2 forward** | CAAAATCGGGAACTTGGAGA |
| **EHMT2 reverse** | CTCGATGTGCTTGTGCTCTG |

## 3.16 Gene expression profiling and data mining tools

Gene expression profiling (GEP) was performed essentially as described in (Bomben et al., 2018). Briefly, total RNA samples derived from OVSAHO cells (parental and 3 different PT-Res clones) were extracting using the TRIZOL Reagent (Thermo Fisher Scientific) according to protocol, and RNA quality was assessed using agarose gel electrophoresis after RNA exposure to 70 °C for 5 min. GEP was performed with 150 ng total RNA labeled with Cyanine(Cy)-3 dye, then hybridized to the Whole Human Genome (8 × 60 K) oligo microarray platform (Agilent Technologies), and analyzed by the Agilent Microarray Scanner, using the Agilent Feature Extraction Software 10.7.3 (Agilent Technologies). The pre-processing steps were carried out according to Agilent instruction, and involved quality check, exponential-normal convolution background subtraction, lowess and quantile normalization. After pre-processing and pre-filtering steps, the final dataset was analyzed using GeneSpring GX 12.7 software (Agilent Technologies, Santa Clara, CA). Differentially expressed genes wGene expression profile results were visualized by hierarchical clustering applying Ward's method with Euclidean distance. Gene Set Enrichment Analysis (GSEA) was used to identify the putative genes sets involved in gene deregulation from the online database available at the GSEA Web site 3 (http://www.broadinstitute.org/gsea/).

## 3.17 Chromatin Immunoprecipitation (ChIP) assay

OVSAHO parental an PT-Res cells were treated with 20 µM of cisplatin and/or 6 µM of UNC0631 for 16 hours. Then, treatment was removed, cells treated with 1% formaldehyde and chromatin was prepared via MNase enxymatic digestion according to the protocol. Chromatin IP was performed using SimpleChIP Enzymatic Chromatin IP kit (Magnetic Beads) #9003 from Cell Signaling Technology (CST). ChIP analyses were performed using the rabbit monoclonal anti-G9a (Cell Signaling)

and the mouse-monoclonal anti-H3K9me2 (abcam) ChIP-grade antibodies. After IPs DNA was purified and region of interest were quantified by qRT-PCR using specific primer for the promoter region of BTRC. Table below reports all the primer sequences. (*Promoter regions are expressed as number of bases from the transcription start site).

| Gene | Promoter region | Sequence 5'-3' |
|---|---|---|
| **BTRC forward** | -1000; -1761 | CTGTATAACCAATTATCACAAACATAGC |
| **BTRC reverse** | 1000; -1761 | AACTGTGGGATGTAAGCCCTGC |
| **BTRC forward** | -782; -535 | GCAGGGCTTACATCCCACAGTT |
| **BTRC reverse** | -782; -535 | TCATGTATCTGGCATCTGCAGG |
| **BTRC forward** | -556; -339 | CCTGCAGATGCCAGATACATGA |
| **BTRC reverse** | -556; -339 | AAGGATGAGAAACGGGAGGGG |
| **BTRC forward** | 358; -161 | CCCTCCCGTTTCTCATCCT |
| **BTRC reverse** | -358; -161 | CTGGTCACGGGATTTGTAG |
| **BTRC forward** | -180; +80 | CTACAAATCCCGTGAGCCAG |
| **BTRC reverse** | -180; +80 | TCCACCGTCTCCTCACCATA |

## 3.18 CRISPR/Cas9 system

Knockout of EHMT1 and EHMT2 in OVSAHO cells was generated by CRISPR-Cas9 system, according to (Ran et al., 2013), using two pairs of guide RNAs (gRNAs) designed using CRISPR Design online tool (https://zlab.bio/guide-design-resources). The first pair of gRNA targets the third exon of EHMT1 (NM_024757), the second pair targets the seventh exon of EHMT2 (NM_006709.5). Table below reports the gRNAs sequences.

| Gene | | Sequence 5'-3' |
|---|---|---|
| **EHMT1** | gRNA1 forward | TCCCAATGGCACCAACACACTAACT |
| **EHMT1** | gRNA1 reverse | AAACAGTTAGTGTGTTGGTGCCATT |
| **EHMT1** | gRNA2 forward | CCTCGCAACACACTAACTCGGATAG |
| **EHMT1** | gRNA2 reverse | AAACCTATCCGAGTTAGTGTGTTGC |
| **EHMT2** | gRNA1 forward | TTGTTTGCACGCGCTCATCCACAGAGT |
| **EHMT2** | gRNA1 reverse | AAACACTCTGTGGATGAGCGCGTGCAA |
| **EHMT2** | gRNA2 forward | CACCGGCGCGTGGACTCCGACAGCA |
| **EHMT2** | gRNA2 reverse | AAACTGCTGTCGGAGTCCACGCGCC |

Both pairs of guide RNAs were cloned into the gRNA expression vector pSpCas9(BB)-2A-GFP plasmid (PX458, Addgene #48138). 293FT cells were transfected with the plasmid and 48 hours and 72 hours after transfection, culture medium containing viral particles was collected and used to transduce OVSAHO PT-Res Clone 56, plated the day before ($5{,}7x10^6$ cells/dish). 72 hours after the transduction, GFP-positive cells were sorted by flow cytometry (Becton Dickinson) and pooled together. GFP single-cell cloning was performed and clones were screened for the expression of G9a and GLP by western blot analysis. In this way, we identified two G9a/GLP knockout clones (KO#1 and KO#3).

To confirm the cut at the gRNA target sites, we purified and sequenced the genomic DNA of the two clones.

## 3.19 Sanger sequencing

For EHMT1 and EHMT2 sequencing of G9a$^{KO\#1}$ and G9a/GLP$^{KO\#3}$ clones, DNA was extracted from cultured cells using Maxwell 16 DNA purification kit (Promega). Then, 50 ng of genomic DNA was amplified using the following primers:

| Gene | | Sequence 5'-3' |
|---|---|---|
| **EHMT1** | forward | TCTTGTGAAAACAGCGATGC |
| **EHMT1** | reverse | AAGAGGCCAGAGTGCTGGTA |
| **EHMT2** | forward | GGAACAAGGAGGACTGGACA |
| **EHMT2** | reverse | AGGAGAAGTGACCCTGACGA |

DNA Sanger sequencing was performed using the BigDye Terminator v.3.1 Cycle Sequencing Kit (Applied Biosystems) and the ABI3130xl instrument (Applied Biosystems, Waltham, MA, USA).

## 3.20 Primary EOC collection and analysis

Human EOC samples were collected by CRO institutional Biobank, immediately frozen and stored in liquid nitrogen until needed. Informed consent was obtained from all patients. The CRO-IRB (Internal Review Board) approved this study. Total RNA was extracted from EOC frozen samples using Trizol solution (Roche Applied Science Mannheim, Germany) according to manufacturer protocol. Total RNA was quantified using NanoDrop (Thermo Fisher Scientific Inc., USA) and retro-transcribed with GoScript reverse transcriptase to obtain cDNAs, according to provider's instruction (Promega). Absolute quantification was evaluated by qRT-PCR, using EvaGreen dye-containing reaction buffer (SsoFastTM EvaGreen®, BioRad) and running the reactions in the MyiQ2 Two Color Real-time PCR Detection System (Biorad). Table below reports the samples of ovarian cancer patients analyzed in **Figure 4.25**. Grade and histotype of primary and recurrent tumor samples are reported. (*n.a.: not available; Gx: not evaluable).

| Number | Tumor | Hystotype | Grade |
|---|---|---|---|
| **1** | Primary | Endometrioid | G2 |
| **5A** | Primary | Endometrioid | G3 |
| **7B** | Primary | Serous | G3 |
| **11** | Primary | Serous | G3 |
| **15** | Primary | Serous | G2 |
| **28** | Primary | Serous | G3 |
| **29** | Primary | Serous | G3 |
| **31** | Primary | Serous | G3 |
| **34** | Primary | Serous | G3 |
| **49** | Primary | Clear Cell | G3 |
| **51** | Primary | Serous | G2/3 |
| **66** | Primary | Serous | G3 |
| **82** | Primary | Serous | n.a. |
| **107** | Primary | Serous papillary | G3 |
| **109** | Primary | Serous papillary | Gx |
| **111** | Primary | Serous papillary | G3 |
| **112** | Primary | Serous papillary | G3 |
| **130** | Primary | Serous | G3 |
| **132** | Primary | Clear Cell | Gx |
| **133** | Primary | Serous papillary | G3 |
| **136** | Primary | Endometrioid | Gx |
| **152A** | Primary | Serous papillary | G3 |
| **9** | Recurrence | Serous | Gx |
| **17** | Recurrence | n.a. | n.a. |
| **27L** | Recurrence | Serous | G3 |
| **32** | Recurrence | Indifferentiated | n.a. |
| **36B** | Recurrence | n.a. | n.a. |
| **39** | Recurrence | n.a. | n.a. |
| **44A** | Recurrence | Serous | G3 |
| **52** | Recurrence | Serous | G3 |
| **54** | Recurrence | Serous | n.a. |
| **59** | Recurrence | Serous | G3 |
| **68** | Recurrence | Serous | n.a. |
| **69** | Recurrence | Serous | n.a. |
| **70** | Recurrence | Serous | n.a. |
| **72** | Recurrence | Serous | n.a. |
| **77** | Recurrence | Serous | Gx |
| **81** | Recurrence | Serous | Gx |
| **128B** | Recurrence | Serous | G3 |
| **141** | Recurrence | Serous papillary | G3 |

## 3.21 Statistical analysis

Statistical significance ($P < 0.05$), means, SD, and 95% confidence intervals (CIs) were determined by using GraphPad PRISM software (version 6.0) using the most appropriate test, as specified in each figure. In all experiments, differences were considered significant when p was ≤0.05 and statistical significance was indicated with: * $p < 0.05$, ** $p < 0.01$, *** $p < 0.001$, **** $p < 0.0001$. For survival analysis, PFS was identified as the relevant clinical endpoint. PFS curves were reported according to the Kaplan-Meier method and were compared with the log-rank test.

# 4. RESULTS

## 4.1 G9a/GLP inhibition significantly reduces cell viability of isogenic PT-Resistant EOC cells

Few models are available to properly study EOC PT-resistance. Thus, to reach our main aim of identifying new biomarkers of PT-resistance and possible therapeutic intervention, we used models of isogenic PT-Resistant (PT-Res) cells, already established in our lab, that encompass the most common EOC hystotypes (**Figure 4.1A**). For each cell line, PT-Res clones have been generated using 20 cycles of treatments either applying the pulse method (high doses of cisplatin for 2 hours) or the incremental method (low doses of cisplatin for 48 hours) (Sonego et al., 2017). In the attempt of finding the mechanism underlying PT-resistance and novel strategies to overcome it, we screened four EOC (OVSAHO, TOV-112D, MDAH-2774 and ES-2) PT-sensitive (parental) and two different PT-Res isogenic clones (**Figure 4.1B**) with a library of 145 epigenetic modifiers (EMs, Cayman), targeting Histone Methyl-Transferases (HMTs), Histone De-Methylases (HDMs), Histone Acetyl-Transferases (HATs), Histone De-Acetylases (HDACs), and acetylated lysine reader proteins (**Figure 4.2A**).

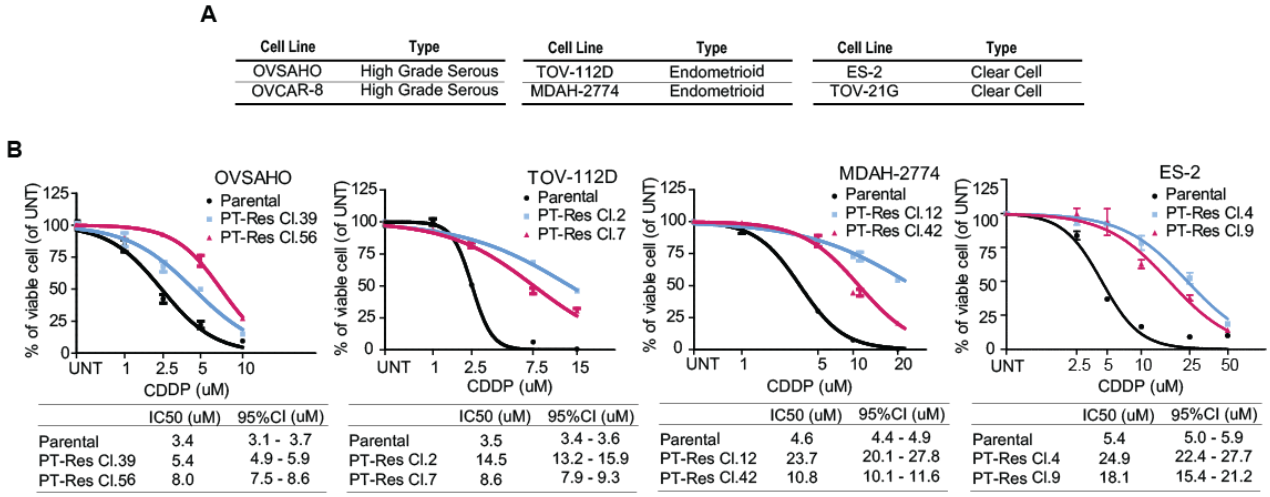


**Figure 4.1. PT-sensitive and PT-Res EOC cell lines. A)** Available isogenic PT-Res cellular models. **B)** Nonlinear regression analyses of cell viability assay in the indicated EOC cell lines, used in the EMs screening, treated with increasing doses of cisplatin (CDDP) for 72 hours. Data are expressed as percentage of viable cells with respect to the untreated (UNT) cells and represent the mean (±SD) of three biological replicates. Tables show the IC50 and the confidence interval (CI) of each condition.

The screening identified the inhibitors of G9/GLP HMTs and of class I HDACs as the most promising drugs in inducing PT-Res EOC cell death. Among the 7 compounds that are supposed to specifically target the G9/GLP HMTs, we observed that all cell permeable G9a/GLP inhibitors (G9a/GLPi)

(BIX01294, UNC0631, UNC0638, UNC0642, UNC0646) were effective in killing all tested cell lines at the fixed dose of 5µM, while the not permeable ones did not (**Figure 4.2B**).

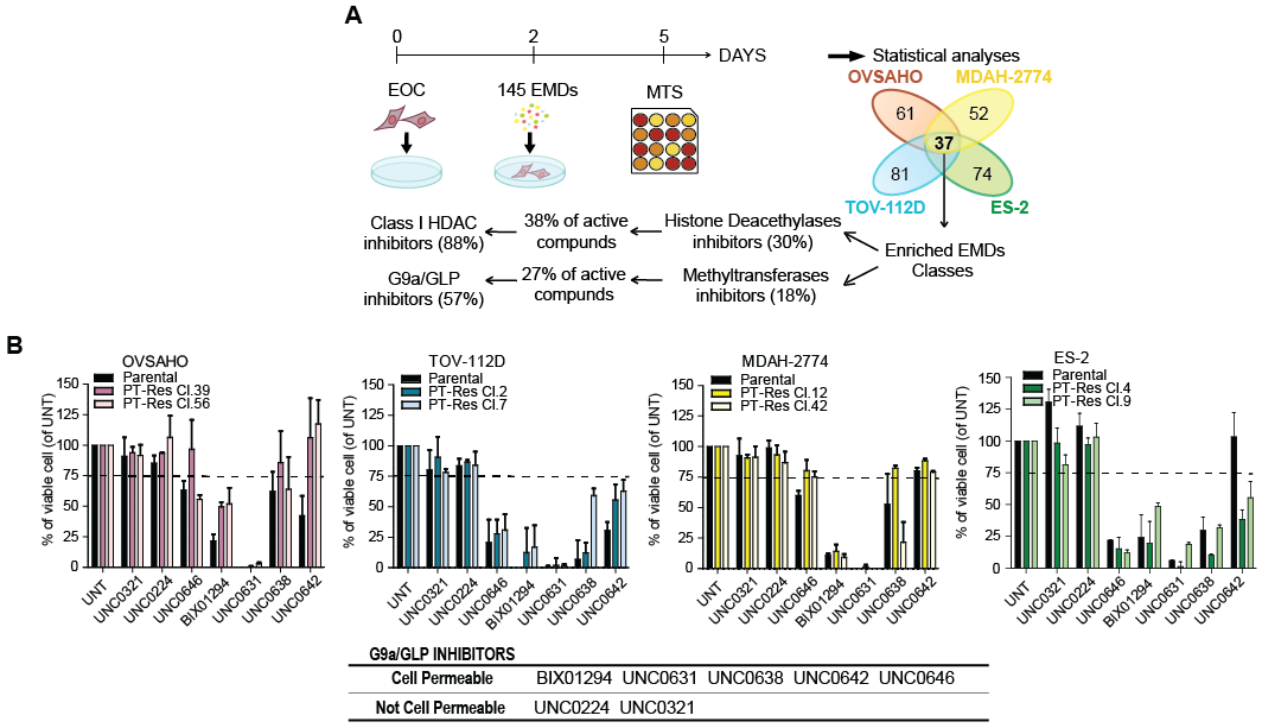


**Figure 4.2. G9a/GLP histone methyltransferases inhibitors significantly reduce cell viability of isogenic PT-sensitive and PT-Res EOC cells. A)** EMs screening experimental design, aimed to identify druggable epigenetic targets. For each EOC cell line (OVSAHO, TOV-112D, MDAH-2774 and ES-2) one PT-sensitive and two PT-Res clones were seeded in 96-well plates in triplicates and treated with 145 EMs at the final concentration of 5µM for 72 hours. Cell viability was evaluated by MTS assay at the end of the treatment. Results are the mean of three independent experiments. Statistical analyses identified 42 compounds able to significantly reduce cell viability in all models, and among these G9a/GLP Histone methyltransferases inhibitors and Class I HDACs inhibitors resulted to be particularly enriched. **B)** Graphs report the cell viability of indicated EOC cell lines treated or not with G9a/GLP specific inhibitors at the final concentration of 5µM for 72 hours. The dotted line indicates the 75% of cell viability selected as limit for EM to be considered active. Data are expressed as percentage of viable cells with respect to the untreated (UNT) cells and represent the mean (±SD) of three biological replicates. The table reports the cell permeable G9a/GLP inhibitors and the not permeable ones.

Next, we confirmed these data using in kill curve analyses the cell permeable compounds on a larger number of EOC PT-Res clones (**Figures 4.3 and 4.4**). Excluding from the study BIX01294, that is known to cause high toxicity in cells, limiting its usefulness as G9a/GLP chemical probe (Vedadi et al., 2011) we decided to test the efficacy of UNC0631, the most potent G9a/GLPi in all tested models, and UNC0638 and UNC0642 that were specifically developed for their higher bio-availability in vivo (Kim et al., 2017). In this manner we calculated the IC50 of UNC0631, UNC0638 and UNC0642 for each cell line and its isogenic PT-Res clones (**Figures 4.3 and 4.4**). Differences among inhibitors were not statistically significant, with the exception of UNC0642, less active than UNC0631 and UNC0638 in OVSAHO parental and PT-Res clones.

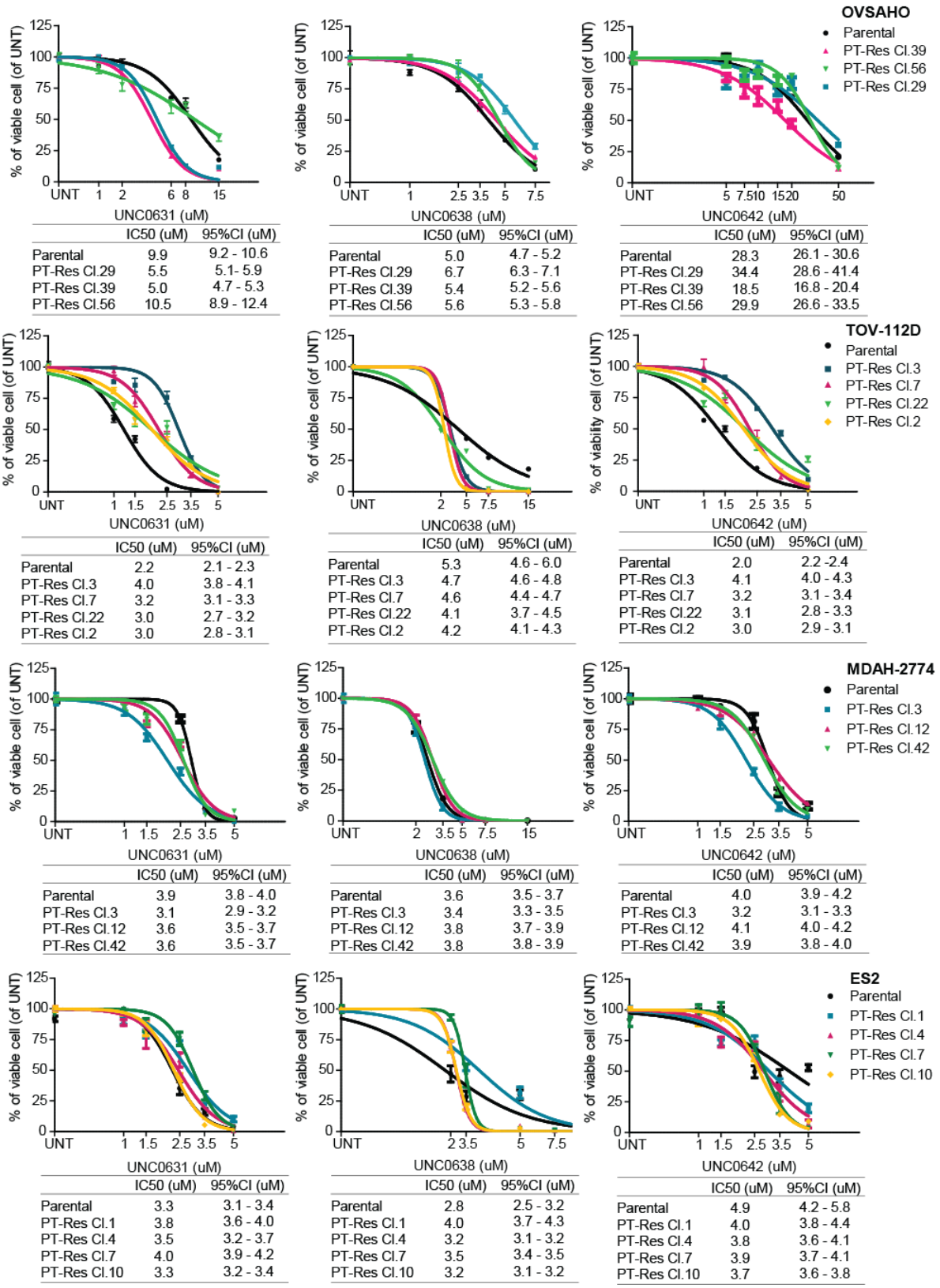


**Figure 4.3.** Nonlinear regression analyses of cell viability assay in OVSAHO, TOV-112D, MDAH-2774 and ES-2 parental and PT-Res cells treated or not with increasing doses of UNC0631, UNC0638 or UNC0642 for 72 hours. Tables show the IC50 and the confidence interval (CI) of each condition. Data are expressed as percentage of viable cells with respect to the untreated (UNT) cells and represent the mean (±SD) of three biological replicates.

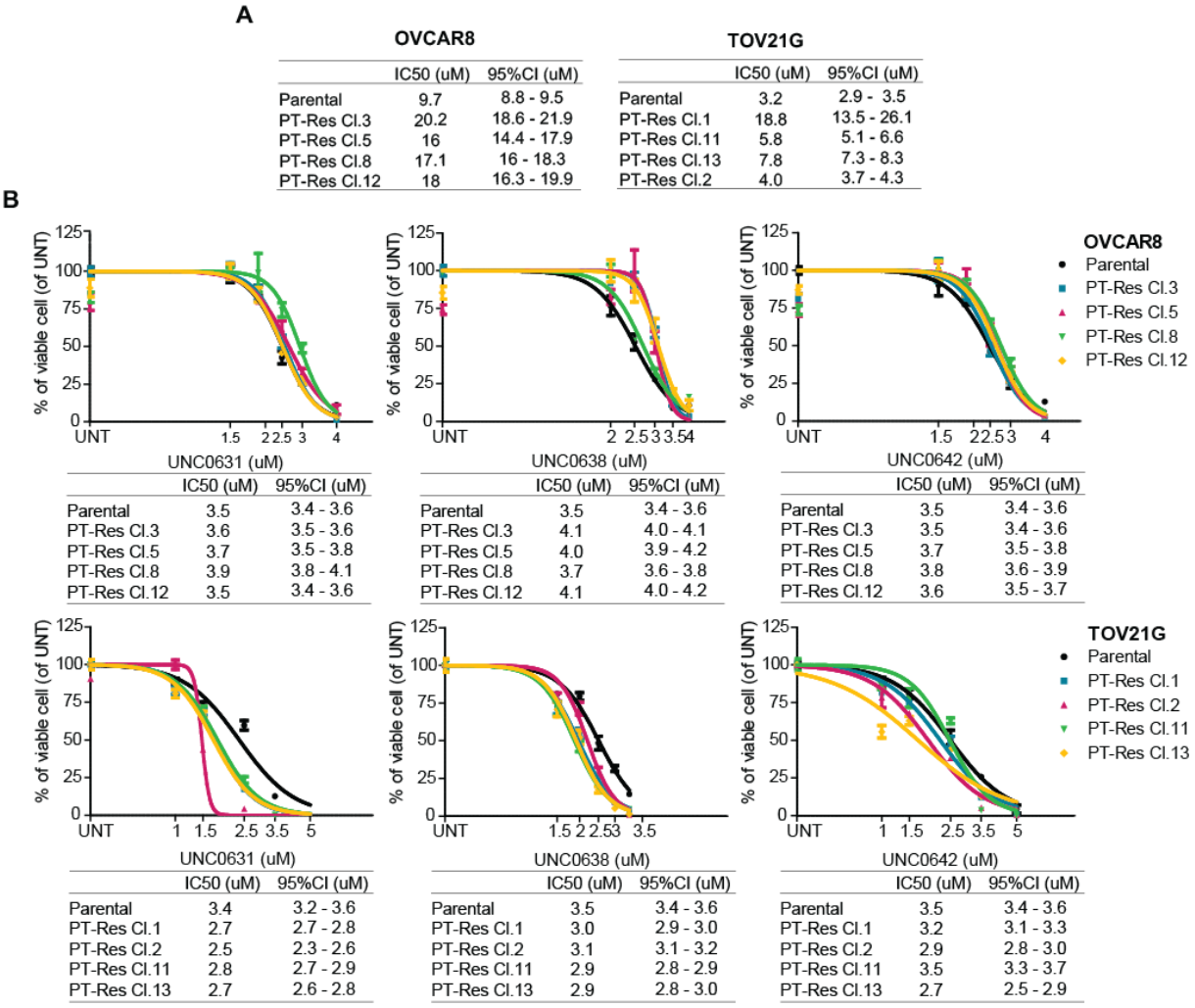


**Figure 4.4. A)** Tables show the IC50 and the confidence interval (CI) for CDDP for OVCAR-8 and TOV-21G. **B)** Nonlinear regression analyses of cell viability assay in OVCAR-8 and TOV-21G cells treated or not with increasing doses of UNC0631, UNC0638 or UNC0642 for 72 hours. Data are expressed as percentage of viable cells with respect to the untreated (UNT) cells and represent the mean (±SD) of three biological replicates. Tables show the IC50 and the confidence interval (CI) of each condition.

Yet, UNC0642 displays very good *in vivo* properties with low general and hematological toxicity in mice (Y. Kim et al., 2017). Therefore, in this thesis we used UNC0631 for *in vitro* experiments.

## 4.2 G9a/GLP inhibition re-sensitizes PT-Resistant cells to PT and second line therapies

Next, we tested if and how G9a/GLPi were able to improve PT-efficacy and/or re-sensitize resistant cells to PT and other drugs commonly used to treat EOC patients (i.e. doxorubicin and taxol). Thus, we tested the effects of UNC0631 and CDDP combination treatment using OVSAHO cells as model. We firstly treated parental and PT-Res OVSAHO cells with UNC0631 for 24 hours, then we removed

the inhibitor and added CDDP for 48 hours (**Figure 4.5A**). When administrated at the same concentration used in the screening (**Figure 4.5B**), UNC0631 slightly increased CDDP activity in parental but not in PT-Res cells. Otherwise, higher doses of inhibitor further reduced both parental and PT-Res cell viability, whether both when administrated alone and in combination with cisplatin (**Figure 4.5C**), probably owed to UNC0631 intrinsic toxicity. Then, we administrated UNC0631 after CDDP (**Figure 4.5D**), observing that the inhibitor increased PT activity in PT-Res clones, having minor or no effects on the ability of PT to kill parental cells (**Figure 4.5E,** compare green with pink columns).

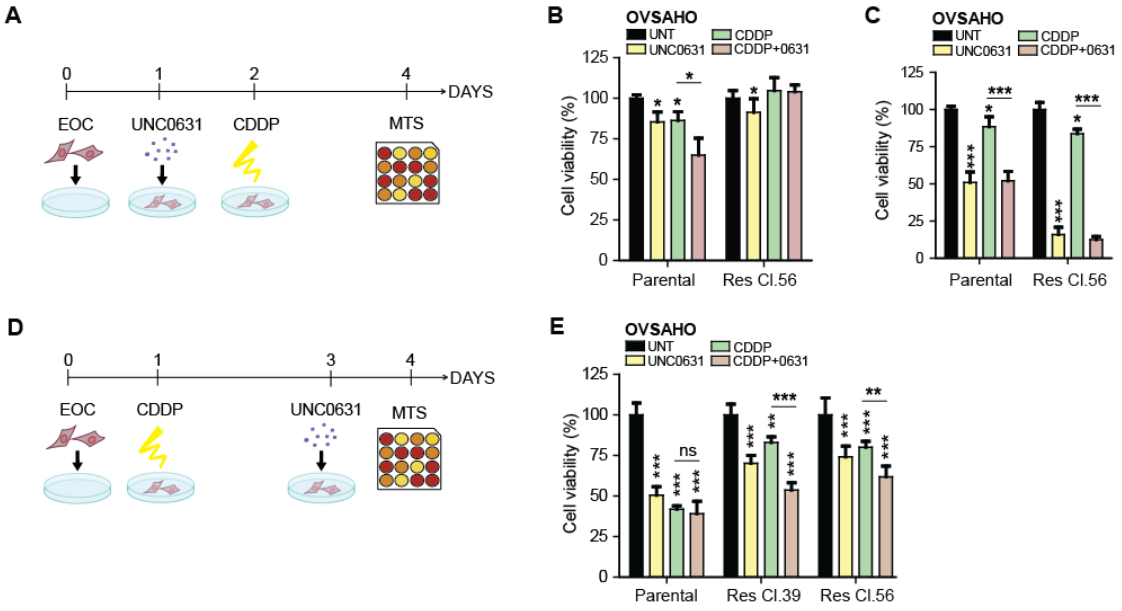


**Figure 4.5. UNC0631 increases parental and PT-Res OVSAHO cells sensitivity to cisplatin. A)** Experimental design of UNC0631 ± CDDP treatment. Cells, plated at high confluence (0), were treated for 24 hours with UNC0631 (1), then the inhibitor was removed and cells were exposed to 2 µM of CDDP for 48 hours (2), finally cell viability was evaluated by MTS assay (4). **B-C)** Graphs show cell viability of OVSAHO parental and PT-Res clones treated or not with 5 µM (**B**) or 8 µM (**C**) of UNC0631 followed by CDDP treatment. **D)** Experimental design of CDDP ± UNC0631 treatment. Cells, plated at high confluence (0), were exposed to 2 µM of CDDP for 48 hours (1), then drug was removed and cells were treated with UNC0631 for 24 hours (3), finally cell viability was evaluated by MTS assay (4). **E)** Graph shows cell viability of OVSAHO parental and PT-Res clones treated or not with CDDP followed by 24 hours of 5 µM of UNC0631. *All data are expressed as percentage of viable cells with respect to the untreated (UNT) cells and represent the mean (±SD) of three biological replicates. Statistical significance was determined by a one-way ANOVA (*$p$<0.05; **$p$<0.01; ***$p$<0.001).

Based on these results, using the schema reported in **Figure 4.5D**, we confirmed the increased PT activity by UNC0631 combined treatment also in all tested PT-Res EOC clones (**Figure 4.6)**.

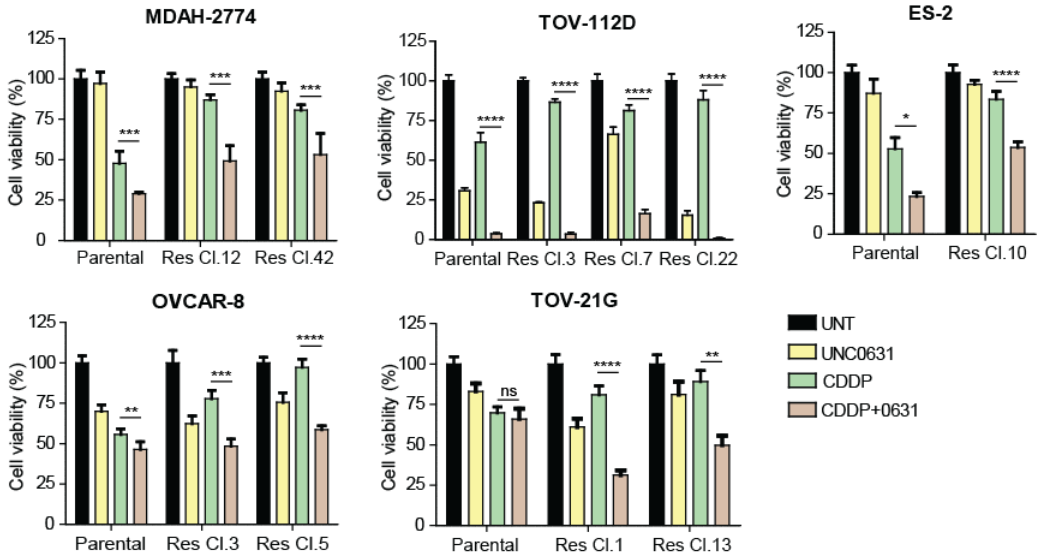


**Figure 4.6. UNC0631 increases parental and PT-Res EOC cells sensitivity to cisplatin.** Graphs show cell viability of parental and PT-Res clones of the indicated EOC cell lines treated or not with CDDP for 48 hours followed by 24 hours of UNC0631. Different doses of CDDP were used to treat the different cell lines: 2,5 µM for TOV-21G, 5 µM for MDAH-2774, ES-2 and OVCAR-8, and 10 µM for TOV-112D. UNC0631 was used at the final concentration of 2,5 µM in MDAH-2774, ES-2 and TOV-21G, 3 µM in OVCAR-8 and 6 µM in TOV-112D. All data are expressed as percentage of viable cells with respect to the untreated (UNT) cells and represent the mean (±SD) of three independent experiments. Statistical significance was determined by a one-way ANOVA (*$p$<0.05; **$p$<0.01; ***$p$<0.001).

To complete this characterization, we evaluated the effect of UNC0631 treatment in combination with cisplatin in ID8 CRISPR/Cas9-modified mouse epithelial ovarian cells, knock-out (KO) for TP53 alone or in combination with the KO of BRCA1, or BRCA2, or PTEN (J. Walton et al., 2018; J. B. Walton et al., 2017). ID8 TP53+BRCA1$^{KO}$ and TP53+BRCA2$^{KO}$ cells have defective homologous recombination DNA repair pathways and, accordingly, increased sensitivity to PT, whereas ID8 TP53+PTEN$^{KO}$ cells exhibit increased resistance to PT treatment respect to ID8 TP53$^{KO}$ cells (**Figure 4.7A**).

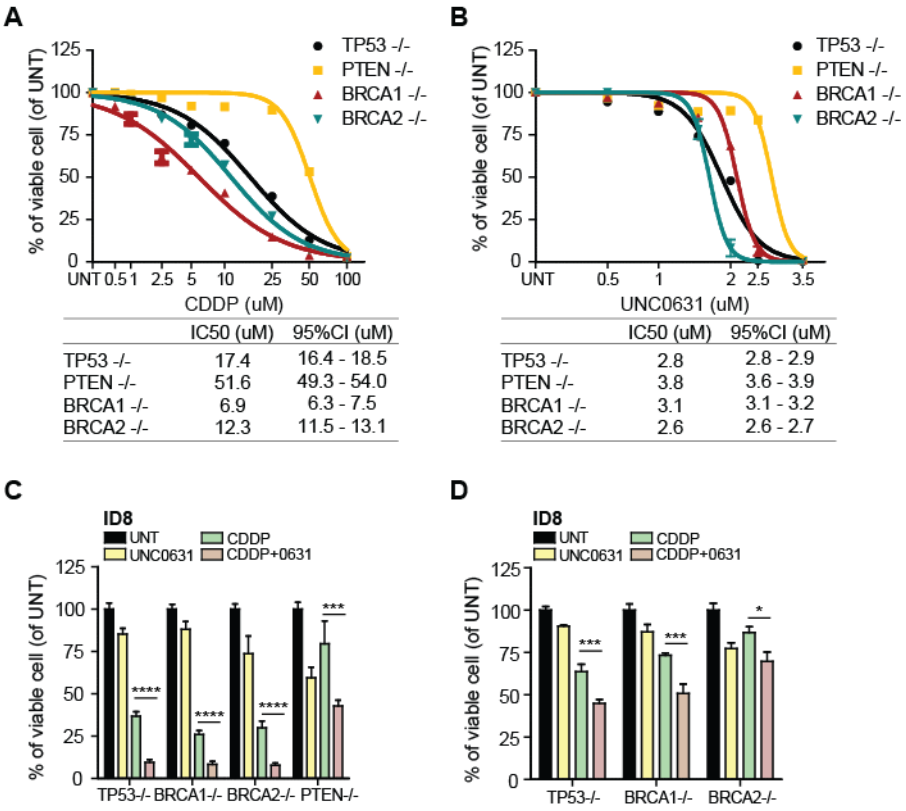


**Figure 4.7. UNC0631 increases ID8 CRISPR/Cas9-modified mouse epithelial ovarian cells sensitivity to cisplatin. A-B)** Nonlinear regression analyses of cell viability assay in ID-8 $TP53^{KO}$, $TP53^{KO}$+$BRCA1^{KO}$, $TP53^{KO}$+$BRCA2^{KO}$, $TP53^{KO}$+$PTEN^{KO}$ cells, treated or not with increasing doses of CDDP (**A**) or UNC0631 (**B**) for 72 hours. Data are expressed as percentage of viable cells with respect to the untreated (UNT) cells and represent the mean (±SD) of three biological replicates. The tables report the IC50 and the confidence interval (CI) of each condition. **C-D)** Graphs show cell viability of the indicated ID-8 cell lines treated or not with 10 µM (**C**) or 2,5 µM (**D**) of CDDP for 48 hours followed by 24 hours of UNC0631. All data are expressed as percentage of viable cells with respect to the untreated (UNT) cells and represent the mean (±SD) of three independent experiments. In **C** and **D** statistical significance was determined by a one-way ANOVA (*$p$<0.05; **$p$<0.01; ***$p$<0.001). (KO is indicated as -/-).

We performed dose response curves treating ID8 PT-sensitive and PT-Res cells with UNC0631 and calculated their IC50 (**Figure 4.7B**), observing that $PTEN^{KO}$ cells were slightly more resistant to the inhibitor than the other cellular models. When the cells were treated with the PT+UNC0631 combination using the schema reported in **Figure 4.5D** we observed that UNC0631 increased PT activity in all models independently on the loss of BRCA1 or BRCA2 and on the dose of cisplatin (**Figure 4.7C and D**, respectively). Importantly, UNC0631 re-sensitized $PTEN^{KO}$ cells to PT treatment (**Figure 4.7C**), recapitulating in this controlled mouse model of HGSOC what observed in human-derived cell lines.

Additionally, using OVSAHO cells as a model, we investigated if UNC0631 increased the activity of doxorubicin and taxol, two other commonly anticancer agents used to treat EOC patients. We have already reported that OVSAHO PT-Res cells display for taxol an IC50 of 2- to 5-fold higher than

parental cells, while they had an IC50 for doxorubicin similar to the one of parental cells (Sonego et al., 2017). By treating OVSAHO parental and PT-Res cells as shown in **Figure 4.8A** we observed that UNC0631 re-sensitized PT-Res cells to taxol (**Figure 4.8B**) and increased the cytotoxic activity of doxorubicin especially in PT-Res clones (**Figure 4.8C**).

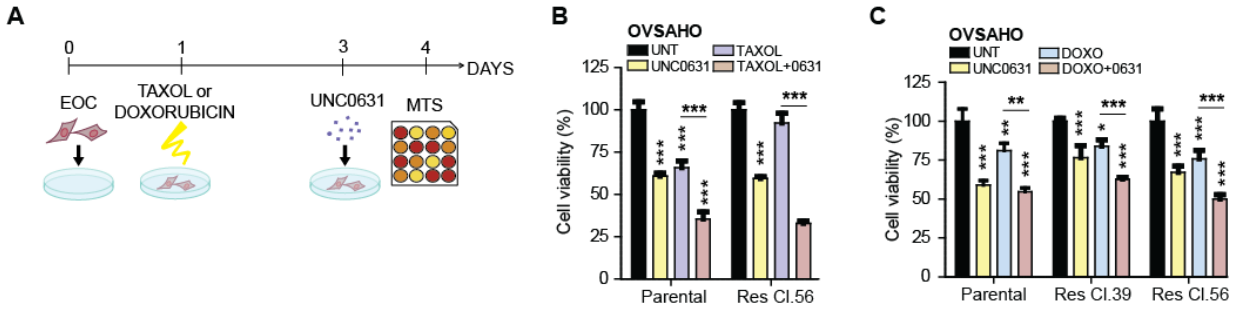


**Figure 4.8. UNC0631 increases OVSAHO parental and PT-Res cells sensitivity to taxol and doxorubicin. A)** Experimental design used in taxol/doxorubicin±UNC0631 combined treatment. Cells, plated at high confluence (0) in a 96-wells plate, were exposed to taxol (100 nM) or doxorubicin (3 µM) for 48 hours (1), then drug was removed and cells were treated with 6 µM of UNC0631 for 24 hours (3), finally cell viability was evaluated by MTS assay (4). **B-C)** Graph shows cell viability of OVSAHO parental and PT-Res clones treated or not with taxol (**B**) or doxorubicin (**C**) followed by 24 hours of UNC0631. All data are expressed as percentage of viable cells with respect to the untreated (UNT) cells and represent the mean (±SD) of three independent experiments. Statistical significance was determined by a one-way ANOVA (*$p$<0.05; **$p$<0.01; ***$p$<0.001).

## 4.3 Functional role of G9a/GLP in EOC

Based on these promising results we evaluated G9a and GLP protein levels in parental and PT-Res OVSAHO cells showing however no significant differences in their expression when whole cell lysates were analyzed (**Figure 4.9A**). Yet, when we evaluated the expression of H3K9me2 (the target of G9a/GLP HMTs activity) in the chromatin fraction of the same cells treated or not with cisplatin for 24 hours, we observed that in untreated conditions all PT-Res clones displayed higher levels of H3K9 di-methylation (**Figure 4.9B**), as also confirmed by the densiometric quantification of the blots (**Figure 4.9C**). After cisplatin treatment H3K9me2 expression increased both in parental and PT-Res cells, although the increase was more evident for parental cells (**Figure 4.9B-D**).

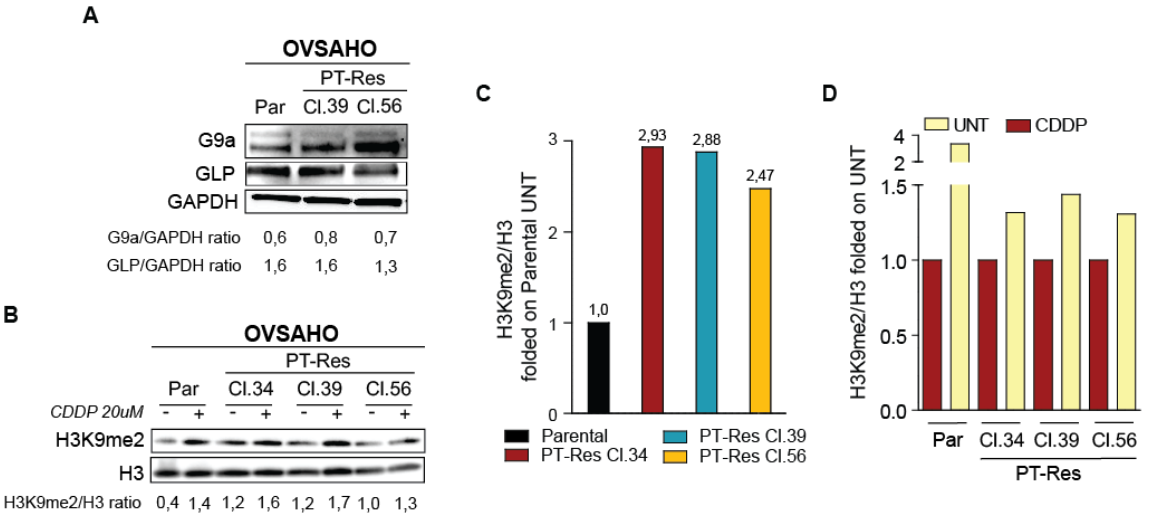


**Figure 4.9. G9a/GLP expression and H3K9 methylation in OVSAHO cells. A)** Western blot evaluating the expression of G9a and GLP in OVSAHO parental and PT-Res cells in basal conditions. GAPDH was used as loading control. Densitometric analysis of G9a/GAPDH and GLP/GAPDH ratio is reported under the blot. **B)** Western blot evaluating the expression of H3K9me2 in the chromatin fraction of OVSAHO parental and PT-Res cells treated or not with CDDP. Histone H3 was used as loading control. Densitometric analysis of H3K9me2/H3 ratio is reported under the blot. **C)** Graph reports the densiometric quantification of di-methylation in parental and PT-Res cells in untreated condition, folded on parental untreated. **D)** Graph reports the densiometric quantification of the experiment in (**B**).

These results were confirmed by cell fraction using ES-2 cells in which we evaluated G9a protein expression and localization and H3K9me2 expression in parental and PT-Res cells, treated with cisplatin and/or UNC0631 for 24 hours, using cytoplasmic, nuclear and chromatin fractions. In untreated conditions G9a was more expressed in PT-Res cells respect to their parental counterpart, both in the nuclear and in the chromatin fractions. Cisplatin treatment increased the expression of G9a in PT-Res cells, especially on chromatin. Interestingly, in both parental and, more evidently, in PT-Res cells the G9a fraction bound to chromatin decreased in cells treated with UNC0631 and with the combination CDDP+UNC0631, with a concomitant increase of its nuclear fraction. As expected, the inhibition of G9a-chromatin binding by the inhibitor treatment, leaded to a decrease of H3K9 di-methylation both in parental and, more pronouncedly, in PT-Res cells (**Figure 4.10A and B**). Overall, these results support the possibility that G9a/GLP activity is commonly increased in PT-Res EOC cells and that it is positively regulated by platinum treatment.

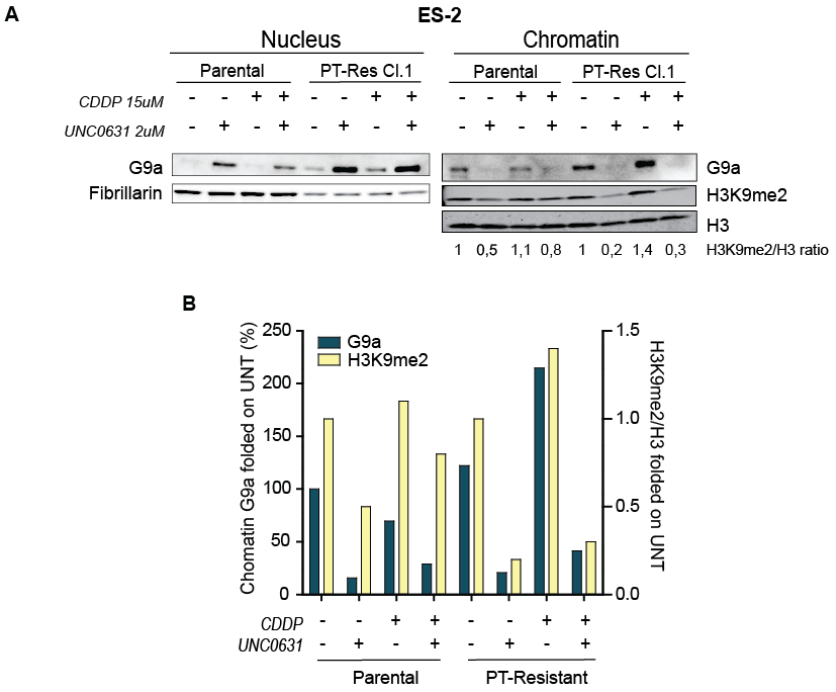


**Figure 4.10. Chromatin binding of G9a is regulated by PT in EOC cells. A)** Western blot evaluating the expression of G9a, H3K9me2 and Histone H3 in ES-2 parental and PT-Res cells treated for 24 hours with CDDP and/or UNC0631, as indicated. Fibrillarin and Histone H3 were used as loading control for nuclear and chromatinic fractions, respectively. Densitometric analysis of H3K9me2/H3 ratio is reported under the blot. **B)** Graph reports the densitometric quantification of the experiment in (**A**).

## 4.4 Role of G9a/GLP inhibition in PT-induced DNA damage response

We have already observed that EOC PT-Res cells accumulate less DNA damage following cisplatin treatment respect to parental cells, as demonstrated by the lower levels of Histone H2AX phosphorylation (γH2AXpS139) (Sonego et al., 2017). We confirmed this observation in the newly generated PT-Res models (**Figure 4.11A-C**). Based on these observations and on the recent evidences proposing a role of G9a/GLP inhibitors in enhancing chemotherapy anti-tumor effects by impairing DNA repair, we investigated the response of PT-Res cells to cisplatin, following UNC0631 treatment. Western blot analyses of phosphorylated S139 Histone H2AX (γH2AX) expression, used as marker of DNA damage, were performed in OVSAHO, OVCAR-8 and ES-2 parental and PT-Res cells, treated or not with cisplatin and/or UNC0631 for 24 hours (**Figure 4.11D**). Cisplatin and UNC0631 strongly increased the expression of γH2AX in all the parental cells, and, slightly, in OVCAR-8 and ES-2 PT-Res clones. Interestingly, in both parental and, more evidently, in PT-Res cells, γH2AX levels increased with cisplatin and UNC0631 combination treatment. γH2AX expression is not influenced by the dose of UNC0631 utilized in OVSAHO PT-Res cells, accordingly with our previous results (see **Results 4.1**), indicating that OVSAHO cells are more resistant to UNC0631 treatment respect to the other EOC cell lines (see **Results 4.1, Figure 4.3**).

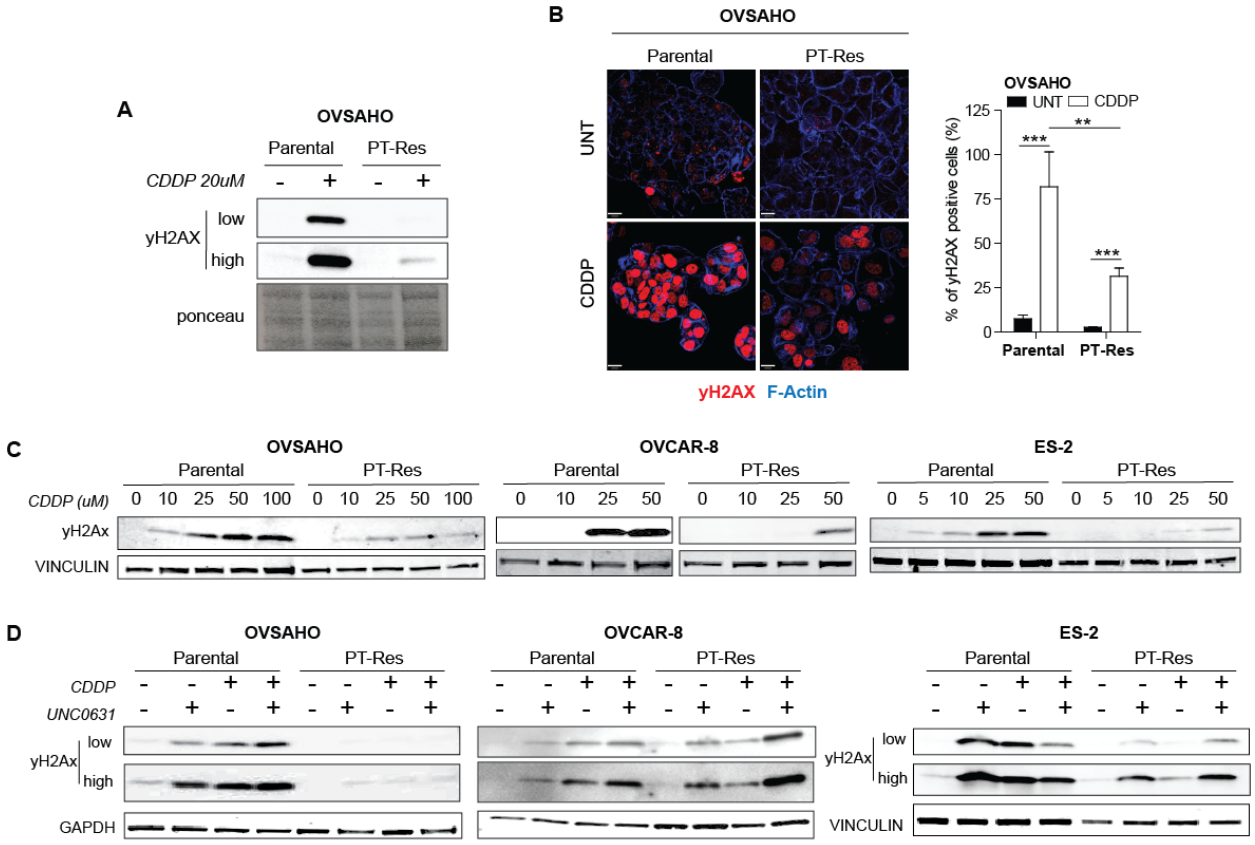


**Figure 4.11. Cisplatin induces DNA damage in EOC cells. A)** Western blot analysis of S139 Histone H2AX (γH2AX) expression, used as marker of DNA damage, in OVSAHO parental and PT-Res cells untreated or treated with cisplatin for 24 hours as indicated. **B)** Immunofluorescence analysis evaluating γH2AX (red) expression in OVSAHO cells untreated (UNT) or treated for 24 hours with 20 μM of CDDP. Graph on the right shows the percentage of γH2AX-positive cells of untreated (UNT) and cisplatin-treated (CDDP) OVSAHO parental and PT-Res cells. Statistical significance is report in the graph and was calculated using Student's t test. **C)** Western blot analysis of γH2AX expression in parental and PT-Res cells of the indicated EOC cell lines untreated or treated with different doses of CDDP for 24 hours. GAPDH was used as loading control. **D)** Western blot analysis γH2AX expression in parental and PT-Res cells of the indicated EOC cell lines untreated or treated with CDDP and/or UNC0631 for 24 hours. GAPDH and Vinculin were used as loading control. Different doses of CDDP were used to treat the different cell lines: 15 μM for OVSAHO parental and ES-2; 20 μM for OVCAR-8 and 25 μM for OVSAHO PT-Res cells. UNC0631 was used at the final concentration of 2 μM in OVSAHO parental, OVCAR-8 parental and ES-2, 2,5 μM in OVCAR-8 PT-Res and 4 μM in OVSAHO PT-Res cells.

PT-Res cells showed a reduced DNA platination and faster removal of platinum from the DNA (Sonego et al., 2017) and, interestingly, here we confirmed these data on the newly generated OVSAHO PT-Res clones. Moreover, using the treatment schedule reported in **Figure 4.12A,** in which OVSAHO cells were treated with cisplatin for 48 hours and then with UNC0631 in cisplatin-free medium for additional 24 hours, we observed that G9a inhibition both in parental and, with lesser extent, in PT-Res cells increased DNA platination in a dose dependent manner (**Figure 4.12B**). These data suggest a possible role for G9a in decreased DNA damage (for PT decreased uptake or increased detoxification/expulsion), increased DNA repair or both.

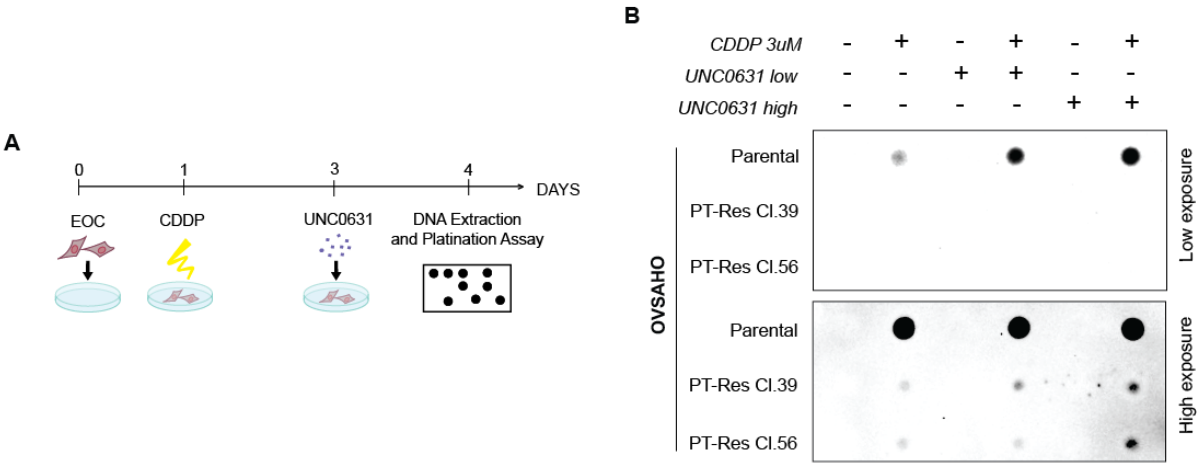


**Figure 4.12. UNC0631 increases DNA platination in OVSAHO cells in a dose dependent manner. A)** Experimental design of DNA platination assay performed on OVSAHO cells. Cells plated at high confluence (0), were exposed to cisplatin (3 µM) for 48 hours (1), then drug was remove and cells were treated with low or high dose of UNC0631 (respectively 3 - 6 µM for parental cells, and 8 - 10 µM for PT-Res cells) for 24 hours (3), finally DNA was extracted to proceed with the dot blot. **B)** Dot blot analyses evaluating the amount of platinated-DNA in parental and PT-Res cells untreated or treated with CDDP for 48 hours and then released in cisplatin-free medium or UNC0631 for additional 24 hours, to allow for DNA repair.

Next, we checked if the increased DNA damage, favored by G9a inhibition, was accompanied by an increased activation of the apoptotic pathway. With this aim, by 3D immunofluorescence analysis, we evaluated the expression of cleaved caspase 3, used as marker of apoptosis, in OVSAHO parental and PT-Res cells treated with cisplatin and/or UNC0631. We treated PT-Res clones for 72 hours, whereas parental cells treatment was stopped at 48 hours because of their reduced ability to growth in matrigel matrix under platinum treatment. Our data showed that PT-Res cells treated with UNC0631 displayed higher levels of cleaved caspase 3 respect to the untreated ones, and CDDP+UNC0631 treatment strongly increased the expression of cleaved caspase 3 respect to cisplatin alone (**Figure 4.13**).

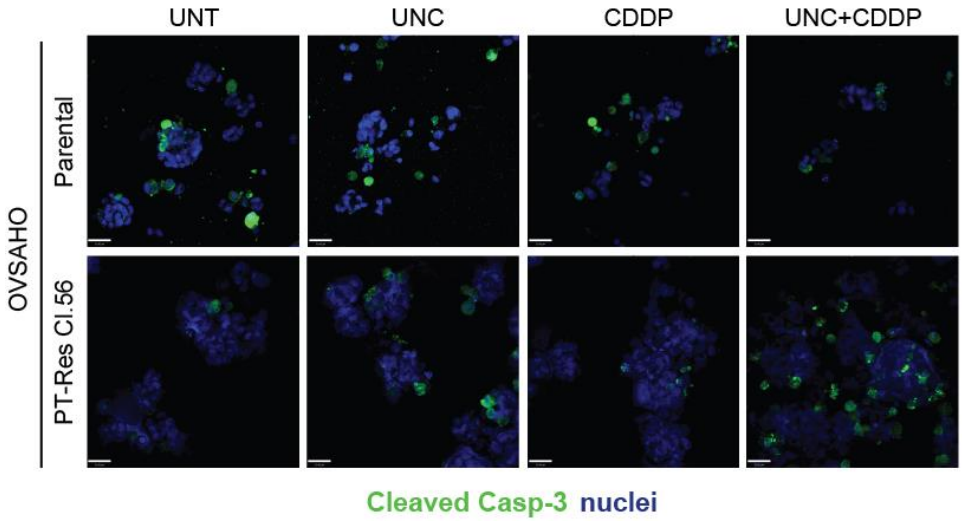


**Figure 4.13. UNC0631 increases cleaved caspase-3 expression in OVSAHO cells when combined with cisplatin.** Immunofluorescence analysis evaluating cleaved caspase 3 (green) expression in OVSAHO cells untreated (UNT) or treated with 2,5 µM of CDDP and/or UNC0631 (UNC) for 48 hours (parental) or 72 hours (PT-Res). Parental and PT-res cells were treated with 4 µM and 7 µM of UNC0631, respectively. Nuclei were stained with propidium iodide (blue).

## 4.5 Role of G9a/GLP complex in cell-cell contact and stemness

The data collected above demonstrated that G9a/GLP inhibition induced cell death and improved PT activity in EOC, especially in the context of PT-Res cells. These effects are likely due to the ability of G9a/GLPi to increase DNA platination and the consequent PT-induced DNA damage, two phenotypes strongly and frequently hampered in PT-Res cells (Sonego et al., 2017). Another phenotype commonly observed in PT-Res EOC cells is the alteration of the Epithelial-Mesenchymal Transition (EMT)/Mesenchymal-Epithelial Transition (MET) processes that confers to PT-Res cells a greater ability to spread, attach and grow (Sonego et al., 2017). Ovary-sphere formation is a validated assay to evaluate the EMT transitions in ovarian cancer cells and their metastatic potential (Sonego et al. Sci Adv. 2019). We thus tested if G9a/GLP could also be involved in the regulation of EMT/MET in OVSAHO PT-sensitive and PT-Res cells. We confirmed that PT-Res clones form a higher number and bigger spheres respect to the parental cells (**Figure 4.14A**). Then, we observed that G9a/GLP inhibition significantly decreased the ability of parental and PT-Res OVSAHO cells to form spheres and potentiate the activity of cisplatin in inhibiting sphere formation (**Figure 4.14B**).

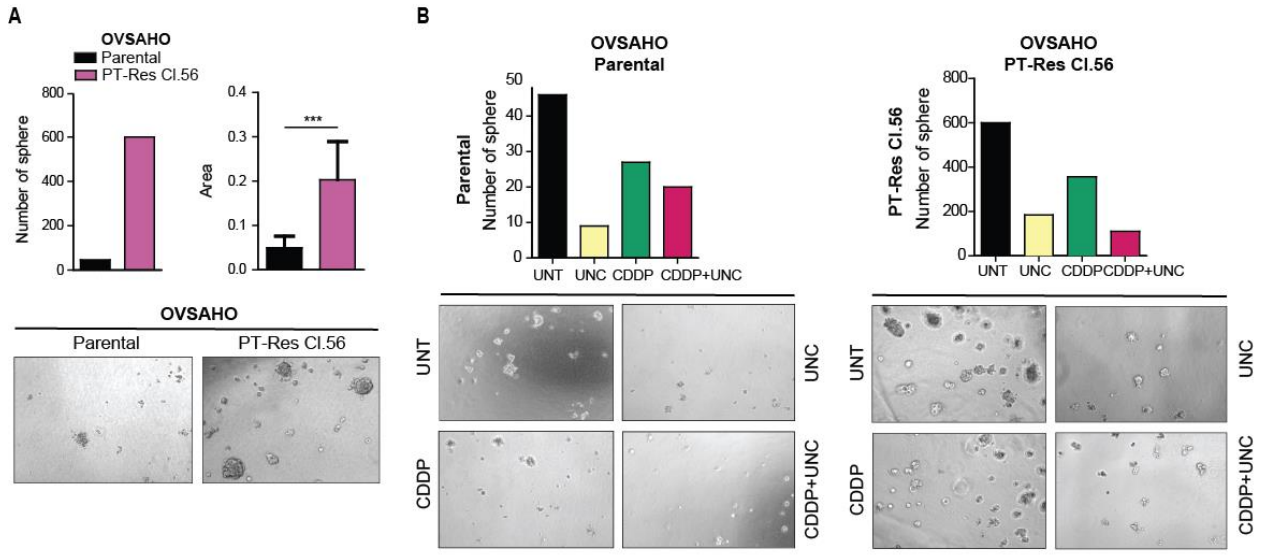


**Figure 4.14. OVSAHO 3D growth assay. A)** Graphs showing number (left) and area (right) of parental and PT-Res spheres. Below, two representative images of spheres formed by OVSAHO parental and PT-Res cells are reported. Statistical significance was determined by a two-tailed unpaired Student's t test (***P < 0.001). **B)** Graphs showing number of spheres formed by OVSAHO parental (left) and PT-Res cells (right) untreated (UNT) or treated with 2,5 µM of cisplatin (CDDP) and/or UNC0631 (UNC) for 48 hours (parental) or 72 hours (PT-Res). Parental and PT-res cells were treated with 4 µM and 7 µM of UNC0631, respectively. Representative images of spheres formed by OVSAHO parental (left) and PT-Res cells (right) for each condition are reported below the graphs.

These results were then corroborated by immunofluorescence (IF) analyses looking at the expression and the localization of proteins involved in cell-cell contacts that are altered in mesenchymal PT-Res cells (Sonego et al., 2017). Indeed, IF analyses showed that in basal conditions, the expression of β-catenin, involved in the adherence junctions' structure, is less expressed and more widespread within OVSAHO PT-Res cells respect to their parental counterpart, in which it is more expressed and mainly localized at cell membrane (**Figure 4.15A).** Treatment with cisplatin induced a decrease in the amount of β-catenin in parental cells and an increased nuclear localization in PT-Res once (**Figure 4.15B**). This effect, mediated by CDDP, seemed to be reverted by UNC0631 both in parental, with a restoration of basal amount of β-catenin, and in PT-Res cells, inducing protein membrane localization (**Figure 4.15B**).

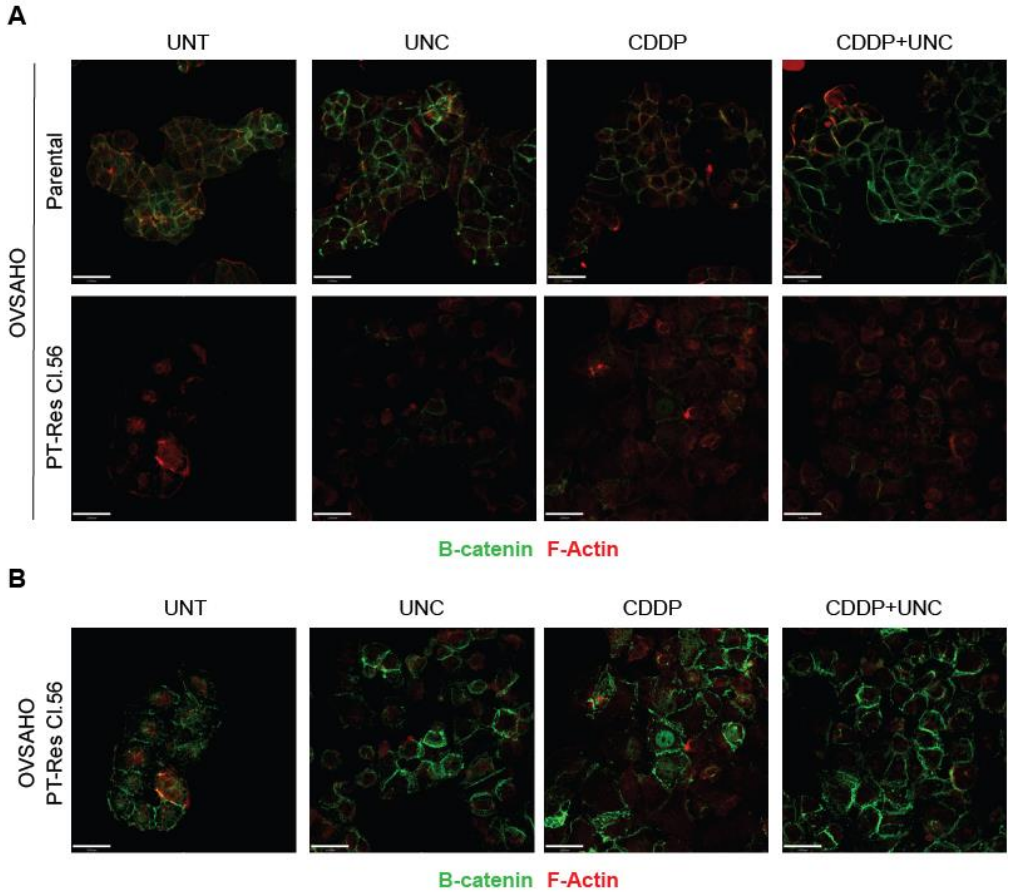


**Figure 4.15. UNC0631 induces β-catenin re-localization. A/B)** Immunofluorescence analysis evaluating the expression of β-catenin (green) in OVSAHO parental and PT-Res cells untreated (UNT) or treated with 20 μM of CDDP and/or 4 μM of UNC0631 (UNC) for 24 hours. In **A** cells were acquired with the same acquisition parameters to highlight the differences between parental and PT-res cells. In **B** is reported the higher exposition times of β-catenin (green) to better highlight its localization in PT-Res cells.

Looking at other cell-cell junction markers, we observed, by IF, different expression and distribution of occludin (marker of tight junctions) and p120-catenin (marker of adherence junctions) between parental and PT-Res cells, treated with CDDP and/or UNC0631 for 24 hours. In particular, at basal condition p120-catenin in PT-Res cells resulted redistributed in the cytosol rather than at the cell membrane, as observed in PT-sensitive cells. In parental cells cisplatin treatment slightly decreased p120-catenin levels at cell membrane, and this effect was reverted by the treatment with UNC0631 (**Figure 4.16A, red)**. Similar observations were made in parental cells for occludin, that in parental cells more localized on membrane and increased under UNC0631 treatment, both alone and in combination with cisplatin (**Figure 4.16A, green)**. In PT-Res cells both p120-catenin and occludin were less localized at cell membrane respect to parental cells and their localization was less affected by both cisplatin and UNC0631 treatment respect to untreated cells (**Figure 4.16B**).

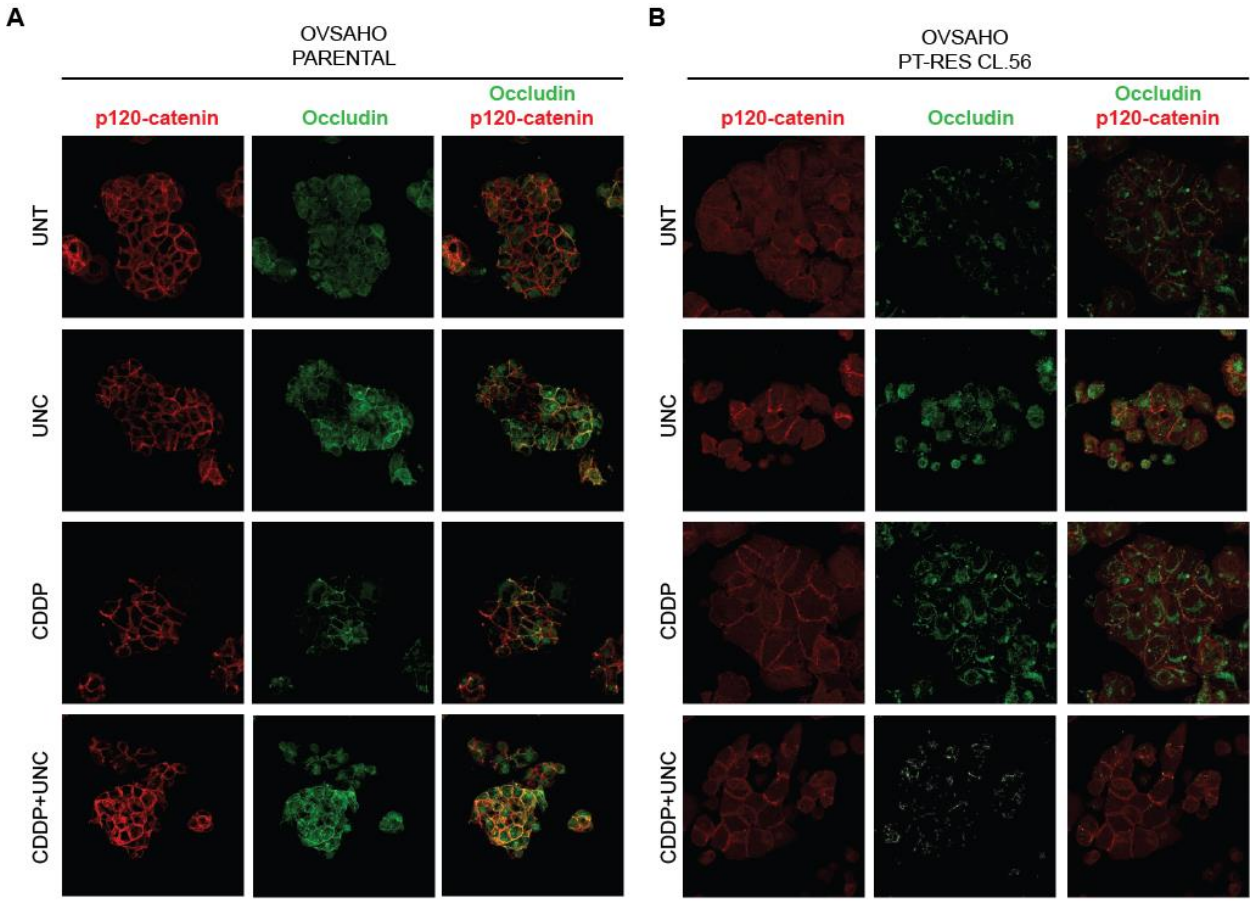


**Figure 4.16. UNC0631 alters occludin and p120-catenin expression and localization. A/B** Immunofluorescence analysis evaluating the expression of occludin (green) and p120-catenin (red) in OVSAHO parental (**A**) and PT-Res cells (**B**) untreated (UNT) or treated with 20 µM of CDDP and/or 4 µM of UNC0631 (UNC) for 24 hrs.

Overall, these data suggest that PT-treatment induce changes in cell-cell contacts and that these changes could be reverted by G9a/GLP inhibition supporting a possible role for G9a/GLP not only in DNA repair but also in EMT regulation.

## 4.6 Genome wide Gene Expression Profile (GEP) showed gene expression regulation by H3K9 methylation in OVSAHO cells

Trying to identify signaling pathways modulated by G9a/GLP inhibitors that could mediate their activity as anticancer drugs, both alone and in combination with cisplatin, we used a genome wide Gene Expression Profile (GEP) on parental and PT-Res cells treated or not with cisplatin and UNC0631. To this aim total RNA was extracted from parental (3 different replicates) and PT-Res (3 different clones) OVSAHO cells, treated as depicted in **Figure 4.17A**. Unsupervised cluster analyses of GEP showed that parental and PT-Res cells segregate by cell type and treatment (**Figure 4.17B**).

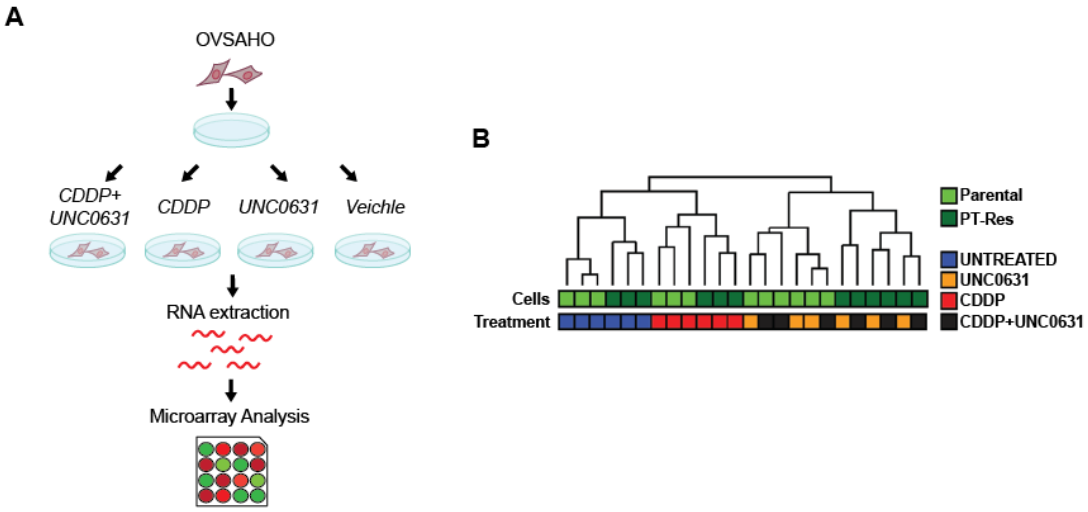


**Figure 4.17. Unsupervised cluster analyses of GEP revealed that parental and PT-Res cells segregate by cell type and treatment. A)** OVSAHO PT-sensitive and PT-Res cells were treated with CDDP (20 µM) and/or UNC0631 (6 µM) for 16 hours. Extracted RNA was used for Microarray Analysis. **B)** Unsupervised cluster analyses of parental and PT-Res cells treated with PT, UNC0361 or PT+UNC0361.

This approach, coupled with Gene Set Enrichment Analyses (GSEA), was highly informative and highlighted several interesting results: first we observed that 3441 genes (1994 up-regulated and 1447 down-regulated in parental vs PT-Res cells) were differentially expressed in untreated parental and PT-Res OVSHAO cells (**Figure 4.18A**), and that this signature in GSEA analyses demonstrated that Focal Adhesion and Canonical Wnt pathways were the most significantly enriched in untreated PT-Res respect to parental cells (**Figure 4.18B**), suggesting a possible molecular explanation for the higher *in vitro* adhesive and invasive capabilities of PT-Res cells.

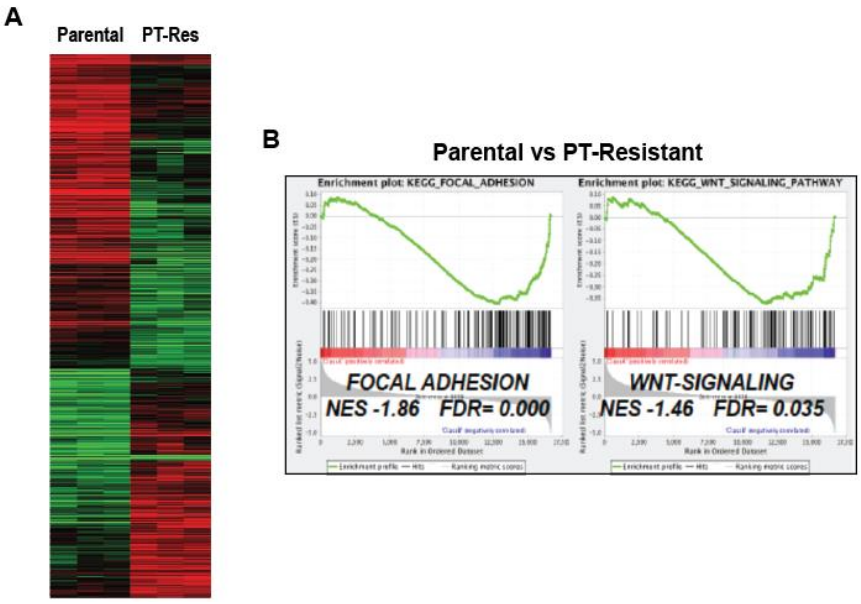


**Figure 4.18. Focal Adhesion and Wnt pathways are enriched in PT-Res cells. A)** Heat map of supervised clustering analyses identified genes differentially expressed between untreated parental and PT-Res cells. **B)** GSEA of genes differentially expressed in untreated parental and PT-Res cells identified Focal Adhesion and Wnt pathways.

Then we analyzed the effects of cisplatin and UNC0631 on GEP of parental and PT-Res cells (**Figure 4.19**). Interestingly while cisplatin did not affect the expression of UNC0631 modified genes, UNC0631 reverted the expression of 10% and 19% of genes modified by cisplatin in parental and PT-Res cells respectively, supporting a role for G9a/GLP in the transcriptional modifications induced by PT.

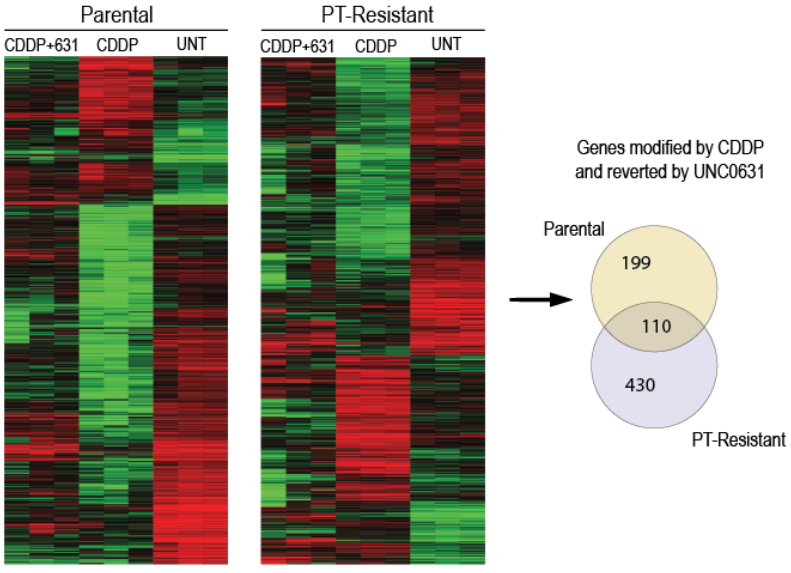


**Figure 4.19. CDDP-modified GEP is partially reverted by UNC0631.** Heat map of supervised clustering analyses identified genes modified by CDDP treatment alone, using fold change ≥2 and $p<0.05$, then compared to GEP from OVSAHO parental and PT-Res cells treated with CDDP and UNC0631. Venn diagram (right) showing the genes differentially modulated by CDDP and reverted by UNC0631 treatment.

GSEA performed on genes differentially expressed among PT-Res OVSAHO cells treated with CDDP versus CDDP+UNC0631 showed that Tight Junction, Canonical Wnt and Focal Adhesion pathways were all highly significantly enriched in PT-treated PT-Res cells and reverted by UNC0631 (**Figure 4.20A**).

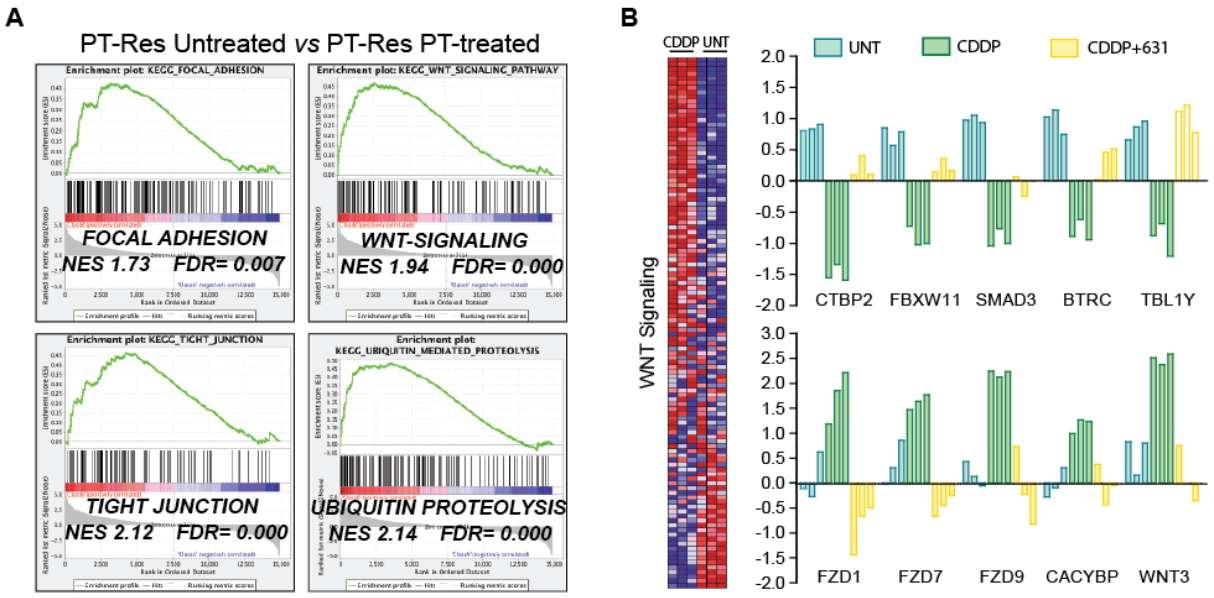


**Figure 4.20. Wnt and Adhesion pathways are modified by PT in PT-Res cells. A)** GSEA of gene differentially expressed in PT-Res cells untreated or PT-treated identified Ubiqutin, Tight Junction, Wnt and Focal Adhesion pathways as the most significantly enriched by PT. The expression of genes belonging to the Ubiquitin pathway was not affected by UNC0631 and therefore not investigated here. NES=Nominal Enrichment Score. FDR= False Discovery Rate. **B)** GSEA of Wnt pathway genes modulated by cisplatin and reverted by UNC0631 in PT-Res cells.

## 4.7 Role of G9a/GLP in the regulation of Wnt pathway in EOC

The biological and molecular results collected so far suggested that G9a/GLP inhibitors could affect EMT and cell-cell contact by altering the expression of Canonical Wnt pathway, a signally pathway deeply involved in the acquisition of PT-resistance and stem-like phenotypes in human cancer, including EOC (Arend et al., 2013). Therefore, we tried to confirm a possible role for UNC0631 in regulating the transcription of selected genes belonging to Canonical Wnt pathway and to verify if this regulation was due to an altered H3K9 methylation. To validate the results obtained by microarray analysis with qRT-PCR, we tested the expression of the 5 most upregulated and downregulated genes by PT and reverted by UNC0631 belonging to Canonical Wnt pathway, and confirmed that three upregulated (the FRIZZLED1, FRIZZLED7 and FRIZZLED9 receptors) and two downregulated genes (FBXW11 and BTRC) (**Figure 4.20B**) were modified by cisplatin in a G9a/GLP-dependent manner in PT-Res cells (**Figure 4.21A**).

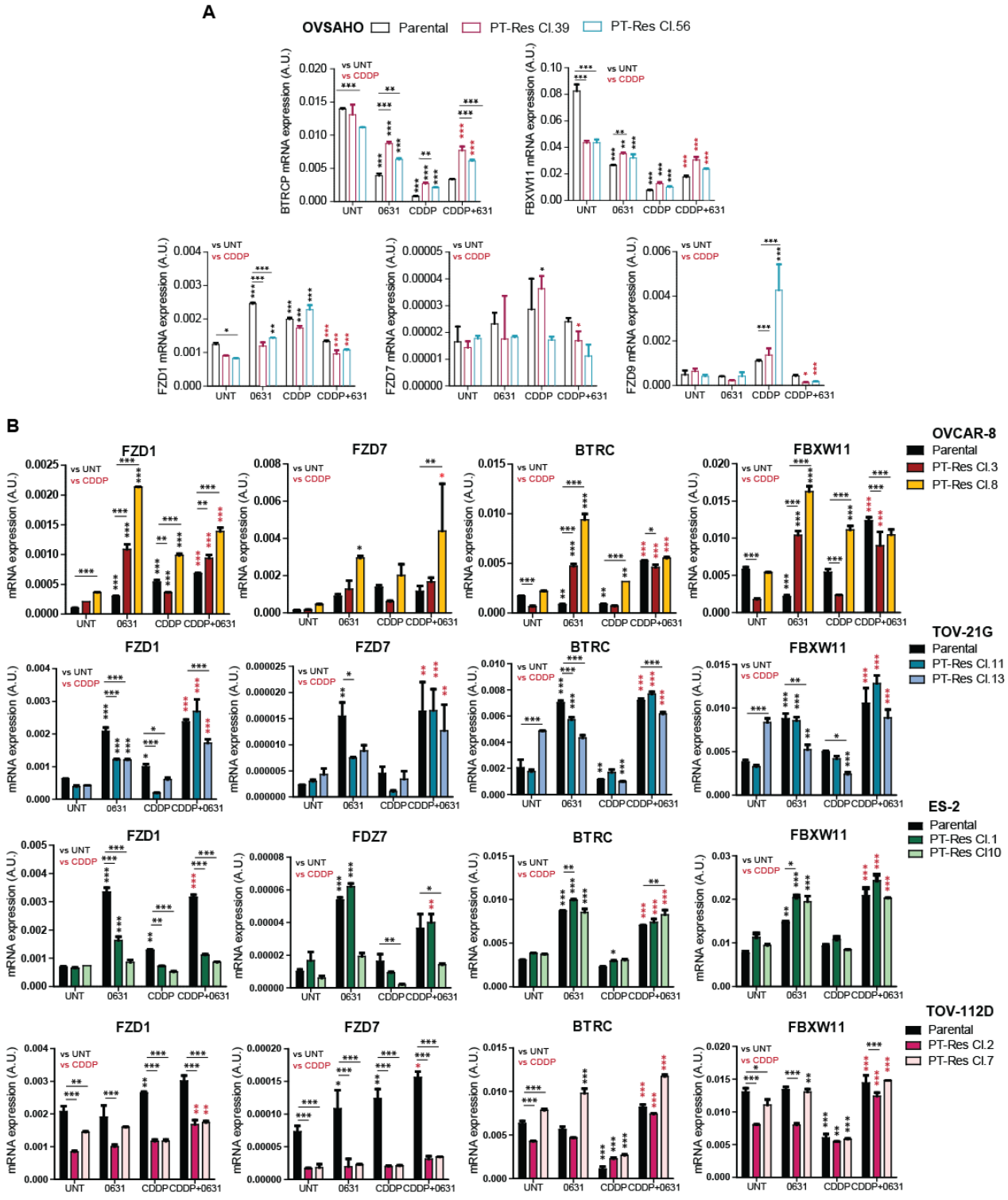


**Figure 4.21. Wnt pathway-related genes modified by PT are partially reverted by UNC0631 in EOC cell lines.** **A)** qRT-PCR reporting the normalize BTRC, FBXW11 and FRIZZLEDs (FZD1, FZD7 and FZD9) mRNA expression in OVSAHO parental and PT-Res cells untreated (UNT) or treated with cisplatin (CDDP) and or UNC0631 (UNC) for 16 hours. **B)** qRT-PCR reporting the normalize FZD1, FZD7, BTRC and FBXW11 mRNA expression in the indicated EOC cell lines untreated (UNT) or treated with cisplatin (CDDP) and or UNC0631 (UNC) for 16 hours.

Based on this evidence, we tested by qRT-PCR if the expression of BTRC, FBXW11 and FRIZ-ZLEDs was regulated by G9a and by PT-treatment also in other available parental and PT-Res EOC

lines. Results showed that the expression of BTRC and FBXW11 is downmodulated by cisplatin and reverted by UNC0631 in all tested cell lines, whereas the FRIZZLEDs genes were differentially modulated in a cell- and treatment-dependent manner (**Figure 4.21B**).

Therefore, we next tested if cisplatin affected the ability of G9a to bound the BTRC promoter (**Figure 4.22A**), performing ChIP analyses on PT-sensitive and PT-Res EOC cells treated with cisplatin. ChIP analysis on the TOV-112D model confirmed that in basal condition, G9a bound to the distal region of BTRC promoter (**Figure 4.22B**). We observed a more efficient binding of G9a to BTRC promoter between bases -339 and -782 from the transcription start site (TSS) and similar binding between -761 and -1000 from TSS in PT-Res respect to the parental cells. At the same time, H3K9me2 was especially present in the same region of BTRC promoter (between -535 and -1000 from TSS) and was higher in PT-Res cells respect to their parental counterpart, supporting an increased G9a activity in PT-Res clones on the regulation of BTRC promoter. Both parental and PT-Res cells treated with cisplatin for 16 hours displayed a general decrease in the G9a binding to BTRC promoter. Yet especially in PT-Res cells we observed a shift of G9a binding to the more proximal regions of the promoter with a peak in the -339 and -556 region (compare yellow empty bars in **Figure 4.22B**). Using the anti-H3K9me2 antibody in the ChIP experiments on the same chromatin we observed a slightly higher H3K9me2 binding to the BTRC promoter especially in PT-Res respect to parental cells under cisplatin treatment (**Figure 4.22C**). Again, the PT-induced increase in H3K9me2 was more evident in the -339 and -556 region of the promoter with a clear parallel between G9a binding modulation and H3K9 di-methylation (compare yellow empty bars in **Figure 4.22C**). We confirmed these findings in OVSHAO cells where an increase in H3K9me2 was evident in PT-Res respect to parental cells (**Figure 4.22D**). In this case, however, cisplatin treatment did not significantly modify the H3K9me2 of BTRC promoter in resistant cells while a reduction of the binding was induced by cisplatin in parental cells (compare empty bars in **Figure 4.22D**).

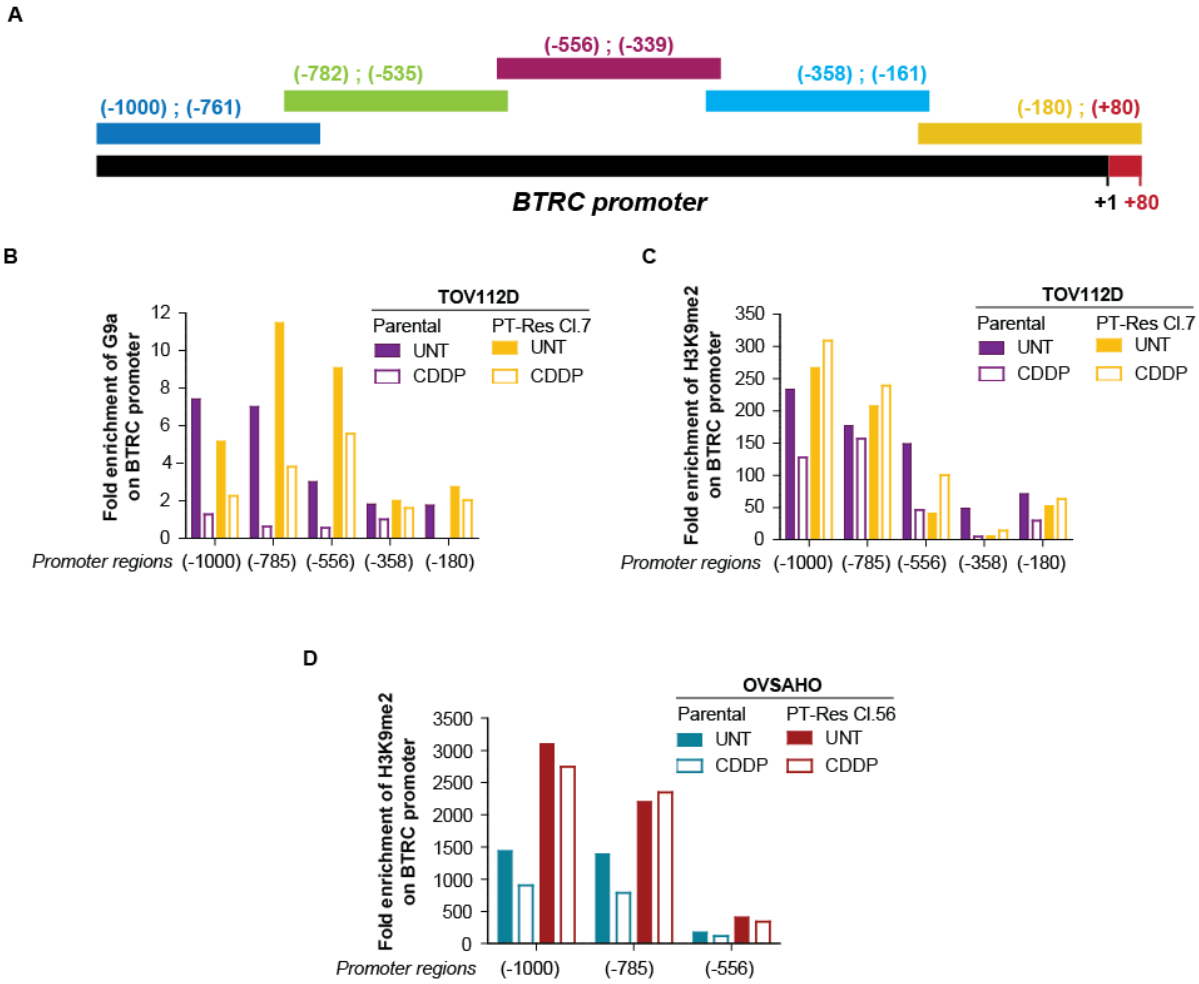


**Figure 4.22. PT-Res EOC cells display higher H3K9me2 levels at BTRC promoters. A)** Scheme of BTRC promoter, subdivided in 5 regions. (+1) indicates the transcription start site. **B-C)** Graphs showing the amount of immunoprecipitated G9a **(B)** bound to BTRC promoter regions and H3K9me2 levels **(C)** in parental and PT-Res cells untreated (UNT) or treated with 50µM of cisplatin (CDDP) for 16 hours. **D)** Graph showing the amount of immunoprecipitated H3K9me2 on BTRC promoter in parental and PT-Res cells untreated (UNT) or treated with 25µM of cisplatin (CDDP) for 4 hours.

Results obtained with GEP and GSEA (**Figures 4.18, 4.19 and 4.20)**, qRT-PCR (**Figure 4.21**) and ChIP analysis (**Figure 4.22**), support the possibility that in our EOC cell lines G9a regulates the transcription of BTRC and, likely FBXW11, both at basal condition and under cisplatin treatment. BTRC and FBXW11 encode for the E3-ubiquitin-ligases β-TRCP1 and β-TRCP2 respectively, which collaborate with other proteins for the degradation of β-catenin (Cui et al., 2020). As β-TRCP1 and β-TRCP2 are paralogs, with similar biochemical properties and thought to be functionally redundant due to their lack of selectivity in the recognition of substrates (Cui et al., 2020), we decided to focus our attention on the most studied, β-TRCP1. Firstly, we performed a time course treatment with cisplatin on OVSAHO parental and PT-Res cells, to evaluate PT-effects on BTRC mRNA expression (**Figure 4.23A**).

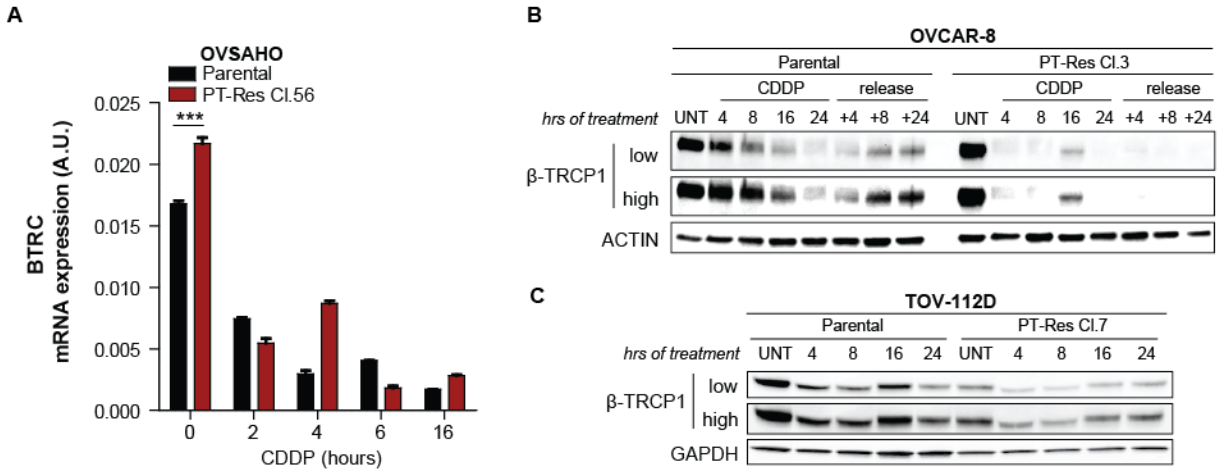


**Figure 4.23. Cisplatin decreases BTRC mRNA expression and protein levels. A)** mRNA expression of BTRC in parental and PT-Res OVSAHO cells untreated (0) or treated with CDDP (25 μM) for 2, 4, 6 and 16 hours. **B)** Western blot analysis of β-TRCP1 expression in OVCAR-8 parental and PT-Res cells treated with CDDP (30 μM) for 4, 8, 16 and 24 hours, and then released in cisplatin-free medium for additional 4 hours (+4), 8 hours (+8) or 24 hours (+24). ACTIN was used as loading control. **C)** Western blot analysis of β-TRCP1 expression in TOV-112D parental and PT-Res cells treated with CDDP (25 μM) for 4, 8, 16 and 24 hours. GAPDH was used as loading control.

OVSAHO displayed decreased BTRC mRNA expression levels as early as 2 hours of cisplatin, and throughout the treatment, respect to the untreated condition. Western blot analysis of β-TRCP1 expression in OVCAR-8 cells, showed decreased protein levels in both parental and PT-Res cells with increasing times of cisplatin (**Figure 4.23B**). Using the same approach, we confirmed the effect of cisplatin on β-TRCP1 also in TOV-112D cells used in ChIP experiments (**Figure 4.23C**).

Next, we investigated the effect of UNC0631 treatment, combined or not with cisplatin, on β-TRCP1 protein levels in OVSAHO, OVCAR-8 and TOV-112D parental and PT-Res cells, treated for 24 hours with CDDP and/or the inhibitor. In the first two cell lines we observed that PT-Res cells displayed lower amount of β-TRCP1 respect to their parental counterpart (**Figure 4.24A and B**) while in the TOV-112D models parental and PT-Res cells had similar levels of the protein (**Figure 4.24C**). Yet, in all tested models, cisplatin alone caused a decrease of β-TRCP1 that was prevented by the combined use of UNC0631 (**Figure 4.24A-C**), except for OVCAR-8 PT-Res clone for which the effects of cisplatin are not evident. In TOV-112D and OVCAR-8 PT-Res cells UNC0631 used as single agent also increased β-TRCP1 protein levels. Overall, these results are in line with the regulation of BTRC mRNA expression by CDDP and/or UNC0631 showed before (**Figures 4.21A-B**).

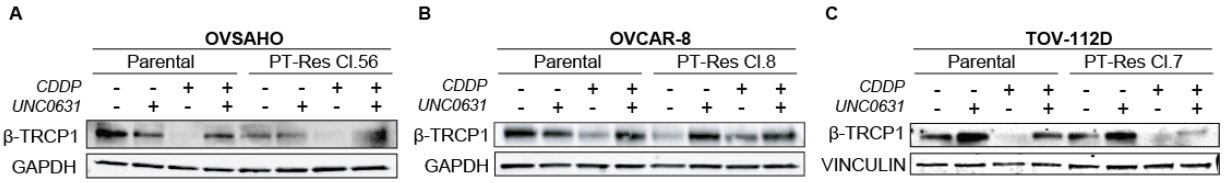


**Figure 4.24. Cisplatin decreased β-TRCP1 protein levels, restored by UNC0631 treatment.** Western blot evaluating the expression of β-TRCP1 in OVSAHO **(A)**, OVCAR-8 **(B)** and TOV-112D **(C)** parental and PT-Res cells treated with CDDP and/or UNC0631 for 24 hours. GAPDH and VINCULIN were used as loading control. Different doses of CDDP were used to treat the different cell lines: 15 μM and 25 μM respectively for OVSAHO parental and PT-Res cells; 20 μM and 40 μM respectively for OVCAR-8 parental and PT-Res cells, and 50 μM for TOV-112D. UNC0631 was used at the final concentration of 1,5 μM in TOV-112D parental, 2 μM in parental OVSAHO and OVCAR-8 and in TOV-112D PT-Res, 2,5 μM in OVCAR-8 PT-Res and 4 μM in OVSAHO PT-Res cells.

To verify if the *in vitro* data were relevant and consistent with the human pathology, we analyzed the expression of G9a and BTRC in HGEOC primary samples collected in our Institute dividing the collected HGEOC samples in naïve (primary) from untreated patients and in pre-treated samples, from patients who already received platinum-based therapy (**Figure 4.25**). The expression of both G9a, and especially BTRC mRNA was reduced in pre-treated respect to the primary samples, overall supporting the possibility that the G9a played a role in the platinum response also *in vivo* by regulating β-TRCP1 expression.

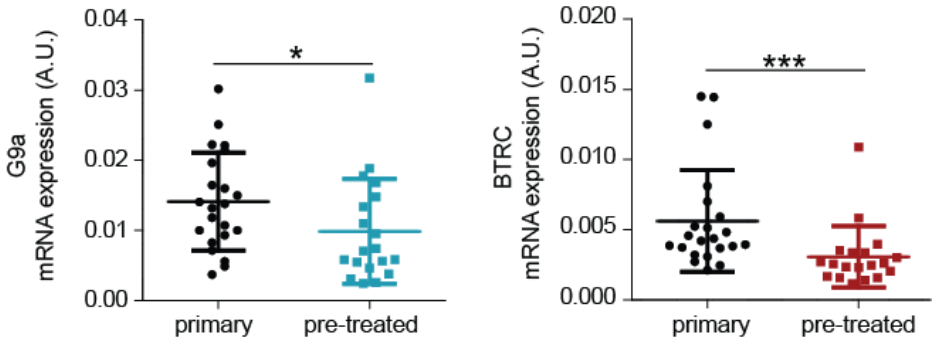


**Figure 4.25. G9a and BTRC mRNA expression in HGSEOC samples from platinum-treated and untreated patients.** qRT-PCR reporting the normalize G9a and BTRC mRNA expression in tumor samples obtained from patients with primary untreated or platinum-treated EOC (pre-treated) (i.e. patients with recurrent disease or treated with neo-adjuvant chemotherapy).

## 4.8 Role of Wnt pathway in mediating the G9a/GLP response to PT and acquisition of PT-resistance

Previous studies demonstrated the involvement of Wnt pathway in response to chemotherapy, platinum response and metastatic progression in EOC (Arend et al., 2013; Krishnamurthy & Kurzrock, 2018). Since BTRC and FBXW11 are central regulators of Wnt pathway by controlling β-catenin protein degradation, we investigated in OVSAHO cells the effects of cisplatin and/or G9a/GLP

inhibition on β-catenin protein expression. In basal condition PT-Res cells displayed lower levels of β-catenin respect to their parental counterpart (**Figure 4.26A**), confirming immunofluorescence results (see **Results 4.5, Figure 4.15A**). Quite unexpectedly cisplatin, UNC0631 or their combined treatment for 24 hours did not affect β-catenin protein levels, neither in parental nor in PT-Res OVSAHO cells (**Figure 4.26B**). Same results were obtained for other EOC cell lines with the exception of ES-2 parental cells in which a modulation of β-catenin protein expression by UNC0631, cisplatin and their combination was observed (**Figure 4.26C**). These results are however compatible with the observation that UNC0631 induces a re-localization of β-catenin to the cell membrane (see **Results 4.5, Figure 4.15A**) since only cytoplasmic and nuclear β-catenin is sensitive to degradation (Shi et al., 2015).

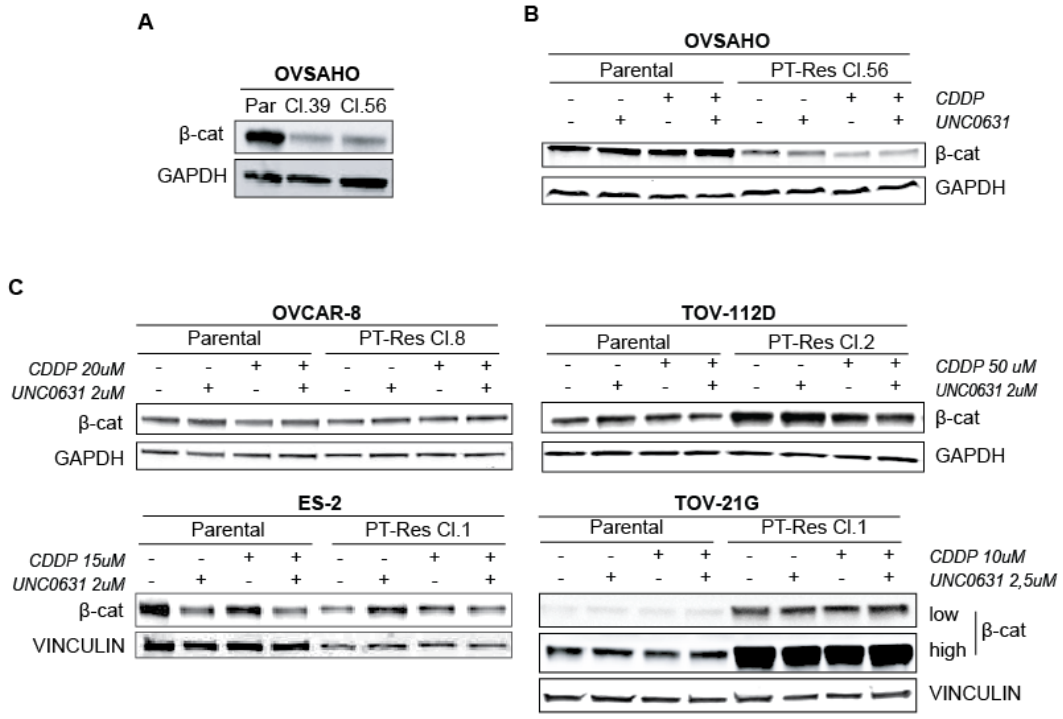


**Figure 4.26. β-catenin protein levels are not affected by cisplatin and UNC0631 treatment. A)** Western blot analysis evaluating the basal expression of β-catenin in OVSAHO parental and PT-Res cells. GAPDH was used as loading control. **B)** Western blot analysis of β-catenin expression in OVSAHO cells untreated (UNT) or treated with CDDP and/or UNC0631 for 24 hours. GAPDH was used as loading control. Parental and PT-Res cells were treated with 15 μM and 25 μM of CDDP, respectively, and with 2 μM and 4 μM of UNC0631, respectively. **C)** Western blot analysis of β-catenin expression in OVCAR-8, TOV-112D, ES-2 and TOV-21G parental and PT-Res cells untreated (UNT) or treated with CDDP and/or UNC0631 for 24 hours, as indicated. GAPDH and VINCULIN were used as loading controls.

Next, we tested if increasing doses of UNC0631 leaded to a decrease in β-catenin protein levels, via BTRC upregulation. We performed a dose-response treatment with UNC0631 in OVSAHO and OVCAR-8 parental and PT-Res clones, then we evaluated the expression of β-catenin by western blot analysis. We observed that in OVSAHO parental cells β-catenin protein expression decreased in a

dose-dependent manner, whereas in OVSAHO PT-Res (**Figure 4.27A**) and in OVCAR-8 cells (**Figure 4.27B**) β-catenin protein expression was insensitive to this treatment.

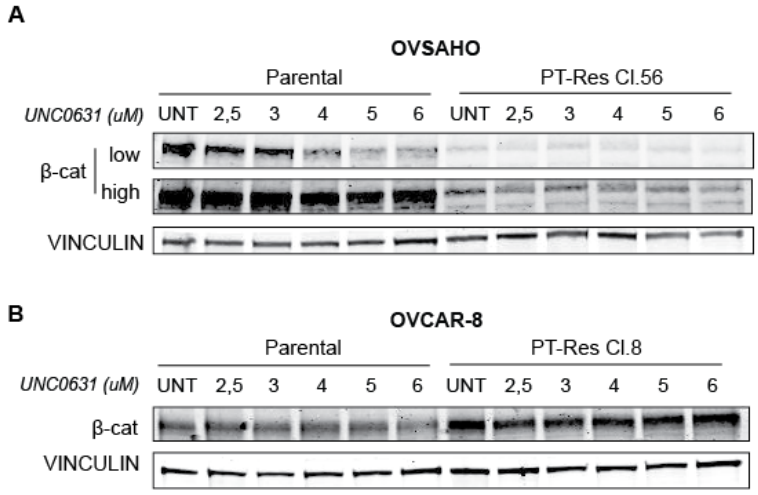


**Figure 4.27. A-B)** Western blot analysis of β-catenin expression in OVSAHO (**A**) and OVCAR-8 (**B**) parental and PT-Res cells, untreated (UNT) or treated for 24 hours with increasing doses of UNC0631. VINCULIN was used as loading control.

The result collected so far suggested that G9a inhibition modulate Wnt/β-catenin pathway by transcriptionally regulating BTRC (see **Results 4.7**) and by favoring the re-localization of β-catenin to the plasma membrane (see **Results 4.5**). Thus, using the TOPFlash/Renilla Wnt receptor assay, we evaluated the transcriptional regulation of the Canonical (β-catenin dependent) Wnt pathway in OVSAHO cells treated with cisplatin and/or UNC0631 for 24 hours. TOPFlash reporter assay demonstrated a significant increase in β-catenin transcriptional activity in OVSAHO parental cells following cisplatin treatment. When combined with cisplatin, UNC0631 inhibited β-catenin transcriptional activity induced by cisplatin alone (**Figure 4.28A**). Based on these results we tested if Wnt/β-catenin pathway stimulation could participate in the response of parental OVSHAO cells to cisplatin-induced death and therefore explain at least in part the PT-Res phenotype. To this aim we used human recombinant Wnt3a (rWnt3a), since Wnt3a encoding gene was among those genes upregulated by PT and reverted by UNC0631 (see **Results 4.6, Figure 4.20B**). Results showed that rWnt3a given alone and in association with UNC0631 after platinum treatment (**Figure 4.28B)** significantly improved cell survival in cells treated with the cisplatin+UNC0631 combination but not with cisplatin alone (**Figure 4.28C**).

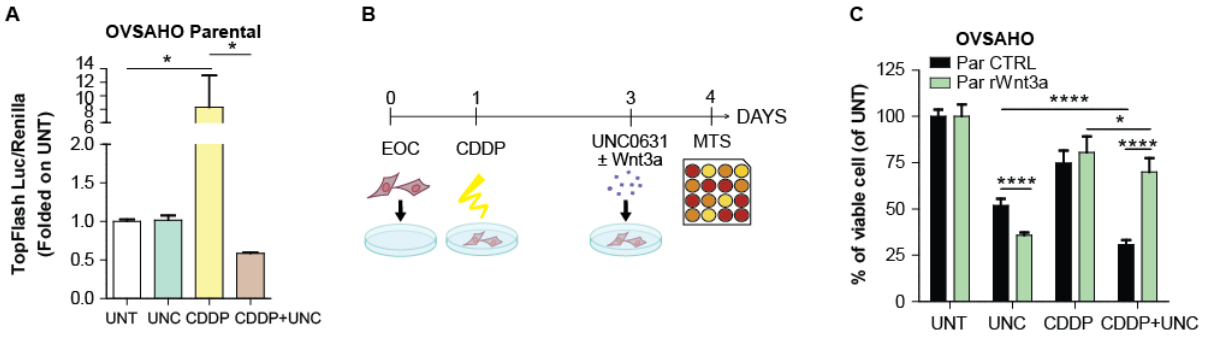


**Figure 4.28. A)** Graph showing the transcriptional activity of β-catenin in OVSAHO parental cells, transfected with a Wnt/β-catenin-reporter plasmid (TOPFlash). Luciferase assay was performed following 24 hours of treatment with 15 µM of cisplatin (CDDP) and/or 2 µM of UNC0631 (UNC). A vector containing Renilla luciferase was used as internal control for transfection efficiency and statistical significance is report in the graph and was calculated using Student t test. **B)** Experimental design of cell viability analysis in (**C**). Cells, plated at high confluence (0), were exposed for 48 hours to 2 µM of cisplatin (CDDP) (1), than the drug was removed and cells were treated for 24 hours with 6 µM of UNC0631 and/or 0,1 µg/µL of recombinant-Wnt3a plasmid (2), finally MTS assay was performed. All data are expressed as percentage of viable cells with respect to the untreated (UNT) cells and represent the mean (±SD) of three independent experiments. Statistical significance was determined by a one-way ANOVA (*$p$<0.05; **$p$<0.01; ***$p$<0.001).

Next, we tested the effect of XAV-939 and WNT-C59, two inhibitors of the Canonical Wnt pathway on OVSAHO cell viability, to verify β-catenin activity contribution to PT-resistance in this model. WNT-C59 is a small-molecule PORCN inhibitor, that acts by blocking the secretion of WNT family ligands (Katoh, 2017), whereas, XAV-939 inhibits TNKS-dependent poly-ADP-ribosylation activity, leading to the stabilization of Axin (a key component of the β-catenin phosphorylation complex) and the abrogation of the Wnt/β-catenin signaling (Guo et al., 2017). Dose-response curves treating OVSAHO parental and PT-Res cells with the two inhibitors for 72 hours showed a small decrease in PT-Res cell viability only when XAV-939 was used (**Figure 4.29A**). Therefore, we next used cisplatin and XAV-939 combination treatments using two different schedules of Wnt-inhibitor administration (**Figure 4.29B and C**). In this manner we observed that XAV-939 increased PT-induced death in PT-Res cells when given after cisplatin treatment (**Figure 4.29C**) having minor or no effects in parental cells and when administered before cisplatin (**Figure 4.29B**). If compared with PT-treatment alone, both parental and PT-Res cells displayed significantly increased cell death when exposed to high doses of XAV-939, before and, especially, after cisplatin treatment (**Figure 4.29C)**.

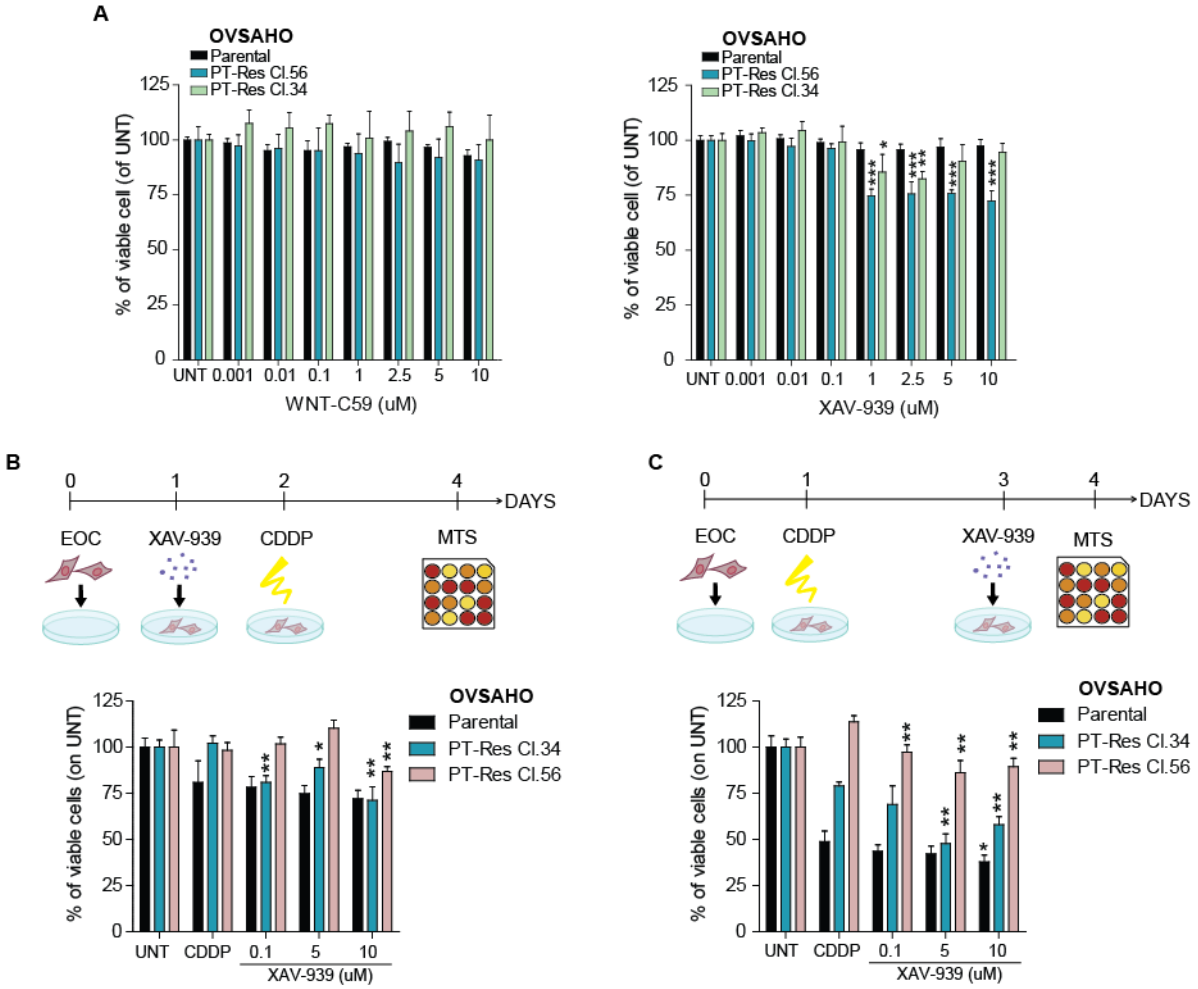


**Figure 4.29. A)** Dose-response curves performed on OVSAHO parental and PT-Res cell treated or not (UNT) with increasing doses of WNT-C59 or XAV-939 for 72 hours. Data are expressed as percentage of viable cells with respect to the untreated (UNT) cells and represent the mean (±SD) of three biological replicates. **B)** Experimental design of XAV-939+CDDP treatment. Cells, plated at high confluence (0), were exposed for 24 hours to increasing doses (0,1 - 5 - 10 µM) of XAV-939 (1), than the inhibitor was removed and cells were treated for 48 hours with 2 µM of CDDP (2), finally cell viability was evaluated by MTS (4 and graph below). **C)** Experimental design of CDDP+XAV-939 treatment. Cells, plated at high confluence (0), were exposed for 48 hours to 2 µM of CDDP (1), than platinum was removed and cells were treated with increasing doses (0,1 -5 - 10 µM) of XAV-939 for 24 hours (3), finally cell viability was evaluated by MTS (4 and graph below).

Overall, our data support the possibility that PT-resistance is driven in EOC cells by G9a/GLP HMTs at least in part by the regulation of Canonical Wnt pathway, a possibility also proposed in recently published manuscripts (Hua et al., 2014b). To verify if the activation of Wnt pathway by G9a could have a significance in the human pathology we interrogated the online resource Kaplan Mayer Plotter testing the expression of the G9a-dependent Wnt signature derived from the GEP and comprising the G9a, WNT3, β-TRCP1, FZD1 and FZD7 genes. Indeed, this Wnt/G9a signature separates EOC patients based on their prognosis both for progression free- and overall-survival (**Figure 4.30**), indirectly confirming the *in vitro* results.

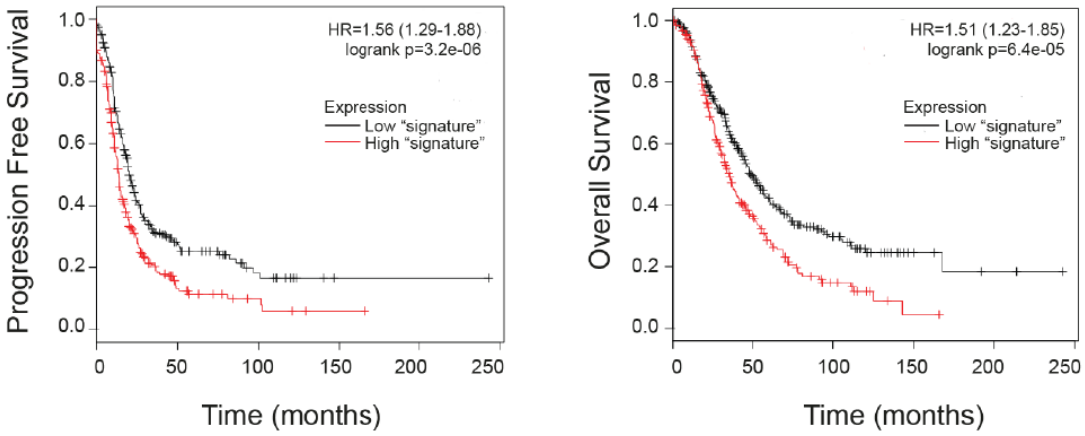


**Figure 4.30. Wnt/G9a signature predict the prognosis in EOC patients.** Kaplan Mayer survival curves predicting the Progression Free Survival (left panel) and the Overall Survival (right panel) of EOC patients (n = 665) divided based on the expression of Wnt/G9a signature (G9a,Wnt3, β-TRCP1, FZD1 and FZD7). Data were obtained using with the online tool Ovmark.

## 4.9 Generation of G9a/GLP knockout PT-Resistant cells

To better address the role of G9a/GLP in PT-response we have generated OVSHAO PT-Res cells knockout for both EHMT1 and EHMT2 genes using the CRISPR/Cas9 technology (**Figure 4.31A and B**). Starting from PT-Res Clone 56, we generated a single knockout, that lacks the EHMT2 gene ($G9a^{KO\#1}$), and a double knockout, missing both EHMT2 and EHMT1 genes ($G9a/GLP^{KO\#3}$). We analyzed the coding sequence of EHMT1/EHMT2 from genomic DNA extracted from OVSAHO PT-Res $G9a^{KO\#1}$ and $G9a/GLP^{KO\#3}$, to confirm the occurred cut of the sequences (**Figure 4.31C**).

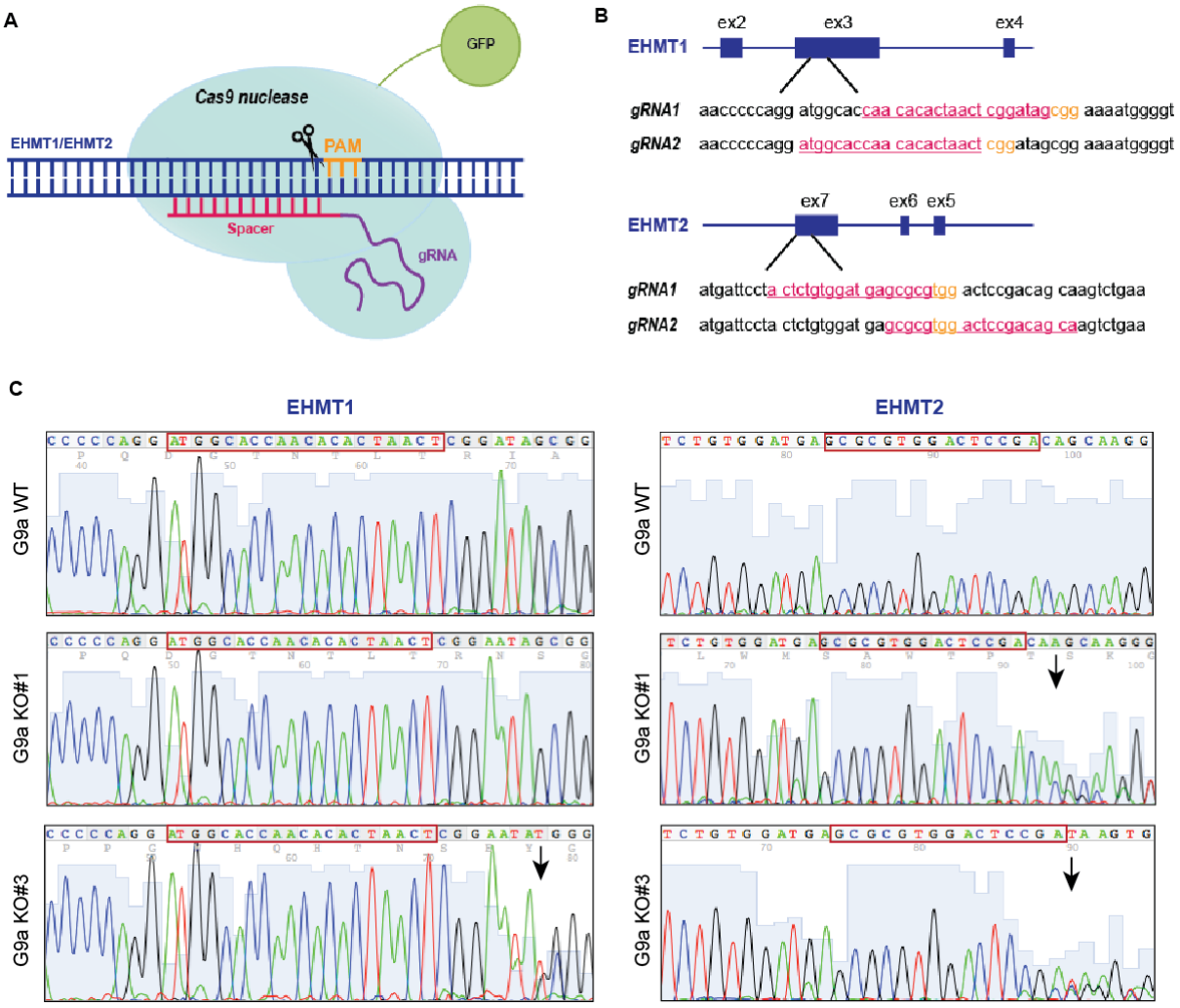


**Figure 4.31. EHMT1/2 knockout OVSAHO cells generated using CRISPR/Cas9 system. A)** Schematic representation of CRISPR/Cas9 system used to produce EHMT1/EHMT2 knockout cells. **B)** For targeting of the EHMT1 exon 3 and EHMT2 exon 7 loci, two pairs of different sets of overlapping gRNAs (gRNA1 and gRNA2) were used. gRNA target sequences are shown in pink and the putative PAM sequence in orange. **C)** Representative four-color fluorescence electropherograms of EHMT1 (left) and EHMT2 (right) Sanger sequence performed on G9a$^{WT}$, G9a$^{KO\#1}$ and G9a/GLP$^{KO\#3}$ OVSAHO cells. Red boxes indicate the sequences recognized by the gRNAs. Black arrows indicate the point where the sequence is no longer aligned with that of the WT, due to the cut made by Cas9 that leads to the modification of the frameshift.

Immunofluorescence and western blot analysis confirmed that CRISPR/Cas9-modified cells did not express G9a (**Figure 4.32A and B**), and lost H3K9 di-methylation (**Figure 4.32B**).

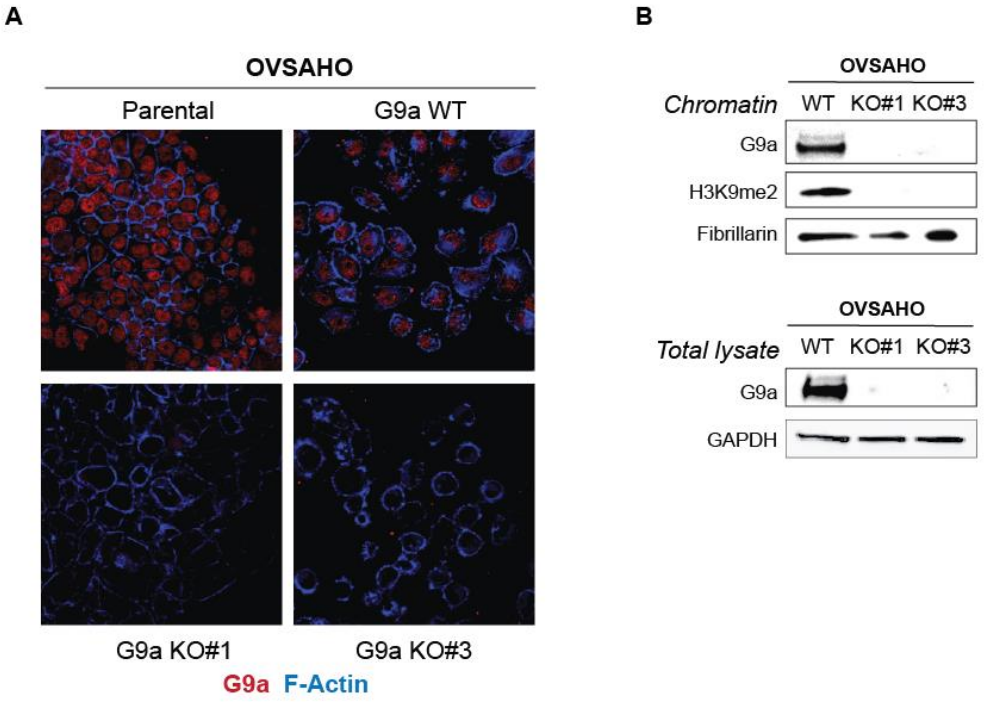


**Figure 4.32. A)** Immunofluorescence analysis of G9a (red) expression in parental and PT-Res G9a/GLP$^{WT/KO}$ OVSAHO cells. **B)** Western blot analysis of chromatin and total lysate G9a and H3K9me2 expression in OVSAHO PT-Res G9a/GLP$^{WT/KO}$ cells. Fibrillarin and GAPDH were used as loading controls, respectively for chromatin and total lysate samples.

## 4.10 G9a/GLP knockout re-sensitizes PT-Resistant cells to PT

Interestingly, both G9a$^{KO\#1}$ and G9a/GLP$^{KO\#3}$ cells significantly increased the sensitivity to cisplatin of PT-Res cells leading to a strong decrease of their cisplatin IC50 (**Figure 4.33A)**. Indeed, we observed that G9a/GLP$^{KO\#3}$ cells had the same sensitivity to cisplatin of parental cells (**Figure 4.33B),** supporting a major role for G9a/GLP in inducing EOC PT-Resistance. Accordingly, PT-treated G9a$^{KO}$ cells exhibited significant increased cleaved-caspase 3 expression respect to untreated condition, not observed in their wild type counterpart (**Figure 4.33C**).

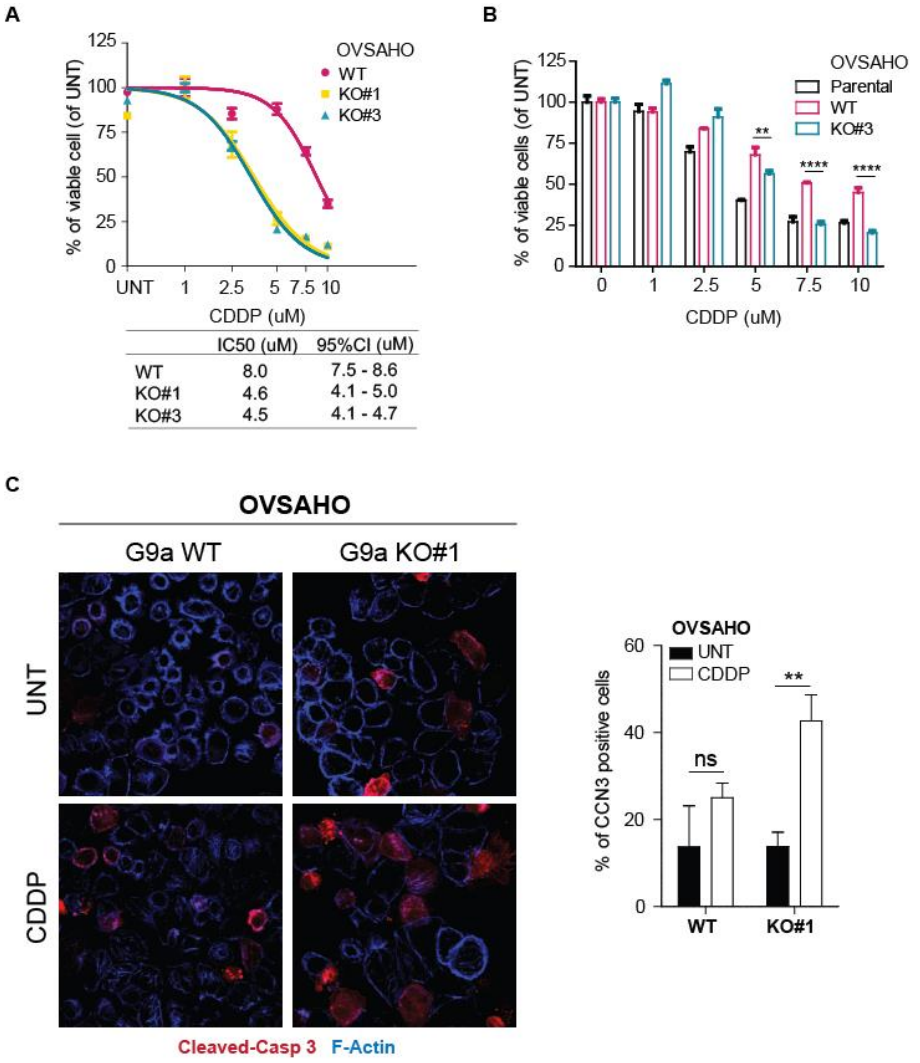


**Figure 4.33. G9a/GLP knockout re-sensitizes PT-Res cells to cisplatin. A)** Nonlinear regression analyses of cell viability assay in OVSAHO G9a/GLP wild type (WT) and knockout (KO#1, KO#3) OVSHAO cells treated with increasing doses of CDDP for 72 hours. Data are expressed as percentage of viable cells with respect to the untreated (UNT) cells and represent the mean (±SD) of three biological replicates. Tables show the IC50 and the confidence interval (CI) of each condition. **B)** Dose-response curve performed on parental and PT-Res G9a/GLP WT/KO cells treated with increasing doses of CDDP for 72 hours. Data are expressed as percentage of viable cells with respect to the untreated (UNT) cells and represent the mean (±SD) of three independent experiments. Statistical significance was determined by a one-way ANOVA (*$p$<0.05; **$p$<0.01; ***$p$<0.001). **C)** Immunofluorescence analysis of cleaved caspase 3 expression in G9a$^{WT/KO}$ OVSAHO cells, untreated (UNT) or treated with 20 µM of cisplatin (CDDP) for 24 hours. Graph (right) shows the percentage of cleaved caspase 3 (CCN3)-positive cells of untreated (UNT) and cisplatin-treated (CDDP) G9a$^{WT/KO}$ OVSAHO. Statistical significance is report in the graph and was calculated using Student's t test.

## 4.11 PT-induced DNA damage response is increased in G9a/GLP knockout cells

In accord with the effect of G9a/GLP knock out on PT-induced death we also observed by immunofluorescence and western blot analyses a strong increase of PT-induced DNA damage, evaluated by the expression of S139 Histone H2AX (γH2AX) in OVSAHO G9a$^{KO\#1}$ respect to WT cells (**Figure 4.34A and B)**. Again, the expression of γH2AX in G9a$^{KO\#1}$ was more similar to the one observed in

parental cells (**Figure 4.11B)** than the one present in PT-Res G9a$^{WT}$ cells (**Figure 4.34B)**. Similarly, G9a$^{KO\#1}$ cells had increased DNA platination respect to both parental and PT-Res G9a$^{WT}$ cells (**Figure 4.34C)**.

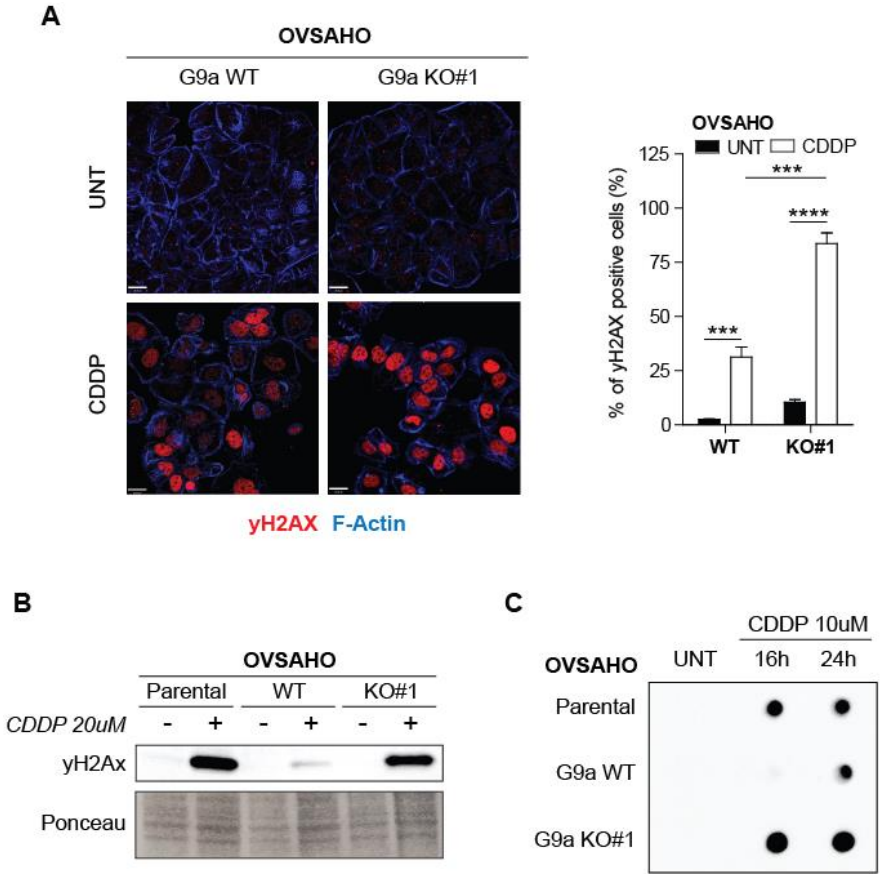


**Figure 4.34. G9a/GLP knockout induces DNA-damage response under cisplatin treatment. A)** Immunofluorescence analysis of γH2AXpS139 (red) in G9a$^{WT/KO}$ OVSAHO cells untreated (UNT) and treated with 20 µM of CDDP for 24 hours. Graph on the right shows the percentage of γH2AXpS139-positive cells of untreated (UNT) and cisplatin-treated (CDDP) G9a$^{WT/KO}$ OVSAHO. Statistical significance is report in the graph and was calculated using Student's t test. **B)** Western blot analysis of γH2AXpS139 expression in G9a$^{WT/KO}$ OVSAHO cells untreated and treated with 20 µM of CDDP for 24 hours. **C)** Dot blot analyses evaluating the amount of platinated-DNA in parental and G9a$^{WT/KO}$ cells untreated (UNT) or treated with 10 µM of CDDP for 24 hours.

## 4.12 BTRC regulation by G9a/GLP complex is partially confirmed by G9a/GLP knockout

Data collected using G9a/GLP inhibitor (see **Results 4.7**) suggested the implication of G9a in Canonical Wnt pathway control, via the regulation of BTRC/FBXW11, WNT3 and FRIZZLEDs transcription, both at basal condition and following cisplatin treatment. To ascertain these observations, we analyzed the expression of β-TRCP1 in G9a/GLP$^{KO}$ cells. An α-H3K9me2-ChIP analysis performed in G9a/GLP$^{WT/KO}$ cells on the most distal region of BTRC promoter showed the loss of dimethylation in KO#3 clone when compared with the WT (**Figure 4.35A)**. However, despite these

quite convincing results, at β-TRCP1 mRNA and protein expression was similar in G9a WT and KO#3 PT-Res OVSHAO cells both in basal condition and under cisplatin treatment (**Figure 4.35B and C)**. Looking at β-TRCP1 targets, as observed in the experiments performed with G9a/GLP inhibitor, also in G9a/GLP$^{KO}$ cells we could not detect any modulation of β-catenin protein levels (**Figure 4.35D)**, but we confirmed, by immunofluorescence, that G9a plays a role in β-catenin plasma membrane localization, since in G9a/GLP knockout but not in WT PT-Res cells β-catenin was prevalently localized at the membrane (**Figure 4.35E)**.

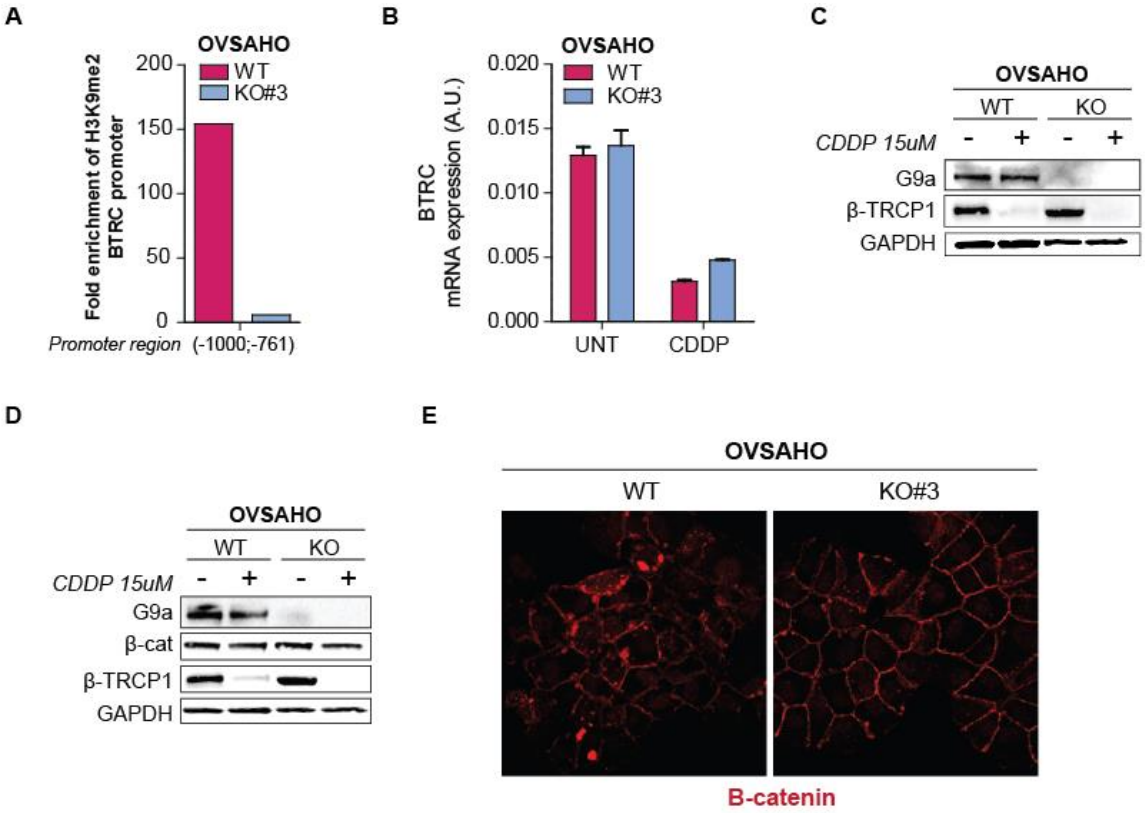


**Figure 4.35. G9a/GLP$^{KO}$ partially confirmed G9a activity in the modulation of BTRC expression. A)** Graph showing the amount of immunoprecipitated H3K9me2 on BTRC promoter in G9a/GLP$^{WT/KO}$ OVSAHO cells, detected by ChIP analysis. **B)** BTRC mRNA expression analysis in G9a/GLP$^{WT/KO}$ OVSAHO cells untreated (UNT) or treated with 25 μM of cisplatin (CDDP) for 16 hours. **C-D)** Western blot analyses of G9a, BTRC and β-catenin expression in G9a/GLP$^{WT/KO}$ OVSAHO cells untreated or treated with cisplatin (CDDP) for 24 hours. GAPDH was used as loading control. **E)** Immunofluorescence analysis of β-catenin (red) in G9a/GLP$^{WT/KO}$ OVSAHO cells.

## 4.13 G9a/GLP knockout confirmed the role of the HMTs complex in cell-cell contact and stemness

Next, we tested G9a/GLP$^{WT/KO}$ cells ability to grow and invade/metastasize *in vitro* when treated or not with cisplatin. Firstly, we checked OVSAHO parental and G9a/GLP$^{WT/KO}$ cells capability to escape matrigel drops an assay used to measure the invasive potential of the cells. While PT-Res

G9a/GLP$^{WT}$ cells were able to escape matrigel drop and spread on the tissue culture dish, the KO#3 clone was less able to escape the protein matrix, showing a behavior similar to the one observed in parental cells, which were unable to escape the matrigel drops (**Figure 4.36A**). Subsequently, we assessed if G9a/GLP loss induced an altered migration of PT-Res OVSAHO cells, compared to the wild type. To this end, a scratch-wound was performed on G9a/GLP$^{WT/KO}$ cells. By this approach, we observed that the G9a/GLP deprivation slightly reduced the ability of PT-Res cells to migrate (**Figure 4.36B)**.

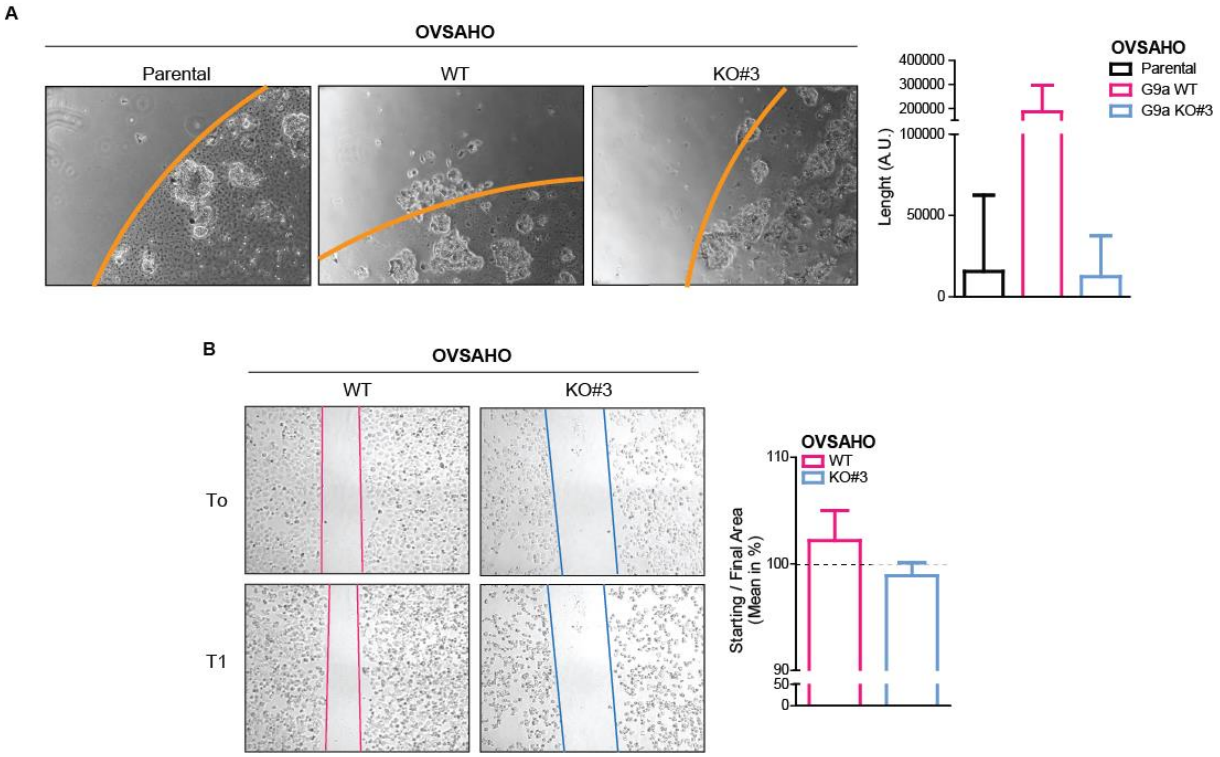


**Figure 4.36. G9a/GLP knockout decreases migration ability of PT-Res cells. A)** Representative images (left) of the evasion assay using OVSAHO parental and PT-Res G9a/GLP$^{WT/KO}$ cells at the beginning (T0) and at the end (T1) of the experiment. Orange lines indicate the matrigel drop border. Graph on the right reports the distance covered by evaded OVSAHO cells after 10 days. **B)** Representative images (left) scratch assay using OVSAHO G9a/GLP wild type and knockout cells. Graph on the right reports the distance covered by migrated OVSAHO cells after 48 hours.

Finally, to better characterize the role of G9a in cell-cell contact, we investigated, by immunofluorescence, the expression of some adherence and tight junction markers in OVAHO G9a$^{KO\#1}$ clone, compared with OVSAHO parental and PT-Res G9a$^{WT}$ cells. As marker for adherence junctions analysis we observed that the decreased and more spread localization of p120-catenin in PT-Res G9a$^{WT}$ cells, respect to the parental cells (see **Results 4.5)**, was reverted in G9a$^{KO}$ cells, where p120-catenin was mainly localized on membrane (**Figure 4.37A, upper panel)**. Similar behavior in γ-catenin was observed, exclusively on membrane in parental and G9a$^{KO}$ cells respect to the G9aWT ones, but less expressed in the KO respect both to PT-sensitive and PT-Res cells **(Figure 4.37A, middle panel)**.

No significant differences were detected between parental and PT-Res G9a$^{WT/KO}$ in the localization of E-cadherin, that however resulted more expressed in both PT-Res G9a WT and KO cells when compared to their parental counterpart (**Figure 4.37A, bottom panel**). When markers of tight junctions were analyzed, we confirmed the decrease in the expression of occludin in PT-Res G9a$^{WT}$ respect to the parental cells, and observed an increase of its membrane localization in G9a$^{KO}$ cells (**Figure 4.37B, upper panels**). No significant differences were observed between parental and PT-Res G9a$^{WT/KO}$ expression and localization of ZO-1 (**Figure 4.37B, lower panels**).

Overall, our data indicated that G9a regulates cell-cell contact organization of PT-Res EOC cells thus questioning if G9a could affect cell permeability by interfere with the formation and the integrity of EOC cells monolayer. With this aim, we performed a permeability assay on OVAHO parental and PT-Res G9a$^{WT/KO}$ cells seeding the cells on transwell filters at confluency, and then by treating them with cisplatin for 16 hours. Functionality of cell-cell junctions was assessed by adding FITC-Dextran on the top of the monolayer and measuring the presence of the compound in the bottom wells, an assay that as measures the FITC-Dextran leakage. As shown in **Figure 4.37C**, the loss of G9a in the KO clone leaded to a decrease in cell permeability, in untreated condition, respect to G9a$^{WT}$ cells. Moreover, cisplatin treatment induced a significant increase in KO cell permeability that, conversely, was not further increased in PT-Res G9a$^{WT}$ cells.

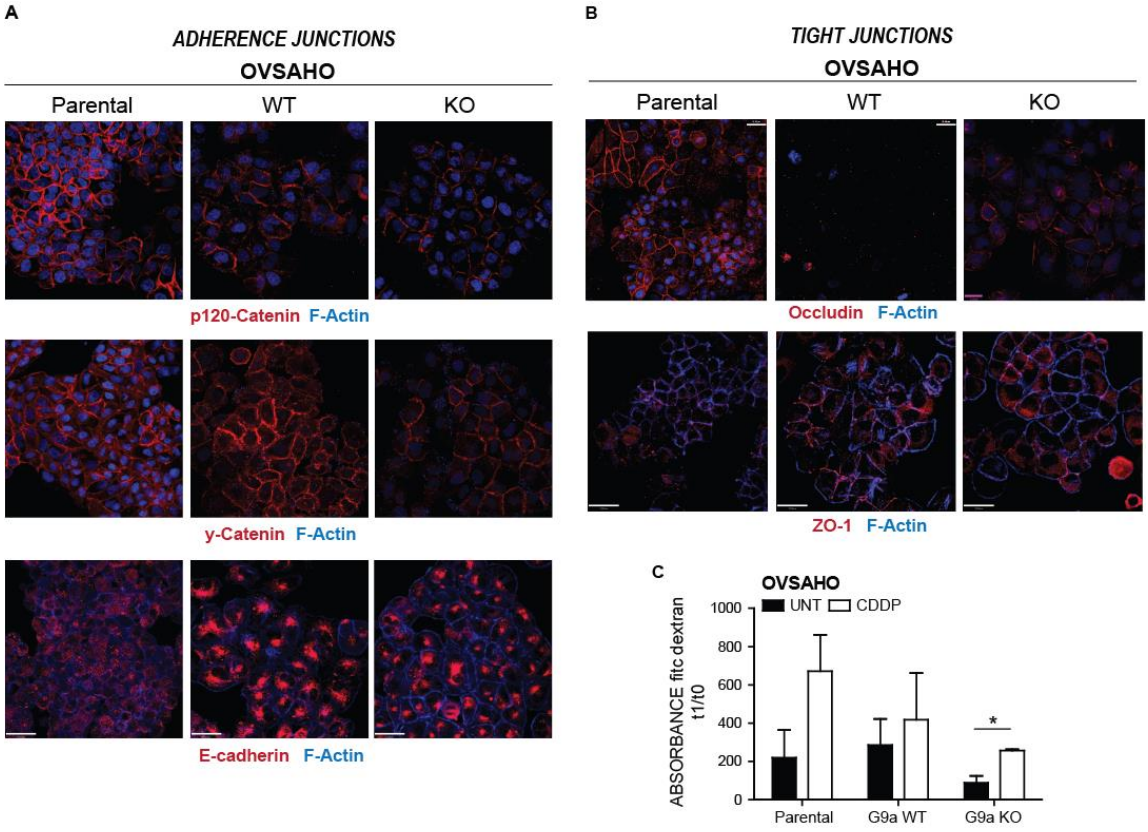


**Figure 4.37. G9a/GLP knockout increases PT-Res cell permeability. A-B)** Immunofluorescence analysis of the expression of adherence junction **(A)** and tight junction **(B)** markers in parental, PT-Res G9a$^{WT}$ and G9a$^{KO}$ cells. **C)** Graph reporting the analysis of the permeability of OVSAHO parental and PT-Res G9a$^{WT/KO}$ cells' monolayers, in untreated condition (UNT) or following cisplatin treatment (CDDP). Statistical significance was determined by a two-tailed unpaired Student's t test (*P < 0.05)

# 5. DISCUSSION

To date, development of PT-resistance remains the main cause of EOC related death, together with the late diagnosis and the high heterogeneity of the disease (Van Zyl et al., 2018). Acquired resistance to chemotherapy has been recently linked to epigenetic alterations, observed early during cell transformation, contribute to define cancer onset, progression and response to therapies, and known to have a central role in the pathology of ovarian carcinomas (Flavahan et al., 2017; H. Zhang et al., 2014).

Here, with the aim to identify possible mechanisms underlying PT-resistance and eventually new strategies to overcome it, we carried out a screening of Epigenetic Modifiers (EMs) used as anticancer drugs. With this approach we identified the inhibitors of G9a/GLP HMTs as the most active drugs in killing isogenic PT-resistant (PT-Res) EOC cells. When given as single agents, G9a/GLP inhibitors (G9a/GLPi) show high efficacy in reducing cell viability of all tested EOC parental and PT-Res cell lines. Moreover, UNC0631 (one of the most effective cell permeable *G9a/GLPi* used as single agent) interferes with platinum activity, improving PT efficacy in parental cells and re-sensitizing to PT the PT-Res ones. The re-sensitization of PT-Res cells to platinum treatment was then confirmed by knocking out G9a and GLP in PT-Res cells, confirming that these HMTs likely mediate the activity of UNC0631. Future experiments will define if *G9a/GLPi* became ineffective in PT-Res KO cells, to definitely prove that, at the doses used, these inhibitors act as expected by altering the activity of G9a/GLP HMTs.

Interestingly, the increased PT-activity in the combined treatment was observed only if UNC0631 was administrated after PT, suggesting that it impairs the ability of EOC cells to repair PT-induced DNA damage. This finding implies that G9a/GLP HMTs plausibly interferes with the DNA repair mechanisms, a possibility supported by recent evidences demonstrating that G9a inhibition leads to increased sensitivity to ionizing radiation of cancer cells, by disrupting DNA repair pathways and that G9a could be recruited on damaged DNA (Ginjala et al., 2017). Accordingly, we observed an increased expression of γH2AX in both parental and PT-Res EOC cells when treated with CDDP+UNC0631 combination compared with the single treatments. Genetic and pharmacological inhibition of G9a/GLP also increased DNA platination in PT-Res cells, suggesting a possible role of G9a/GLP activity not only in improving DNA-repair following PT-induced DNA damage, but also in reducing the efficacy of PT in induce DNA damage. Further experiments are needed to precisely define how G9a/GLP affect the ability of PT to bound the DNA and/or if the decreased platination is the results of a faster PT adducts resolution.

Overall the functional results are in line with the possibility that PT induces G9a chromatin localization with a consequent increase of H3K9 di-methylation (H3K9me2) and the suppression of transcription in genes possibly involved in the regulation of PT-response, pointing to a dynamic

epigenetic regulation of acquired PT-resistance in EOC cells. This possibility is in line with our observation that UNC0631, that is a substrate competitive inhibitor of G9a that specifically binds the substrate site in the enzyme (Cao et al., 2019), hampered the bond of the HMT with DNA, resulting in a decrease of both chromatin-G9a and H3K9me2 levels of PT-Res cells.

In search for possible molecular pathways modified by PT and *G9a/GLPi* we used genome wide Gene Expression Profile (GEP) analyses recovered several interesting information. First both PT and UNC0631 profoundly affect the GEP of both parental and PT-Resistant cell. Yet, while PT treatment had no effects on the expression of genes regulated by UNC0361 the *G9a/GLPi* reverted the expression of 10% and 19% of genes modified by PT in parental and PT-Res cells, respectively. These evidences allowed us to identify a signature (i.e. genes modified by PT in a G9a/GLP-dependent manner in PT-Res cells) that might play a role in the onset of acquired PT-resistance. Gene Set Enrichment Analysis (GSEA) interrogated with this signature evidences four pathways significantly modified by PT in a G9a/GLP-dependent manner in PT-Res cells. Quite surprisingly among these we did not identified pathways related to DNA damage but, principally, pathways that regulates cell-cell contacts and EMT regulation. Among these we focused on the possible regulation of Canonical Wnt pathway by a G9a/GLP, being Wnt pathway previously linked to PT-resistance in EOC (Arend et al., 2013). Moreover, the enrichment of Wnt/β-catenin signaling pathway in PT-Res cells compared with the parental once, with the addition of Tight Junction and Focal Adhesion pathways under cisplatin treatment, represents a possible molecular explanation for the higher *in vitro* adhesive and invasive capabilities of PT-Res cells (Sonego et al. and **Figure 4.36**) and is in accord with their greater ability to form a higher number and bigger spheres respect to their parental counterpart, regardless of PT treatment. The data collected on PT-Res G9a/GLP$^{KO}$ cells also support the role of G9a in cell-cell contacts, since the KO differ from the wild type PT-Res cells in the localization of most of the analyzed markers of adherence (β-catenin, p120-cantenin and γ-catenin), and tight junctions (occludin), becoming similar to that observed in parental cells.

Despite our data demonstrate a role for G9a/GLP HMTs in the regulation of Canonical WNT pathway in PT-Res EOC, the behavior of β-catenin in PT+UNC0631-treated PT-Res wild type and PT-treated G9a/GLP$^{KO}$ cells remain not entirely clear. The redistribution of β-catenin in the cytosol rather than at the cell membrane in PT-Res untreated cells, with its entry in the nucleus after cisplatin treatment, suggests the activation of the Wnt/β-catenin pathway, in accord with GSEA and its discussed involvement in cancer progression in ovarian cancer (Arend et al., 2013). However, the increased expression of β-TRCP1 and β-TRCP2, demonstrated by GEP and mRNA and protein expression analyses in parental and PT-Res cells treated with UNC0631, was not associated with the expected decrease of β-catenin protein expression. Among the possible explanations of these findings is the fact that β-

catenin is sensitive to degradation only if located into the cytoplasm and the nucleus (Shi et al., 2015). Thus, the re-localization of β-catenin on plasma membrane by G9a/GLP inhibition could prevent its degradation by β-TRCP1/2 bond. It is already known that, on cell membrane, β-catenin contributes to the maintenance of the adherence junctions, by interacting with E-cadherin (Arend et al., 2013; Zhou & Hung, 2005), and that PT induce downregulation of E-cadherin via stabilization of Snail (Sonego et al., 2019; Yu et al., 2017). We can speculate that under cisplatin treatment Snail-associated downregulation of E-cadherin leads to a greater availability of β-catenin, that can enter the nucleus and activate gene target transcription. In this context, it would be interesting evaluating if and why the principal target of β-TRCP1/2 in PT-Res cells is Snail, a proved target of β-TRCP1/2 (Yu et al., 2017). This possibility will reconcile the observed increased expression of E-cadherin on the plasma membrane, which in turn recruits β-catenin preventing its degradation, as observed with G9a/GLP pharmacological inhibition.

We believe that BTRC and FBXW11 genes (encoding for β-TRCP1/2) are regulated by G9a/GLP through H3K9me2 regulation, since we observed a direct binding of G9a on the BTRC promoter and a correspondent H3K9me2 in ChIP experiments. Yet, some contrasting data has been obtained with the analyses of H3K9me2 ChIP in PT-treated cells. Here we expected an increase of H3K9me2 on the BTRC promoter after PT treatment that however was not observed. A possible explanation of this unexpected results come however from the preliminary analyses of ChIP Seq experiments we performed in parental, PT-Res and PT-Res G9a/GLP$^{KO}$ cells treated or not with PT in which the chromatin was immunoprecipitated with an anti-H3K9me2 antibody. These preliminary analyses clearly demonstrated that genes downregulated by PT are more methylated on H3K9 after PT treatment and the degree of methylation increased in PT-Res cells. Moreover, we observed that the increased methylation was present not only in the promoter region but also, and especially after the TSS and the TES of the genes, suggesting that H3K9me2 after platinum regulates not only the promoters but also other regulatory elements like enhancers and repressors regions (**Figure 5.1**).

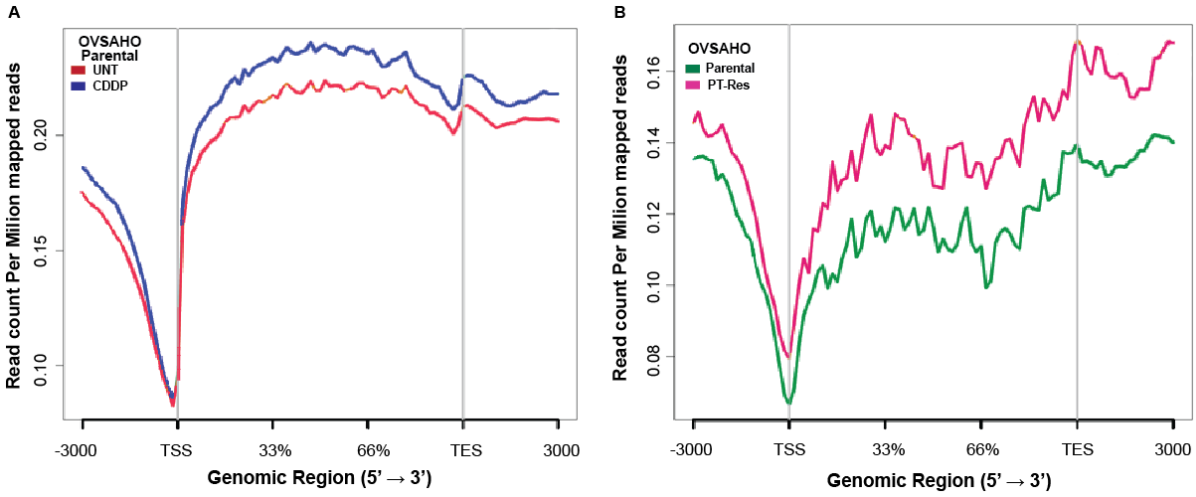


**Figure 5.1. The higher H3K9 methylation of PT-downregulated genes is confirmed by ChIP-seq analysis. A-B)** ChIP-seq reads as normalized read counts per million of H3K9me2 signal in regions 3000 bp upstream the TSS and 3000 bp downstream the TES of genes downregulated by PT (**A**) in untreated (red) *vs* PT-treated (blu) parental OVSAHO cells, and (**B**) in PT-treated parental (green) *vs* PT-Res (pink) OVSAHO cells. (TSS = Transcription start sites, TES = transcription End sites).

We were also surprised in verifying that in PT-Res G9a/GLP$^{KO}$ cells PT did not regulate BTRC and FBXW11 genes expression as expected. We believe that in solving these doubts the ongoing analyses of ChIP Seq experiments on these cells will help in clarifying the key role of G9a/GLP in the regulation of Wnt pathway. Then we have already planned to treat PT-Res G9a/GLP$^{KO}$ cells with UNC0631 to verify if possible off target effects of this inhibitor are related to the regulation of Wnt pathway.

Despite the above mentioned possible limitations, here starting from an unbiased pharmacological screening to identify possible vulnerabilities in the epigenome of PT-Res EOC cells we identified a previously undisclosed role of G9a/GLP HMTs in the regulation of WNT/β-catenin pathway in PT-Res EOC cells. The fact that the G9a/GLP complex is a druggable HMTs and that the *G9a/GLPi* have good *in vivo* properties and low toxicity open new possible therapeutic options for PT-Res EOC patients. Of course, several aspects of this work should be further developed and, toward a possible clinical development of our results, it would be important to define the *in vivo* tolerability of the PT+*G9a/GLPi* combination and its activity in the control of tumor growth and spreading. Appropriate xenograft and syngeneic models are necessary to explore this possibility.

# 6. REFERENCES

Agarwal, P., & Jackson, S. P. (2016). G9a inhibition potentiates the anti-tumour activity of DNA double-strand break inducing agents by impairing DNA repair independent of p53 status. *Cancer Letters*, *380*(2), 467–475. https://doi.org/10.1016/j.canlet.2016.07.009

Agarwal, R., & Kaye, S. B. (2003). Ovarian cancer: Strategies for overcoming resistance to chemotherapy. *Nature Reviews Cancer*, *3*(7), 502–516. https://doi.org/10.1038/nrc1123

Arend, R. C., Londoño-Joshi, A. I., Straughn, J. M., & Buchsbaum, D. J. (2013). The Wnt/β-catenin pathway in ovarian cancer: A review. *Gynecologic Oncology*, *131*(3), 772–779. https://doi.org/10.1016/j.ygyno.2013.09.034

Audia, J. E., & Campbell, R. M. (2016). Histone modifications and cancer. *Cold Spring Harbor Perspectives in Biology*, *8*(4), 1–31. https://doi.org/10.1101/cshperspect.a019521

Baldassarre, G., Belletti, B., Nicoloso, M. S., Schiappacassi, M., Vecchione, A., Spessotto, P., Morrione, A., Canzonieri, V., & Colombatti, A. (2005). p27Kip1-stathmin interaction influences sarcoma cell migration and invasion. *Cancer Cell*, *7*(1), 51–63. https://doi.org/10.1016/j.ccr.2004.11.025

Binju, M., Padilla, M. A., Singomat, T., Kaur, P., Suryo Rahmanto, Y., Cohen, P. A., & Yu, Y. (2019). Mechanisms underlying acquired platinum resistance in high grade serous ovarian cancer - a mini review. *Biochimica et Biophysica Acta - General Subjects*, *1863*(2), 371–378. https://doi.org/10.1016/j.bbagen.2018.11.005

Bomben, R., Ferrero, S., D'Agaro, T., Dal Bo, M., Re, A., Evangelista, A., Carella, A. M., Zamò, A., Vitolo, U., Omedè, P., Rusconi, C., Arcaini, L., Rigacci, L., Luminari, S., Piccin, A., Liu, D., Wiestner, A., Gaidano, G., Cortelazzo, S., … Gattei, V. (2018). A B-cell receptor-related gene signature predicts survival in mantle cell lymphoma: Results from the Fondazione Italiana Linfomi MCL-0208 trial. *Haematologica*, *103*(5), 849–856. https://doi.org/10.3324/haematol.2017.184325

Brown, R., Curry, E., Magnani, L., Wilhelm-Benartzi, C. S., & Borley, J. (2014). Poised epigenetic states and acquired drug resistance in cancer. *Nature Reviews Cancer*, *14*(11), 747–753. https://doi.org/10.1038/nrc3819

Cabasag, C. J., Arnold, M., Butler, J., Inoue, M., Trabert, B., Webb, P. M., Bray, F., & Soerjomataram, I. (2020). The influence of birth cohort and calendar period on global trends in ovarian cancer incidence. *International Journal of Cancer*, *146*(3), 749–758. https://doi.org/10.1002/ijc.32322

Cao, H., Li, L., Deying, Y., Liming, Z., Yewei, X., Yu, B., Liao, G., & Chen, J. (2019). Recent progress in histone methyltransferase (G9a) inhibitors as anticancer agents. *European Journal of Medicinal Chemistry*, *179*, 537–546. https://doi.org/10.1016/j.ejmech.2019.06.072

Casciello, F., Windloch, K., Gannon, F., & Lee, J. S. (2015). Functional role of G9a histone methyltransferase in cancer. *Frontiers in Immunology*, *6*(SEP), 3–9. https://doi.org/10.3389/fimmu.2015.00487

Chandra, A., Pius, C., Nabeel, M., Nair, M., Vishwanatha, J. K., Ahmad, S., & Basha, R. (2019). Ovarian cancer: Current status and strategies for improving therapeutic outcomes. *Cancer Medicine*, *8*(16), 7018–7031. https://doi.org/10.1002/cam4.2560

Chetrit, A., Hirsh-Yechezkel, G., Ben-David, Y., Lubin, F., Friedman, E., & Sadetzki, S. (2008). Effect of BRCA1/2 mutations on long-term survival of patients with invasive ovarian cancer: The National Israeli Study of Ovarian Cancer. *Journal of Clinical Oncology*, *26*(1), 20–25.

https://doi.org/10.1200/JCO.2007.11.6905

Chi, P., Allis, C. D., & Wang, G. G. (2010). Covalent histone modifications-miswritten, misinterpreted and mis-erased in human cancers. *Nature Reviews Cancer*, *10*(7), 457–469. https://doi.org/10.1038/nrc2876

Collins, R., & Cheng, X. (2010). A case study in cross-talk: The histone lysine methyltransferases G9a and GLP. *Nucleic Acids Research*, *38*(11), 3503–3511. https://doi.org/10.1093/nar/gkq081

Cooke, S. L., & Brenton, J. D. (2011). Evolution of platinum resistance in high-grade serous ovarian cancer. *The Lancet Oncology*, *12*(12), 1169–1174. https://doi.org/10.1016/S1470-2045(11)70123-1

Cui, D., Dai, X., Shu, J., Ma, Y., Wei, D., Xiong, X., & Zhao, Y. (2020). The cross talk of two family members of β-TrCP in the regulation of cell autophagy and growth. *Cell Death and Differentiation*, *27*(3), 1119–1133. https://doi.org/10.1038/s41418-019-0402-x

Damia, G., & Broggini, M. (2019). Platinum resistance in ovarian cancer: Role of DNA repair. *Cancers*, *11*(1), 1–15. https://doi.org/10.3390/cancers11010119

Daugherty, R. L., & Gottardi, C. J. (2007). Phospho-regulation of β-catenin adhesion and signaling functions. *Physiology*, *22*(5), 303–309. https://doi.org/10.1152/physiol.00020.2007

Dawson, M. A., & Kouzarides, T. (2012). Cancer epigenetics: From mechanism to therapy. *Cell*, *150*(1), 12–27. https://doi.org/10.1016/j.cell.2012.06.013

Debnath, J., Muthuswamy, S. K., & Brugge, J. S. (2003). Morphogenesis and oncogenesis of MCF-10A mammary epithelial acini grown in three-dimensional basement membrane cultures. *Methods*, *30*(3), 256–268. https://doi.org/10.1016/S1046-2023(03)00032-X

E. L. Greer, Y. S. (2002). Histone methylation: a dynamic mark in health, disease and inheritance. *Nature Reviews Genetics*, *13*(5), 343–357. https://doi.org/10.1038/nrg3173.Histone

Estève, P. O., Patnaik, D., Chin, H. G., Benner, J., Teitell, M. A., & Pradhan, S. (2005). Functional analysis of the N- and C-terminus of mammalian G9a histone H3 methyltransferase. *Nucleic Acids Research*, *33*(10), 3211–3223. https://doi.org/10.1093/nar/gki635

Fang, F., Munck, J., Tang, J., Taverna, P., Wang, Y., David, F. B., Pilrose, J., Choy, G., Azab, M., Pawelczak, K. S., Wagner, M., Lyons, J., Matei, D., & John, J. (2014). The novel, small molecule DNA methylation inhibitor SGI-110 as an ovarian cancer chemosensitizer. *Clinial Cancer Research*, *20*(24), 6504–6516. https://doi.org/10.1158/1078-0432.CCR-14-1553.The

Ferlay, J., Colombet, M., Soerjomataram, I., Mathers, C., Parkin, D. M., Piñeros, M., Znaor, A., & Bray, F. (2019). Estimating the global cancer incidence and mortality in 2018: GLOBOCAN sources and methods. *International Journal of Cancer*, *144*(8), 1941–1953. https://doi.org/10.1002/ijc.31937

Flavahan, W. A., Gaskell, E., & Bernstein, B. E. (2017). Epigenetic plasticity and the hallmarks of cancer. *Science*, *357*(6348). https://doi.org/10.1126/science.aal2380

Fong et al. (2009). Inhibition of Poly(ADP-Ribose) Polymerase in Tumors from BRCA Mutation Carriers. *The New England Journal of Medicine*, *361*(2), 123–134.

Freimund, A. E., Beach, J. A., Christie, E. L., & Bowtell, D. D. L. (2018). Mechanisms of Drug Resistance in High-Grade Serous Ovarian Cancer. *Hematology/Oncology Clinics of North*

*America*, *32*(6), 983–996. https://doi.org/10.1016/j.hoc.2018.07.007

Gao, Y., Liu, X., Li, T., Wei, L., Yang, A., Lu, Y., Zhang, J., Li, L., Wang, S., & Yin, F. (2017). Cross-validation of genes potentially associated with overall survival and drug resistance in ovarian cancer. *Oncology Reports*, *37*(5), 3084–3092. https://doi.org/10.3892/or.2017.5534

Ginjala, V., Rodriguez-Colon, L., Ganguly, B., Gangidi, P., Gallina, P., Al-Hraishawi, H., Kulkarni, A., Tang, J., Gheeya, J., Simhadri, S., Yao, M., Xia, B., & Ganesan, S. (2017). Protein-lysine methyltransferases G9a and GLP1 promote responses to DNA damage. *Scientific Reports*, *7*(1), 1–12. https://doi.org/10.1038/s41598-017-16480-5

Guo, W., Shen, F., Xiao, W., Chen, J., & Pan, F. (2017). Wnt inhibitor XAV939 suppresses the viability of small cell lung cancer NCI-H446 cells and induces apoptosis. *Oncology Letters*, *14*(6), 6585–6591. https://doi.org/10.3892/ol.2017.7100

Haslehurst, A. M., Koti, M., Dharsee, M., Nuin, P., Evans, K., Geraci, J., Childs, T., Chen, J., Li, J., Weberpals, J., Davey, S., Squire, J., Park, P. C., & Feilotter, H. (2012). EMT transcription factors snail and slug directly contribute to cisplatin resistance in ovarian cancer. *BMC Cancer*, *12*(1), 91. https://doi.org/10.1186/1471-2407-12-91

Holmes, D. (2015). Ovarian cancer: beyond resistance. *Nature*, *527*(7579), S217. https://doi.org/10.1038/527S217a

Hu, S., Yu, L., Li, Z., Shen, Y., Wang, J., Cai, J., Xiao, L., & Wang, Z. (2010). Overexpression of EZH2 contributes to acquired cisplatin resistance in ovarian cancer cells in vitro and in vivo. *Cancer Biology and Therapy*, *10*(8), 788–795. https://doi.org/10.4161/cbt.10.8.12913

Hua, K. T., Wang, M. Y., Chen, M. W., Wei, L. H., Chen, C. K., Ko, C. H., Jeng, Y. M., Sung, P. L., Jan, Y. H., Hsiao, M., Kuo, M. L., & Yen, M. L. (2014a). The H3K9 methyltransferase G9a is a marker of aggressive ovarian cancer that promotes peritoneal metastasis. *Molecular Cancer*, *13*(1), 1–13. https://doi.org/10.1186/1476-4598-13-189

Hua, K. T., Wang, M. Y., Chen, M. W., Wei, L. H., Chen, C. K., Ko, C. H., Jeng, Y. M., Sung, P. L., Jan, Y. H., Hsiao, M., Kuo, M. L., & Yen, M. L. (2014b). The H3K9 methyltransferase G9a is a marker of aggressive ovarian cancer that promotes peritoneal metastasis. *Molecular Cancer*, *13*(1), 1–13. https://doi.org/10.1186/1476-4598-13-189

Ivanov, M., Barragan, I., & Ingelman-Sundberg, M. (2014). Epigenetic mechanisms of importance for drug treatment. *Trends in Pharmacological Sciences*, *35*(8), 384–396. https://doi.org/10.1016/j.tips.2014.05.004

Javadi, S., Ganeshan, D. M., Qayyum, A., Iyer, R. B., & Bhosale, P. (2016). Ovarian cancer, the revised FIGO staging system, and the role of imaging. *American Journal of Roentgenology*, *206*(6), 1351–1360. https://doi.org/10.2214/AJR.15.15199

Jayson, G. C., Kohn, E. C., Kitchener, H. C., & Ledermann, J. A. (2014). Ovarian cancer. *The Lancet*, *384*(9951), 1376–1388. https://doi.org/10.1016/S0140-6736(13)62146-7

Jones, P. M., & Drapkin, R. (2013). Modeling high-grade serous carcinoma: How converging insights into pathogenesis and genetics are driving better experimental platforms. *Frontiers in Oncology*, *3 AUG*(August), 1–10. https://doi.org/10.3389/fonc.2013.00217

Katoh, M. (2017). Canonical and non-canonical WNT signaling in cancer stem cells and their niches: Cellular heterogeneity, omics reprogramming, targeted therapy and tumor plasticity (Review). *International Journal of Oncology*, *51*(5), 1357–1369. https://doi.org/10.3892/ijo.2017.4129

Ke, X. X., Zhang, D., Zhu, S., Xia, Q., Xiang, Z., & Cui, H. (2014). Inhibition of H3K9 methyltransferase G9A repressed cell proliferation and induced autophagy in neuroblastoma. *PLoS ONE*, *9*(9). https://doi.org/10.1371/journal.pone.0106962

Kilari, D., Guancial, E., & Kim, E. S. (2016). Role of copper transporters in platinum resistance. *World Journal of Clinical Oncology*, *7*(1), 106–113. https://doi.org/10.5306/wjco.v7.i1.106

Kim, S., Han, Y., Kim, S. I., Kim, H.-S., Kim, S. J., & Song, Y. S. (2018). Tumor evolution and chemoresistance in ovarian cancer. *Npj Precision Oncology*, *2*(1), 1–9. https://doi.org/10.1038/s41698-018-0063-0

Kim, Y., Lee, H., Xiong, Y., Sciaky, N., Hulbert, S. W., Everitt, J. I., Jin, J., Roth, B. L., Jiang, Y., Carolina, N., Hill, C., Carolina, N., Hill, C., Carolina, N., Sciences, O., Carolina, N., Carolina, N., Drug, P., Program, S., & Carolina, N. (2017). Targeting the histone methyltransferase G9a activates imprinted genes and improves survival of a mouse model of Prader–Willi syndrome. *Nat Med*, *23*(2), 213–222. https://doi.org/10.1038/nm.4257.Targeting

Konstantinopoulos, P. A., & Matulonis, U. A. (2018). Targeting DNA Damage Response and Repair as a Therapeutic Strategy for Ovarian Cancer. *Hematology/Oncology Clinics of North America*, *32*(6), 997–1010. https://doi.org/10.1016/j.hoc.2018.07.006

Kossaï, M., Leary, A., Scoazec, J. Y., & Genestie, C. (2018). Ovarian Cancer: A Heterogeneous Disease. *Pathobiology*, *85*(1–2), 41–49. https://doi.org/10.1159/000479006

Koukoura, O., Spandidos, D. A., Daponte, A., & Sifakis, S. (2014). DNA methylation profiles in ovarian cancer: Implication in diagnosis and therapy (Review). *Molecular Medicine Reports*, *10*(1), 3–9. https://doi.org/10.3892/mmr.2014.2221

Kouzarides, T. (2007). Chromatin Modifications and Their Function. *Cell*, *128*(4), 693–705. https://doi.org/10.1016/j.cell.2007.02.005

Krishnamurthy, N., & Kurzrock, R. (2018). Targeting the Wnt/beta-catenin pathway in cancer: Update on effectors and inhibitors. *Cancer Treatment Reviews*, *62*, 50–60. https://doi.org/10.1016/j.ctrv.2017.11.002

Krishnan, S., Horowitz, S., & Trievel, R. C. (2011). Structure and Function of Histone H3 Lysine 9 Methyltransferases and Demethylases. *ChemBioChem*, *12*(2), 254–263. https://doi.org/10.1002/cbic.201000545

Kurman, R. J., & Shih, I. M. (2016). The dualistic model of ovarian carcinogenesis revisited, revised, and expanded. *American Journal of Pathology*, *186*(4), 733–747. https://doi.org/10.1016/j.ajpath.2015.11.011

Lisio, M. A., Fu, L., Goyeneche, A., Gao, Z. H., & Telleria, C. (2019). High-grade serous ovarian cancer: Basic sciences, clinical and therapeutic standpoints. *International Journal of Molecular Sciences*, *20*(4). https://doi.org/10.3390/ijms20040952

Marsh, D. J., Shah, J. S., & Cole, A. J. (2014). Histones and their modifications in ovarian cancer - drivers of disease and therapeutic targets. *Frontiers in Oncology*, *4 JUN*(June), 1–12. https://doi.org/10.3389/fonc.2014.00144

Mirza, M. R., Coleman, R. L., González-Martín, A., Moore, K. N., Colombo, N., Ray-Coquard, I., & Pignata, S. (2020). The forefront of ovarian cancer therapy: update on PARP inhibitors. *Annals of Oncology*, *31*(9), 1148–1159. https://doi.org/10.1016/j.annonc.2020.06.004

Morera, L., Lübbert, M., & Jung, M. (2016). Targeting histone methyltransferases and

demethylases in clinical trials for cancer therapy. *Clinical Epigenetics*, *8*(1), 16. https://doi.org/10.1186/s13148-016-0223-4

Mozzetta, C., Pontis, J., Fritsch, L., Robin, P., Portoso, M., Proux, C., Margueron, R., & Ait-Si-Ali, S. (2014). The Histone H3 Lysine 9 Methyltransferases G9a and GLP Regulate Polycomb Repressive Complex 2-Mediated Gene Silencing. *Molecular Cell*, *53*(2), 277–289. https://doi.org/10.1016/j.molcel.2013.12.005

Nogales, V., Reinhold, W. C., Varma, S., Martinez-Cardus, A., Moutinho, C., Moran, S., Heyn, H., Sebio, A., Barnadas, A., Pommier, Y., & Esteller, M. (2016). Epigenetic inactivation of the putative DNA/RNA helicase SLFN11 in human cancer confers resistance to platinum drugs. *Oncotarget*, *7*(3), 3084–3097. https://doi.org/10.18632/oncotarget.6413

Oronsky, B., Ray, C. M., Spira, A. I., Trepel, J. B., Carter, C. A., & Cottrill, H. M. (2017). A brief review of the management of platinum-resistant–platinum-refractory ovarian cancer. *Medical Oncology*, *34*(6), 1–7. https://doi.org/10.1007/s12032-017-0960-z

Palomer, E., Buechler, J., & Salinas, P. C. (2019). Wnt signaling deregulation in the aging and Alzheimer's brain. *Frontiers in Cellular Neuroscience*, *13*(May), 1–8. https://doi.org/10.3389/fncel.2019.00227

Poulard, C., Bittencourt, D., Wu, D., Hu, Y., Gerke, D. S., & Stallcup, M. R. (2017). A post-translational modification switch controls coactivator function of histone methyltransferases G9a and GLP. *EMBO Reports*, *18*(8), 1442–1459. https://doi.org/10.15252/embr.201744060

Ramalingam, P. (2016). Morphologic, Immunophenotypic, and Molecular Features of Epithelial Ovarian Cancer. *Oncology (Williston Park, N.Y.)*, *30*(2), 166–176.

Ran, F. A., Hsu, P. D., Wright, J., Agarwala, V., Scott, D. A., & Zhang, F. (2013). Genome engineering using the CRISPR-Cas9 system. *Nature Protocols*, *8*(11), 2281–2308. https://doi.org/10.1038/nprot.2013.143

Reid, B. M., Permuth, J. B., & Sellers, T. A. (2017). Epidemiology of ovarian cancer: a review. *Cancer Biology and Medicine*, *14*(1), 9–32. https://doi.org/10.20892/j.issn.2095-3941.2016.0084

Rocha, C. R. R., Silva, M. M., Quinet, A., Cabral-Neto, J. B., & Menck, C. F. M. (2018). DNA repair pathways and cisplatin resistance: An intimate relationship. *Clinics*, *73*(8), 1–10. https://doi.org/10.6061/clinics/2018/e478s

Rojas, V., Hirshfield, K. M., Ganesan, S., & Rodriguez-Rodriguez, L. (2016). Molecular characterization of epithelial ovarian cancer: Implications for diagnosis and treatment. *International Journal of Molecular Sciences*, *17*(12). https://doi.org/10.3390/ijms17122113

Samimi, G., Safaei, R., Katano, K., Holzer, A. K., Rochdi, M., Tomioka, M., Goodman, M., & Howell, S. B. (2004). Increased expression of the copper efflux transporter ATP7A mediates resistance to cisplatin, carboplatin, and oxaliplatin in ovarian cancer cells. *Clinical Cancer Research*, *10*(14), 4661–4669. https://doi.org/10.1158/1078-0432.CCR-04-0137

Schiappacassi, M., Lovat, F., Canzonieri, V., Belletti, B., Berton, S., Di Stefano, D., Vecchione, A., Colombatti, A., & Baldassarre, G. (2008). p27Kip1 expression inhibits glioblastoma growth, invasion, and tumor-induced neoangiogenesis. *Molecular Cancer Therapeutics*, *7*(5), 1164–1175. https://doi.org/10.1158/1535-7163.MCT-07-2154

Schwarzenbach, H., & Gahan, P. B. (2019). Resistance to cis- and carboplatin initiated by epigenetic changes in ovarian cancer patients. *Cancer Drug Resistance*.

https://doi.org/10.20517/cdr.2019.010

Segatto, I., Berton, S., Sonego, M., Massarut, S., Fabris, L., Armenia, J., Mileto, M., Colombatti, A., Vecchione, A., Baldassarre, G., & Belletti, B. (2014). P70S6 kinase mediates breast cancer cell survival in response to surgical wound fluid stimulation. *Molecular Oncology*, *8*(3), 766–780. https://doi.org/10.1016/j.molonc.2014.02.006

Segatto, I., De Marco Zompit, M., Citron, F., D'Andrea, S., Vinciguerra, G. L. R., Perin, T., Berton, S., Mungo, G., Schiappacassi, M., Marchini, C., Amici, A., Vecchione, A., Baldassarre, G., & Belletti, B. (2019). Stathmin is required for normal mouse mammary gland development and D16Her2-driven tumorigenesis. *Cancer Research*, *79*(2), 397–409. https://doi.org/10.1158/0008-5472.CAN-18-2488

Shankar, S. R., Bahirvani, A. G., Rao, V. K., Bharathy, N., Ow, J. R., & Taneja, R. (2013). G9a, a multipotent regulator of gene expression. *Epigenetics*, *8*(1), 16–22. https://doi.org/10.4161/epi.23331

Sharma, A., Albahrani, M., Zhang, W., Kufel, C. N., James, S. R., Odunsi, K., Klinkebiel, D., & Karpf, A. R. (2019). Epigenetic activation of POTE genes in ovarian cancer. *Epigenetics*, *14*(2), 185–197. https://doi.org/10.1080/15592294.2019.1581590

Shen, D. W., Pouliot, L. M., Hall, M. D., & Gottesman, M. M. (2012). Cisplatin resistance: A cellular self-defense mechanism resulting from multiple epigenetic and genetic changes. *Pharmacological Reviews*, *64*(3), 706–721. https://doi.org/10.1124/pr.111.005637

Shen, H., & Laird, P. W. (2013). Interplay between the cancer genome and epigenome. *Cell*, *153*(1), 38–55. https://doi.org/10.1016/j.cell.2013.03.008

Shi, J., Liu, Y., Xu, X., Zhang, W., Yu, T., Jia, J., & Liu, C. (2015). Deubiquitinase USP47/UBP64E Regulates β-Catenin Ubiquitination and Degradation and Plays a Positive Role in Wnt Signaling. *Molecular and Cellular Biology*, *35*(19), 3301–3311. https://doi.org/10.1128/mcb.00373-15

Shinkai, Y., & Tachibana, M. (2011). H3K9 methyltransferase G9a and the related molecule GLP. *Genes and Development*, *25*(8), 781–788. https://doi.org/10.1101/gad.2027411

Smith, H. J., Straughn, J. M., Buchsbaum, D. J., & Arend, R. C. (2017). Epigenetic therapy for the treatment of epithelial ovarian cancer: A clinical review. *Gynecologic Oncology Reports*, *20*, 81–86. https://doi.org/10.1016/j.gore.2017.03.007

Sonego, M., Pellarin, I., Costa, A., Vinciguerra, G. L. R., Coan, M., Kraut, A., D'Andrea, S., Dall'Acqua, A., Castillo-Tong, D. C., Califano, D., Losito, S., Spizzo, R., Couté, Y., Vecchione, A., Belletti, B., Schiappacassi, M., & Baldassarre, G. (2019). USP1 links platinum resistance to cancer cell dissemination by regulating Snail stability. *Science Advances*, *5*(5). https://doi.org/10.1126/sciadv.aav3235

Sonego, M., Pellizzari, I., Dall'Acqua, A., Pivetta, E., Lorenzon, I., Benevol, S., Bomben, R., Spessotto, P., Sorio, R., Gattei, V., Belletti, B., Schiappacassi, M., & Baldassarre, G. (2017). Common biological phenotypes characterize the acquisition of platinum-resistance in epithelial ovarian cancer cells. *Scientific Reports*, *7*(1), 1–12. https://doi.org/10.1038/s41598-017-07005-1

Sonego, M., Schiappacassi, M., Lovisa, S., Dall'Acqua, A., Bagnoli, M., Lovat, F., Libra, M., D'Andrea, S., Canzonieri, V., Militello, L., Napoli, M., Giorda, G., Pivetta, B., Mezzanzanica, D., Barbareschi, M., Valeri, B., Canevari, S., Colombatti, A., Belletti, B., … Baldassarre, G.

(2013). Stathmin regulates mutant p53 stability and transcriptional activity in ovarian cancer. *EMBO Molecular Medicine*, *5*(5), 707–722. https://doi.org/10.1002/emmm.201201504

Spitzwieser, M., Pirker, C., Koblmüller, B., Pfeiler, G., Hacker, S., Berger, W., Heffeter, P., & Cichna-Markl, M. (2016). Promoter methylation patterns of ABCB1, ABCC1 and ABCG2 in human cancer cell lines, multidrug-resistant cell models and tumor, tumor-adjacent and tumor-distant tissues from breast cancer patients. *Oncotarget*, *7*(45), 73347–73369. https://doi.org/10.18632/oncotarget.12332

Stein, J., Majores, M., Rohde, M., Lim, S., Schneider, S., Krappe, E., Ellinger, J., Dietel, M., Stephan, C., Jung, K., Perner, S., Kristiansen, G., & Kirfel, J. (2014). KDM5C is overexpressed in prostate cancer and is a prognostic marker for prostate-specific antigen-relapse following radical prostatectomy. *American Journal of Pathology*, *184*(9), 2430–2437. https://doi.org/10.1016/j.ajpath.2014.05.022

Stewart, C., Ralyea, C., & Lockwood, S. (2019). Ovarian Cancer: An Integrated Review. *Seminars in Oncology Nursing*, *35*(2), 151–156. https://doi.org/10.1016/j.soncn.2019.02.001

Testa, U., Petrucci, E., Pasquini, L., Castelli, G., & Pelosi, E. (2018). Ovarian Cancers: Genetic Abnormalities, Tumor Heterogeneity and Progression, Clonal Evolution and Cancer Stem Cells. *Medicines*, *5*(1), 16. https://doi.org/10.3390/medicines5010016

To, K. K. W., Polgar, O., Huff, L. M., Morisaki, K., & Bates, S. E. (2008). Histone modifications at the ABCG2 promoter following treatment with histone deacetylase inhibitor mirror those in multidrug-resistant cells. *Molecular Cancer Research*, *6*(1), 151–164. https://doi.org/10.1158/1541-7786.MCR-07-0175

Toh, T. B., Lim, J. J., & Chow, E. K. H. (2017). Epigenetics in cancer stem cells. *Molecular Cancer*, *16*(1), 1–20. https://doi.org/10.1186/s12943-017-0596-9

Van Zyl, B., Tang, D., & Bowden, N. A. (2018). Biomarkers of platinum resistance in ovarian cancer: What can we use to improve treatment. *Endocrine-Related Cancer*, *25*(5), R303–R318. https://doi.org/10.1530/ERC-17-0336

Vedadi, M., Barsyte-Lovejoy, D., Liu, F., Rival-Gervier, S., Allali-Hassani, A., Labrie, V., Wigle, T. J., Dimaggio, P. A., Wasney, G. A., Siarheyeva, A., Dong, A., Tempel, W., Wang, S. C., Chen, X., Chau, I., Mangano, T. J., Huang, X. P., Simpson, C. D., Pattenden, S. G., … Jin, J. (2011). A chemical probe selectively inhibits G9a and GLP methyltransferase activity in cells. *Nature Chemical Biology*, *7*(8), 566–574. https://doi.org/10.1038/nchembio.599

Walton, J. B., Farquharson, M., Mason, S., Port, J., Kruspig, B., Dowson, S., Stevenson, D., Murphy, D., Matzuk, M., Kim, J., Coffelt, S., Blyth, K., & McNeish, I. A. (2017). CRISPR/Cas9-derived models of HGSOC targeting Brca1, Pten and Nf1, and correlation with platinum sensitivity. *Scientific Reports*, *7*(1), 1–11. https://doi.org/10.1038/s41598-017-17119-1

Walton, J., Blagih, J., Ennis, D., Leung, E., Dowson, S., Farquharson, M., Tookman, L. A., Orange, C., Athineos, D., Stevenson, D., Blyth, K., Strathdee, D., Balkwill, F. R., Lockley, M., & Mcneish, I. A. (2018). CRISPR / Cas9-mediated Trp53 and Brca2 KO to generate improved murine models of HGSOC. *Cancer Research*, *76*(20), 6118–6129. https://doi.org/10.1158/0008-5472.CAN-16-1272.CRISPR/Cas9-mediated

Xiaodong Cheng and Robert M. Blumenthal. (2010). Coordinated Chromatin Control: Structural and Functional Linkage of DNA and Histone Methylation. *Biochemistry*, *49*(14), 2999–3008. https://doi.org/10.1038/jid.2014.371

Yang, Q., Yang, Y., Zhou, N., Tang, K., Lau, W. B., Lau, B., Wang, W., Xu, L., Yang, Z., Huang, S., Wang, X., Yi, T., Zhao, X., Wei, Y., Wang, H., Zhao, L., & Zhou, S. (2018). Epigenetics in ovarian cancer: Premise, properties, and perspectives. *Molecular Cancer*, *17*(1), 1–21. https://doi.org/10.1186/s12943-018-0855-4

Yu, Q., Zhou, B. P., Wu, Y., Sciences, N., & Biochemistry, C. (2017). The regulation of snail: on the ubiquitin edge. *Cancer Cell & Microenvironment*, *4*(2). https://doi.org/10.14800/ccm.1567

Zhang, H., Liu, T., Zhang, Z., Payne, S. H., Zhang, B. B., Jason, E., Zhou, J., Petyuk, V. A., Chen, L., Ray, D., Sun, S., Yang, F., Chen, L., Wang, J., Shah, P., Cha, S. W., Aiyetan, P., Woo, S., Tian, Y., … Von Ruecker, A. (2014). The Histone H3 Lysine 9 Methyltransferases G9a and GLP Regulate Polycomb Repressive Complex 2-Mediated Gene Silencing. *Nature Genetics*, *53*(1), 1–13. https://doi.org/10.1038/ng.297.Large

Zhang, X. Y., & Zhang, P. Y. (2016). Recent perspectives of epithelial ovarian carcinoma (Review). *Oncology Letters*, *12*(5), 3055–3058. https://doi.org/10.3892/ol.2016.5107

Zhou, B. P., & Hung, M. C. (2005). Wnt, hedgehog and snail: Sister pathways that control by GSK-3β and β-Trcp in the regulation of metastasis. *Cell Cycle*, *4*(6), 772–776. https://doi.org/10.4161/cc.4.6.1744

# 7. PUBLICATIONS

Sonego M, Pellarin I, **Costa A**, Vinciguerra GLR, Coan, M, Kraut A, D'Andrea S, Dall'Acqua A, Castillo-Tong DC, Califano D, Losito S, Spizzo R, Couté Y, Vecchione A, Belletti B, Schiappacassi M, Baldassarre G. USP1 links platinum resistance to cancer cell dissemination by regulating Snail stability. *Science Advances, 2019; 5*: eaav3235. DOI: 10.1126/sciadv.aav3235

Lombardi R, Sonego M, Pucci B, Addi L, Iannelli F, Capone F, Roca MS, Milone MR, Moccia T, **Costa A**, Di Gennaro E, Bruzzese F, Baldassarre G, Budillon A. HSP90 identified by a proteomic approach as druggable target to reverse platinum-resistance in ovarian cancer. *Molecular Oncology, 2020.* DOI:10.1002/1878-0261.12883

# 8. ACKNOWLEDGEMENTS

I am grateful to all my group members, but in particular to Dr. Gustavo Baldassarre and Dr. Maura Sonego for accepting me in the lab and for giving me the opportunity to carry out my PhD project, helping and supporting me. I like also to thank the Biasotto M.D. Foundation OGAP O.N.L.U.S. founding for supported my PhD.